SYNTHESIS OF PRECIPITATED CALCIUM CARBONATE USING CALCIUM CARBIDE WASTE FOR ACID MINE DRAINAGE REMEDIATION

LYE XIN YAN

UNIVERSITI TUNKU ABDUL RAHMAN

SYNTHESIS OF PRECIPITATED CALCIUM CARBONATE USING CALCIUM CARBIDE WASTE FOR ACID MINE DRAINAGE REMEDIATION

LYE XIN YAN

A project report submitted in partial fulfilment of the requirements for the award of Bachelor of Engineering (Hons.) Environmental Engineering

Faculty of Engineering and Science
Universiti Tunku Abdul Rahman

January 2019

DECLARATION

I hereby declare that this project report is based on my original work except for citations and quotations which have been duly acknowledged. I also declare that it has not been previously and concurrently submitted for any other degree or award at UTAR or other institutions.

Signature : _____

Name : _____

ID No. : _____

Date : _____

APPROVAL FOR SUBMISSION

I certify that this project report entitled "**SYNTHESIS OF PRECIPITATED CALCIUM CARBONATE USING CALCIUM CARBIDE WASTE FOR ACID MINE DRAINAGE REMEDIATION**" was prepared by **LYE XIN YAN** has met the required standard for submission in partial fulfillment of the requirements for the awards of Bachelor of Engineering (Hons.) Environmental Engineering at Universiti Tunku Abdul Rahman.

Approved by,

Signature : _____

Supervisor : Ts. Dr. Lam Sze Mun

Date : _____

ACKNOWLEDGEMENTS

This project would not have been a success without unconditional guidance and patience given to me by my supervisor, Ts. Dr. Lam Sze Mun. She has provided me with opportunities to challenges and has also motivated me to advance throughout this course. The entire journey is swift and consistently manageable with schedules for which I am very grateful with. Appreciation to be given for my co-supervisor, Ts. Dr. Sin Jin Chung, as well.

I would also like to take this opportunity to express my surmount gratitude for the unfaltering supports of my family who, friends and seniors. Family and friends who have endowed overflowing encourage and care during the entire period. My utmost gratefulness to seniors Wong Kok Ann, Kee Ming Wei, Chai Huey Yee and Quek Jian Ai, who have all nourished me with knowledge and guidance. I would like to extend my thankfulness to senior Wai Kok Poh of UTAR Sg Long who has demonstrated endless patience and help in performing ICP-OES analysis for us.

Utmost gratitude to all of the lab officers and lecturers who have provided immense advices and helps. This was especially emphasized for Mr Chin Kah Seng for his guidance on the preparations for ICP-OES analysis. Nonetheless, Ms Amelia Ng Suk Ting who has patiently provided materials, advices as well as instructions for performing analyses, in which Mr. Voon Kah Loon, Mr. Yong Tzyy Jeng and Ms. Mirohsha a/p Mohan have also provided. A special acknowledgement to UTAR for the provision of numerous research instrumentations. Last but not least, a sincere gratitude and acknowledgement to be given to MCB Industries Sdn. Bhd. for the ample supplies of calcium carbide sludge provided for this research.

SYNTHESIS OF PRECIPITATED CALCIUM CARBONATE USING CALCIUM CARBIDE WASTE FOR ACID MINE DRAINAGE REMEDIATION

ABSTRACT

Calcium carbide sludge represents a by-product of acetylene gas production in which this waste material is converted to yield precipitated calcium carbonate (PCC) via surfactant-polymer template precipitation method. In this present study, the synthesized PCC products were employed for the remediation of acid mine drainage (AMD) which manifested a major concern to the environment as a potent surface and ground water contamination due to its high acidity, concentration of dissolved heavy metal ions and anions. The PCC synthesized by hexadecyltrimethylammonium bromide (CTAB), Pluronics® P-123/CTAB (P123/CTAB), polyethylene glycol/CTAB (PEG/CTAB) and polyvinyl alcohol/CTAB (PVA/CTAB) surfactant-polymer templates were characterized by X-Ray Diffraction (XRD), Fourier Transform Infrared Spectroscopy (FTIR), Brunauer, Emmett and Teller (BET) surface area and Particle Size Distribution (PSD) analyses. It was demonstrated that the synthesized PCC consisted primarily of high thermodynamically stable calcite with high crystallinity and the presence of C=O and O-H bonds. Additionally, BET surface areas of PCC products were determined to range from 8.2487 m^2/g to 25.0417 m^2/g and were defined as macroporous with pore size of more than 50 nm. PCC products exhibited a uniform mean particle size of 0.158 µm with a narrow size distribution of 0.046 – 0.316 µm. The neutralizing capacity of PCC synthesized by various surfactant-polymer templates was evaluated in terms of pH, oxidative reductive potential (ORP), conductivity and removal of heavy metal ions as well as anions. As a result, the final pH readings of all PCC products complied with national (Department of Environment (DOE) National Water Quality Standards (NWQS) for

Malaysia Class IIA as well as Standards A and B of Environmental Quality Act 1974 (EQA) Environmental Quality (Industrial Effluent) Regulations 2009) and international (World Health Organization (WHO) Guidelines for Drinking Water Quality and United States Environmental Protection Agency (EPA) Ore Mining and Dressing Effluent Guidelines 1975 for Iron Ore) standards and guidelines. The PCC synthesized by P123/CTAB was selected as the optimum surfactant-polymer templates due to its achievement of highest pH of 8.22 within standard compliances, lowest ORP of -60.4 mV, highest conductivity of 238.4 µS, high removal efficiency of 87.63 % Al and other heavy metal ions as well as 68.39 % of SO_4^{2-} ion. In the findings for PCC dosage tests, PCC synthesized by P123/CTAB template with a dosage of 0.40 g/L attained a final pH of 8.36, ORP of -61.4 mV and conductivity of 230.1 µS with a removal efficiency of 32.52 % for Mn and 72.77 % for SO_4^{2-} ions. It represented the optimum dosage due to its close proximity with the high neutralizing performance of 0.50 g/L dosage, yet would be more economical for use in large-scaled treatment of AMD. For sludge settling, PCC synthesized by P123/CTAB template of 0.40 g/L dosage successfully acted as a weighing material to precipitate heavy metal and SO_4^{2-} ions in AMD.

TABLE OF CONTENTS

LIST OF TABLES

LIST OF FIGURES

LIST OF SYMBOLS / ABBREVIATIONS

Al	Aluminium
AMD	Acid Mine Drainage
AMD-PCC	Acid Mine Drainage Treated Using Optimized PCC
As	Arsenic
ASTM	American Society for Testing and Materials
BET	Brunauer, Emmett and Teller
Ca^{2+}	Calcium ion
$CaCO_3$	Calcium Carbonate
$CaSO_4.2H_2O$	Gypsum
CCD	Charge-Coupled Device
Class IIA	Department of Environment (DOE) National Water Quality Standards (NWQS) for Malaysia Class IIA
CTAB	Hexadecyl-Trimethylammonium Bromide
Cu	Copper
DI	Distilled Water
DIW	Deionized Water
DIW-PCC	Deionized Water Treated Using Optimized PCC
DOE	Department of Environment
E_h	Electrode Potential
EPA	United States Environmental Protection Agency
EQA	Environmental Quality Act 1974
Fe	Iron
FTIR	Fourier Transform Infrared Spectroscopy
H^+	Hydrogen ion

HCO_3^-	Bicarbonate ion
HNO_3	Anhydrous Nitric Acid
IC	Ion Chromatography
ICP-OES	Inductively Coupled Plasma Optical Emission Spectrometry
JCPDS	Joint Committee on Powder Diffraction Standards
K	Potassium
Mg	Magnesium
Mn	Manganese
N	No
Na	Sodium
Na_2CO_3	Sodium Carbonate
ND	Not detectable (~0 mg/L)
Ni	Nickel
NO_3^-	Nitrate ion
NWQS	National Water Quality Standards
OH^-	Hydroxyl ion
ORP	Oxidative-Reductive Potential, mV
P123	*Pluronics® P-123*
PCC	Precipitated Calcium Carbonate
PEG	Polyethylene Glycol
PO_4^{3-}	Phosphate ion
PVA	Polyvinyl Alcohol
SO_4^{2-}	Sulphate Ion
Standard A	Environmental Quality Act 1974 (EQA) Environmental Quality (Industrial Effluent) Regulations 2009 Standard A
Standard B	Environmental Quality Act 1974 (EQA) Environmental Quality (Industrial Effluent) Regulations 2009 Standard B
SVI	Sludge Volume Index
TSP	Total Suspended Particles
WHO	World Health Organization
X_i	Final Reading

X_o	Initial Reading
XRD	X-Ray Diffraction
Y	Yes
Zn	Zinc

LIST OF APPENDICES

CHAPTER 1

INTRODUCTION

1.1 Acid Mine Drainage Treatment with Precipitated Calcium Carbonate

Every year, in the production of metals, several billion tonnes of inorganic wastes either in the solid form or effluent has been produced due to mineral processing as a part of global mining industry activities. According to the statistical report by International Organising Committee for the World Mining Congresses (2018), Malaysia had produced 4123 metric tonnes of tin in 2016. Tin production has mostly been concentrated in Perak state with a total of 30 active tin mines (Kaur, 2013; Ahmad and Jones, 2013). During the mining of tin, acid mine drainage (AMD) is developed due to the oxidation of iron sulphide which is also known as pyrite and other sulphide minerals in mine wastes in the presence of oxygen, water and oxidizing bacteria. The production of AMD has occurred in mines regardless of its state of activity, either active, or terminated.

Acid mine water possesses high metal concentrations of heavy metal ions and semi-heavy metals, for example, iron (Fe), copper (Cu), lead (Pb), zinc (Zn), cadmium (Cd), cobalt (Co), chromium (Cr), nickel (Ni), mercury (Hg), arsenic (As) and antimony (Sb), as well as anions, such as sulphate (SO_4^{2-}) ion (Othman, Sulaiman and Sulaiman, 2017). High concentration of heavy metals poses threats to both health and the environment, while high concentration of SO_4^{2-} ions develops toxicity (Tolonen, et al., 2014). The exposure of mineral rocks and water resources with AMD has rendered toxic

metals to leach into and pollute both resources, hence resulted in the resources being unsuitable for intended use. The release of AMD into surface waters or groundwaters has degraded water quality, injured aquatic life, and corroded or encrusted engineering structures over a significant area, including its neighbouring area due to interconnectivity of water bodies (Bigham and Cravotta, 2016; Kaur, et al., 2018).

Due to the different characteristics of each mine waters, a vast range of remediation techniques was established to treat mine water with effective methods for pH neutralization and removal of harmful ions and suspended solids in order to ensure good water quality for aquatic life and further usage of water (Heviánková, et al., 2013). Treatment methods for acid mine drainage can be categorized as either using chemical or biological mechanisms, active or passive systems. The application of alkalis for acid mine water treatment, a type of active AMD treatments, which is well documented, has included slaked lime ($Ca(OH)_2$), sodium hydroxide (NaOH) and limestone ($CaCO_3$). In a study performed by Heviánková, et al. (2013), it was mentioned that the use of calcium carbonate as the neutralising agent for AMD had been favoured due to its lower costs per weight. Their results showed the production of higher density sludge for easier drainage, better pH control as well as reduced occurrence of over-dosage, in comparison to that of conventional AMD treatment agent, calcium hydroxide or caustic soda. Other than AMD neutralization, calcium carbonate can also be used in cement production and as a fluxing agent in steel manufacturing.

On the other hand, precipitated calcium carbonate (PCC), a high-purify form of calcium carbonate can serve a wide range of industrial uses such as being a polymer composite, filler, additives, proving use in the pharmaceuticals and food industry as well as aiding in flue gas desulphurization (De Beer, et al., 2015). The particle of PCC differs than ground calcium carbonate (GCC) in terms of a higher uniformity in shape and narrower size distribution. PCC displays three types of crystalline polymorphs which are calcite, aragonite and vaterite. In a study performed by Jimoh, et al. (2018), it was concluded that PCC polymorphs merited wastewater treatment by membrane technology, whereby the introduction of aragonite PCC in polyethersulfone hollow fibre (PES HF)

membrane had resulted in more than 99 % efficiency in oil filtration. Moreover, Nakamura, Kasuga and Sakka (2017) found that vaterite with high silicon content of carbamate-functionalized siloxane effectively increased strontium precipitation in wastewater. Among the vast range of application, PCC may show yet another promising use in pH neutralization and heavy metal removal of AMD, which has not been studied previously.

1.2 Problem Statement

The composition and pH of AMD govern the intensity of environmental pollution (Kefeni, Msagati and Mamba, 2017). High concentration of heavy metals is characteristic to all AMD with its percolating capacity and presence of very active bacteria which render AMD self-perpetuating and a major concern for the environment (Bwapwa, Jaiyeola and Chetty, 2017). The richest constitute in AMD, Fe(II) can be oxidized to form iron oxide precipitates, which may sink and attach to bed of water bodies, and suffocate aquatic life at the bottom of water resources. The impact can be continued up the food chain and cause small aquatic life which feed on the bottom to die out in the worst case scenario (Kefeni, Msagati and Mamba, 2017). Ferric hydroxide precipitation can elevate the effect of AMD by causing pH reduction and damages to microorganisms. Several thousands of mg/L of SO_4^{2-} ion present in high concentrations in AMD can stimulate the production of hydrogen sulphide and hence, develop toxicity and the formation of thick anoxic sediment layers at the beds of river and lakes (Tolonen, et al., 2014).

For AMD treatment, the synthesis of PCC from calcium carbide sludge as a neutralizing agent serves to provide environmental benefits. Calcium carbide, the raw material in the production of acetylene gas, has yielded by-product calcium carbide sludge, which mainly consisted of calcium hydroxide. Acetylene gas represented a raw material, particularly for the production of polyvinyl chloride (PVC) in the chemical field, meanwhile calcium carbide sludge was usually disposed of in landfills, amounting to 21 500 tons and 1200 million tons per year in Thailand and China (Latif, et al., 2015).

Possessing high pH of greater than 12, and metal content of Mg, Fe, and such, calcium carbide sludge could result in groundwater contamination, one of the environmental pollutions. Thus, it was diverted from disposal and utilized in concrete production by mixing with various chemicals such as bagasse ash mixtures and fly ash to provide cementitious property and compressive strength respectively (Rattanashotinunt, et al., 2013).

Furthermore, an increased attention is garnered to the adoption of industrial by-products in other fields, such as conversion into commercial products, in order to reduce the occurrence of waste, decrease environmental concern and constraint on disposal, while increasing surplus to the economy (Tolonen, et al., 2014; De Beer, et al., 2015). The use of synthesized PCC in AMD treatment promotes the reuse of waste, by extracting beneficial constitutes present in calcium carbide sludge, rather than other neutralizing chemicals which are manufactured from scratch. According to Kanoje, Patel and Kuperkar (2017), the modification of PCC crystallization by polymer-surfactant templates for PCC synthesis enhanced the mechanical properties of PCC and enlarged their scope of applications. This could be extended to AMD treatment, where zero application was seen through findings and hence, PCC will be studied in this work in regards to its ability in environmental protection of AMD. Overall, the possibility of groundwater contamination may be restricted by the diversion of calcium carbide sludge into PCC synthesis, in which the resulting alkaline agent can be utilized in suppressing the detrimental effects of high acidity, concentration of dissolved metal ions and anions in AMD

1.3 Objectives

The specific objectives of this study are:

1. To synthesize PCC using calcium carbide sludge with the aid of various surfactant-polymer template.

2. To analyze the physical and chemical characteristics of synthesized PCC using various characterization techniques.
3. To evaluate AMD treatment process using PCC synthesized by different surfactant-polymer templates and different dosages of PCC.

1.4 Scope of Study

In this study, the synthesis of PCC will be carried out by the conversion of calcium carbide sludge using surfactant-polymer templates. The templates include polyvinyl alcohol (PVA), polyethylene glycol (PEG), and Pluronics® P-123 (P123) as the polymers and cetyltrimethylammonium bromide (CTAB) as the cationic surfactant. The synthesized PCC will be characterized by X-Ray Diffraction (XRD), Fourier Transform Infrared Spectroscopy (FTIR), Brunauer, Emmett and Teller (BET) surface area and particle size distribution (PSD) measurements to determine crystallinity structure, functional group, surface area and particle size, respectively. These characterization techniques were selected to analyze the variations due to different surfactant-polymer template on the resulting thermodynamic stability and adsorption capacity of PCC. Subsequently, the synthesized PCC will be tested on AMD for its ability to neutralize pH and remove metal ions and anions. The pH, oxidative-reductive potential (ORP) and conductivity readings of treated AMD will be measured using a portable water quality meter to evaluate the generation of net alkalinity, reducing power and dissolution rate of PCC. Various concentration of heavy metals such as Al, Cu, Fe, Mn, Ni, Zn and As will be determined by Inductively Coupled Plasma Optical Emission Spectrometry (ICP-OES) so as to assess the effect of PCC on selective precipitation of metal ions in AMD. On the other hand, SO_4^{2-} ions of AMD will be monitored by ion chromatography (IC) to analyse the precipitation capability of PCC on sulphide minerals.

CHAPTER 2

LITERATURE REVIEW

2.1 Acid Mine Drainage

Mining activities are known to deposit rocks on ground surface and underground voids in natural water bodies and have caused heavy metal components to leach out from the rock structure. Mine water discharge may be classified as acidic, neutral or alkaline. The difference in pH of mine waters is due to the differing sum of acidity and alkalinity, in which the former depends on the concentration of hydrogen ion (H^+) and that of all soluble metals combined, while the latter is contributed by the concentration of alkaline minerals, mainly in bicarbonate (HCO^-) form (Johnson and Hallberg, 2005; Moodley, et al., 2018). According to Pfitzner, et al. (2018), both neutral and alkaline mine waters have shown saline properties, while acid generating mine tailings have exhibited enhanced metal solubility. Owing to elevated dissolved metal concentrations in streams and unfavourable pH for aquatic life, acid mine drainage (AMD) deteriorated downstream water bodies and caused undesirable biological influence, hence there has been increasing focus on its properties and treatment.

Being a type of water and wastewater, AMD is highly acidic and exhibits an elevated concentration of salts and metal sulphates, in the form of dissolved ferrous and non-ferrous. These compounds have resulted from mining sites which consisted of polymetallic sulphide. AMD is produced regardless of the state of operation of the mines

(Simate and Ndlovu, 2014). Crushing of acid-generating rock induces exposure to oxygen and the surface environment, hence leading to acid generation which persists for years until sulphide material becomes limiting. AMD from active mine production is of lesser significance due to low water tables established by pumping. When the pumps are no longer in operation due to closing down or abandonment of the mines, water tables revert to their original depth, hence the AMD discharge would be drastic (Simate and Ndlovu, 2014).

Many researchers have mentioned different pH values were observed for AMD. It was found to be equal to 2 or below (Masindi, et al. 2017), below 5.5, (Othman, Sulaiman and Sulaiman, 2017), within the pH range of 2 to 6 (Bigham and Cravotta III, 2016) or around 3 (Heviánková, et al., 2013). The vast range of pH reported was due to different geologies in which the mine waters were obtained. Hydrochemical water mixtures of one geological structure may possibly show different results. Moreover, mine water differed in terms of type and chemistry from one mining company to another due to time, space and technology. For active mines, factors influencing the chemistry of mine water included pollution due to various process and refuse substances, products of weathering, as well as bacterial and biological decomposition, and others. The natural chemistry of mine water before mining activity may also re-develop after the termination of mining activities. The influence of a large number of factors thus imposes difficulty in the determination of typical mine water (Heviánková, et al., 2013).

Regardless of the above mentioned difficulty, it can be agreed that four major contributions shared by all AMD are acidity, salinization, metal toxicity and sediment toxicity (Tolonen, et al., 2014). The reactions which give rise to the properties of AMD are commonly shared as well. It begins with the widely available sulphide mineral, pyrite which is usually present in metals ores, mainly existing in the form of sulphide ores (Johnson and Hallberg, 2005). Eq. (2.1) represents the complicated process of pyrite oxidation which produces hydrogen (H^+), sulphate (SO_4^{2-}) and ferrous (Fe^{2+}) ions. (Kaur, et al., 2018; Simate and Ndlovu, 2014). According to Fernando, et al. (2018) and Simate and Ndlovu (2014), the oxidation of Fe^{2+} to ferric iron (Fe^{3+}) ion was stimulated under

adequately oxidizing condition and subjected to oxygen concentration, performance of bacteria as well as a pH higher than 3.5, as shown in Eq. (2.2). This reaction was followed by the formation of ochre ($Fe(OH)_3$) due to precipitation at pH values of 2.3 to 3.5 as presented in Eq.(2.3) or additional Fe^{2+} and acidity by reacting with pyrite as shown in Eq. (2.4).

A pH lower than 2 caused instability of $Fe(OH)_3$, hence the remaining Fe^{3+} would undergo reaction of Eq. (2.4) rather than Eq. (2.3). Eq. (2.5) expresses the oxidation of metal sulphides which forms metallic ions. A model for pyrite oxidation is shown in Figure 2.1. This phenomenon implied that the release of metal ions would pollute groundwater, which rendered it unsafe for drinking and agricultural uses. Meanwhile, low pH did not support fish and crustacean living in AMD-polluted water bodies.

$$2FeS_{2\,(s)} + 2H_2O_{\,(l)} + 7O_{2\,(g)} \rightarrow 2Fe^{2+}_{(aq)} + 4SO_4^{2-}{}_{(aq)} + 4H^+_{(aq)} \quad (2.1)$$

$$2Fe^{2+}_{(aq)} + 2H^+_{(aq)} + \frac{1}{2}O_{2\,(g)} \rightarrow 2Fe^{3+}_{(aq)} + H_2O_{\,(l)} \quad (2.2)$$

$$Fe^{3+}_{(aq)} + 3H_2O_{\,(l)} \rightarrow Fe(OH)_{3\,(s)} + 3H^+_{(aq)} \quad (2.3)$$

$$FeS_{2\,(s)} + 14Fe^{3+}_{(aq)} + 8H_2O_{\,(l)} \rightarrow 15Fe^{2+}_{(aq)} + 16H^+_{(aq)} + 2SO_4^{2-}{}_{(aq)} \quad (2.4)$$

$$MS_{\,(s)} + 2H_2O_{\,(l)} + O_{2\,(g)} \rightarrow M^{2+}_{(aq)} + SO_4^{2-}{}_{(aq)} + 4H^+_{(aq)} \quad (2.5)$$

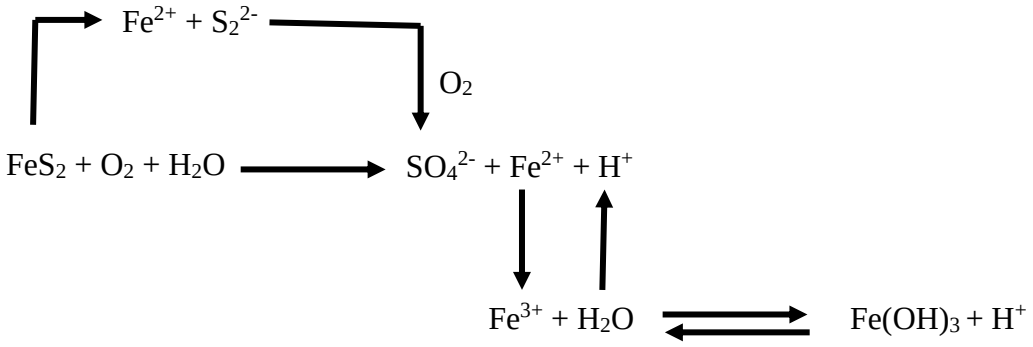

Figure 2.1: Model for Pyrite Oxidation (Simate and Ndlovu, 2014).

Overall, these reactions resulted in the generation of cations and anion. In particular, the reactions shown in Eqs. (2.2) and (2.4) were enhanced with the action of

acidophilic bacteria for example *Thiobacillus ferroxidans*, which elevated the rate of iron conversion. The high acidity and dissolved metal ions content renders AMD hazardous, impacts ecosystems and infrastructure, and may limit water supply if AMD leaches into the source. Heavy metal ions have exhibited long-lasting persistence in the environment, and their accumulation up the food chain would cause disruption in the performance of important organs and glands of higher-level consumers and may hinder absorption of nutrients. Plants and aquatic life were prone to oxidative stress due to heavy metal ion exposure which may result in damage or ionic homeostasis to plants cell. Aquatic life may face mortality due to acute or chronic exposure, in which the latter may cause non-lethal outcomes for example stunted growth, lower reproduction, impairment or injuries. On the other hand, pH indirectly resulted in the formation of ochre, which has been found to be bright orange in colour. Ochre settled and bound with substances on the bed of water bodies, including the nutrients of benthic organisms, which belong at the base of the food chain. Similar to the effect of heavy metal ions, organisms up the biological chain were then affected due to the depletion of resource at the bottom. The introduction of AMD in water bodies altered the physiological performance of aquatic life as it has been governed by ambient water pH, and may lead to sub-lethal or lethal possibilities (Simate and Ndlovu, 2014; Heviánková, et al., 2013).

Actions must be taken in order to control the discharge of AMD in water resources and avoid multiple consequences of AMD. Feris and Kotze (2017) stated that there has been mining regulation implemented in South Africa which covered pollution prevention, reduction, remediation and liability provisions in addressing water and AMD problems. Tolonen, et al. (2014) mentioned that emission limit of SO_4^{2-} ions in Finland was established specifically for mine discharge water. According to US EPA (2017), the maximum contaminant level (MCL) of SO_4^{2-} ions in drinking water was 250 mg/L. In Malaysia, law enforcement has been made on mining under Mineral Development Act 1994, whereby it was stated at Part I, 18, that "as to ensure that water so used shall, before it leaves the mine or waste retention area in which it has been used, comply with such water quality standards as may be prescribed". In addition, the Malaysia government has established both Environmental Quality Act (1974) (EQA 1974) and Mineral

Development Act (1994) to control mining activities in terms of mine termination and contamination discharge (Wan Zuhairi, Syuhadah, and Hazwani, 2009). This research study did not utilized AMD obtained from natural sources that would be subjected to water quality standards. Instead, the AMD for this study represented an effluent from the mining industry and has been classified as an industrial discharge. Hence the regulations in EQA 1974 would be used to regulate each listed chemical prior to being discharged according to standard A and B as shown in Table 2.1.

Table 2.1: Acceptable Conditions for Discharge of Industrial Effluent or Mixed Effluent of Standards A and B (Department of Environment, 2010).

Fifth Schedule
[Paragraph 11(1) (a)]

Parameter	Unit	Standard	
		A	**B**
Temperature	^{0}C	40	40
pH value	-	6.0 – 9.0	5.5 – 9.0
BOD_5	mg/L	20	40
Suspended Solids	mg/L	50	100
Mercury	mg/L	0.005	0.05
Cadmium	mg/L	0.01	0.02
Chromium, Hexavalent	mg/L	0.05	0.05
Chromium, Trivalent	mg/L	0.20	1.0
Arsenic	mg/L	0.05	0.10
Cyanide	mg/L	0.05	0.10
Lead	mg/L	0.10	0.5
Copper	mg/L	0.20	1.0
Manganese	mg/L	0.20	1.0
Nickel	mg/L	0.20	1.0
Tin	mg/L	0.20	1.0
Zinc	mg/L	2.0	2.0
Boron	mg/L	1.0	4.0
Iron (Fe)	mg/L	1.0	5.0
Silver	mg/L	0.1	1.0
Aluminium	mg/L	10	15
Selenium	mg/L	0.02	0.5
Barium	mg/L	1.0	2.0
Fluoride	mg/L	2.0	5.0
Formaldehyde	mg/L	1.0	2.0
Phenol	mg/L	0.001	1.0
Free Chlorine	mg/L	1.0	2.0
Sulphide	mg/L	0.50	0.50
Oil and Grease	mg/L	1.0	10
Ammoniacal Nitrogen	mg/L	10	20
Colour	ADMI*	100	200

Notes:
*: American Dye Manufactures Institute

2.2 Methods for AMD Treatment

It was mentioned by Heviánková, et al. (2013) that vast difference of each mine water characteristics resulted in the introduction of a large number of AMD treatments, to effectively raise pH and capture potentially toxic ions and solids for disposal. The outcome of an effective treatment should produce suitable water quality for aquatic life and extended application of water in other fields. As discussed earlier, AMD remediation technologies have been divided into abiotic or biological mechanisms, which are both further separated as active or passive systems depending on chemical addition, infrastructure, maintenance and monitoring requirements. Othman, Sulaiman and Sulaiman (2017) reported that the former requires continuous input, while the latter requires only a small amount during operation. Abiotic and biological processes differ in terms of biological activities which are not incorporated in the former but are included in the latter. Figure 2.2 presents the division and classification, while Table 2.2 summarizes the function, advantages and disadvantages of typical AMD treatments.

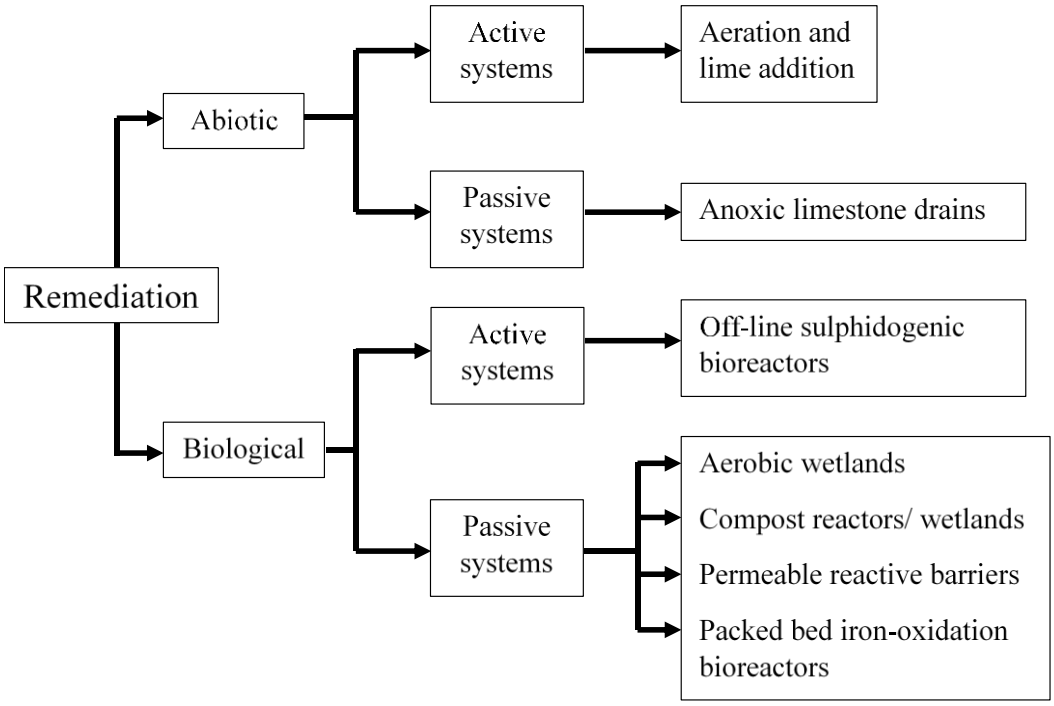

Figure 2.2: Classification of AMD Remediation Technologies (Simate and Ndlovu, 2014; Johnson and Hallberg, 2005).

Table 2.2: Summary of Various AMD Treatment Remediation.

Treatment processes	Function	Advantages	Limitations	References
Abiotic treatments (Active)				
Addition of alkaline industrial chemicals	• Chemical-neutralizing agent resulted in pH increase, accelerated rate of oxidation of Fe^{2+} ion. • Precipitation of dissolved metal ions as (oxy)hydroxides, sulphides and carbonates. • Removal of SO_4^{2-} ion as gypsum.	• Easily applied for any AMD treatment forms. • Removed certain amount of SO_4^{2-} ions if calcium based agent was used.	• High operation costs. • Not effective in SO_4^{2-} removal. • Produced large volume of sludge. • Sensitivity of metals in sludge to pH change.	Johnson and Hallberg (2005), Bwapwa, Jaiyeola and Chetty, (2017), Moodley, et al. (2018)
Addition of alkaline industrial by-products	• Diverted by-products of industries for AMD neutralization. • Common by-products used included cement and lime kiln dust, red mud bauxite, coal fly ash and blast furnace slag.	• Cost-effective. • Reduced waste volume and cost of waste disposal. • Sustainable and environmental friendly. • Comparable effectiveness to and considerable replacement for industrial chemicals.	• Pre-treatment of by-products may be required prior to use. • Required further processing and extraction of recovered metals.	Kefeni, Msagati and Mamba (2017)
Alkaline barium calcium (ABC) desalination process	• Consisted of three major steps: neutralization for metal removal, SO_4^{2-} ions removal and sludge processing.	• High removal of SO_4^{2-} ions. • Recovery and recycling of barium carbonate ($BaCO_3$) for treatment. • Low production of sludge. • Possible recovery of drinking water.	• Required suitable kiln for the conversion of $BaSO_4/CaCO_3$ sludge to barium sulphide (BaS).	Mulopo (2015), Kefeni, Msagati and Mamba (2017)

Table 2.2: Summary of Various AMD Treatment Remediation (continued).

Treatment processes	Function	Advantages	Limitations	References
(Passive)				
Anoxic limestone drain	• An impervious limestone drain which allowed passage of AMD in the absence of air. • Elevated partial pressure of carbon dioxide increased the dissolution rate of limestone and released alkali for neutralization.	• High alkalinity was produced compared to open system. • Lower cost of alkaline production. • Required little maintenance. • Small land space.	• Not suitable for all AMD. • Reduction in permeability due to clogging. • Difficulty in maintenance of anoxic condition. • Dissolution of limestone. • Time-consuming. • Low SO_4^{2-} ion removal.	Johnson and Hallberg (2005), Kefeni, Msagati and Mamba (2017), Moodley, et al. (2018)
Membrane distillation	• Utilized membrane to reject the permittivity of certain substances, retaining them from the effluent.	• Rejected dissolved non-volatile compounds. • Low energy consumption. • Reduced treatment discharge. • Lower water requirement for treatment.	• Expensive membranes. • High membrane fouling. • Efficiency might be lowered.	Simate and Ndlovu (2014), Kefeni, Msagati, and Mamba (2017)
Biological treatments (Active)				
Sulphidogenic bioreactors	• Produced hydrogen sulphide which increased alkalinity and converted metal ions into insoluble sulphides.	• Predictable and controllable performance. • Recovery of heavy metal ions for future usage. • Reduced SO_4^{2-} ion greatly. • Low cost. • Easy installation.	• Uncertain long term performance.	Johnson and Hallberg (2005), Moodley, et al. (2018)

Table 2.2: Summary of Various AMD Treatment Remediation (continued).

Treatment processes	Function	Advantages	Limitations	References
(Passive)				
Aerobic wetlands	• Focused on Fe^{2+} oxidation and Fe^{3+} hydrolysis, ion exchange and adsorption. • Usually applied for net alkaline mine waters due to net acid generating reactions.	• Accumulated ochre stabilized by macrophytes. • Removed As. • Low investment and operating cost. • No additional energy input.	• Required additional treatment for mine water of insufficient net alkalinity. • Long duration. • Large area of land. • Oxygenated for oxidation.	Sheoran and Sheoran (2006), Fernando, et al. (2018)
Anaerobic wetlands/ compost bioreactors	• Anaerobic microbially driven process resulted in net alkalinity and biogenic sulphide. Electron donors were obtained from compost for reductive reactions.	• Filtered suspended and colloidal substances. • Adsorbed metal ions onto structure of compost. • Stable metal precipitates. • Low cost material and waste.	• Required anaerobic condition. • Introduction of oxygen harmed the process. • Large area of land. • Long duration.	Johnson and Hallberg (2005), Fernando, et al. (2018)
Composite aerobic and anaerobic "wetlands"	• Consisted of oxidation, holding and Acid Reduction Using Microbiology (ARUM) cells. • Produced alkali and sulphide using floating macrophytes.	• Effective in high latitude and subtropical areas. • Oxidation and precipitation of Fe^{2+} ions. • Produced SO_4^{2-} ion reducing organic matter.	• Required high AMD volume and complete coverage of floating vegetation for higher efficiency. • Effectiveness changed with seasons.	Johnson and Hallberg (2005), Kalin and Caetano (2003)
Permeable reactive barriers	• A trench or pit was made to interrupt the flow of AMD contaminated groundwater and filled with permeable organics and limestone.	• Effluent groundwater could be treated. • No land space needed. • No waste disposal. • Low cost.	• Multiple substrates needed to increase effectiveness. • Required characterizing of mine site. • Unpredictable performance.	Moodley, et al. (2017), Kefeni, Msagati and Mamba (2017)
Iron-oxidizing bioreactors	• Incorporated iron-oxidizing prokaryotes into reactors.	• Increased oxidation of Fe^{2+} to Fe^{3+} ions.	• No recovery of heavy metals. • Unpredictable performance.	Johnson and Hallberg (2005)

Firstly, active abiotic treatment consisted of methods such as adding alkaline for metal precipitation, adsorption, ion exchange, membrane technology as well as alkaline barium calcium (ABC) desalination process (Kefeni, Msagati and Mamba, 2017). The widely adopted method in AMD remediation has been the addition of alkaline neutralizing agent which includes limestone, quicklime, hydrated lime, dolomite, kiln dust, sodium bicarbonate, ammonia, potassium hydroxide, barium carbonate, barium hydroxide, magnesite to calcium peroxide (Moodley, et al., 2018). Factors such as concentration, individual identity and complex interaction between dissolved species in water governed the rate and extend of metal precipitation (Kaur, et al., 2018). The most commonly used and widely available alkaline agent for AMD has been industrial chemical lime (Kaur, et al., 2018). Table 2.3 shows the efficiency of removal of heavy metal ions and anions as well as pH neutralization of different neutralizing agents performed by various researchers.

In contrast, passive abiotic treatment consisted of membrane distillation. As an example, Aguiar, et al. (2016) studied on the evaluation of RO (reverse osmosis) and NF (nanofiltration) membranes on AMD of a gold mining company in Minas Gerais, Brazil. It was found that NF270 (NF of low salt retention) membrane at pH 5.5 resulted in 93.1 % calcium and 94.9 % magnesium retentions with highest permeate flux at water recovery rate (RR) of 40 %. Anoxic limestone drain (ALD) represented another treatment in this category, which is presented in Figure 2.3. Modification of ALD by using phosphatic waste-rock instead of limestone showed pH neutralization and reduction of 80 % Fe^{2+} ions, 98.9 % Al^{3+} ions and 99.9 % Cu^{2+} ions (Ouakibi, Hakkou and Benzaazoua, 2014).

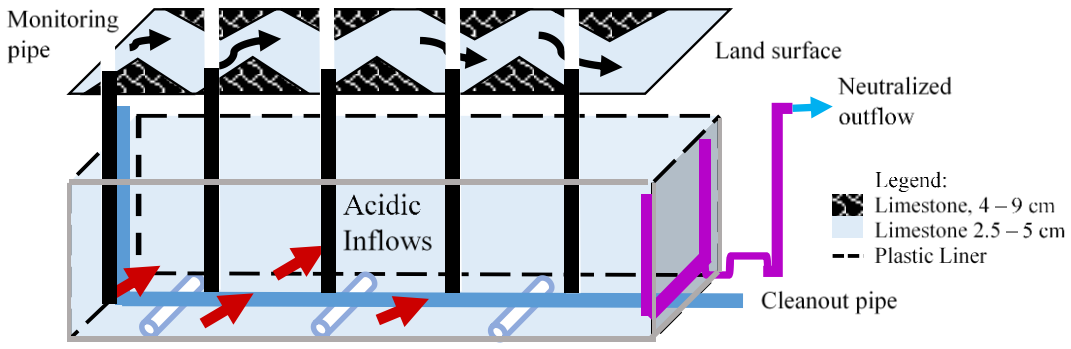

Figure 2.3: Schematic Illustration of Anoxic Limestone Drains (Kefeni, Msagati and Mamba, 2017).

Table 2.3: Various Neutralizing Agents Used in AMD Treatment.

Neutralizing Agent	Amount	Optimum Amount	Volume of AMD (mL)	Contact Time (h)	Initial pH	Final pH	Removal Efficiency	References
Lime[1]	1.6 – 3.3 mmol	3.3 mmol	25	24	3.74	9.19	• Al (99.9 %), Mn (99.7 %), Cu (99.9 %), Zn (99.9 %), Fe (99.7 %) and Ni (96.8 %).	Kaur, et al. (2018)
Sodium hydroxide	3.12 – 7.1 mmol	7.1 mmol	25	24	3.74	9.46	• Al (99.7 %), Mn (99.9 %), Cu (96.64 %), Zn (99.9 %), Fe (99.7 %) and Ni (96.8 %).	Kaur, et al. (2018)
Sodium carbonate	1.7 – 4.9 mmol	4.9 mmol	25	24	3.74	9.15	• Al (99.8 %), Mn (95.8 %), Cu (95.8 %), Zn (99.9 %), Fe (99.7 %) and Ni (96.8 %).	Kaur, et al. (2018)
Bayer liquor	2.5 – 5.0 mL	5.0 mL	25	24	3.74	8.95	• Al (99.6 %), Mn (97.6 %), Cu (99.3 %), Zn (99.9 %), Fe (99.7 %) and Ni (96.8 %).	Kaur, et al. (2018)
Bayer precipitate	0.5025 – 1.500 g	1.500 g	25	24	3.74	8.00	• Al (99.9 %), Mn (82.82 %), Cu (99.9 %), Zn (99.9 %), Fe (99.7 %) and Ni (96.8 %).	Kaur, et al. (2018)
Calcium lime waste	0.5 – 2.5 g	1.5 g	1000	1 h 10 min	~2.75	~8	• Al (>90 %), Cu (>90 %), Fe (~99.9 %), Mn (~40 %), Ni (~90 %), Zn (~90 %) and As (~98 %).	Othman, Sulaiman and Sulaiman (2017)
Caustic soda	0 – 20 g	10 g	1000	1	<2	12.5 – 13.5	• Fe (99.8 %), Mg (85.3 %), Mn (99.9 %), K (99.9 %), Na (0 %), Al (66.1 %), SO_4^{2-} (2.9 %), TSP (21.6 %) and Hardness (85.2 %).	Masindi, et al. (2017)
Soda ash	0 – 20 g	10 g	1000	1	<2	7	• Fe (97.6 %), Mg (0 %), Mn (33.3 %), K (0 %), Na (0 %), Al (99.9 %), SO_4^{2-} (0.4 %), TSP (0 %) and Hardness (12.3 %).	Masindi, et al. (2017)
Periclase	0 – 20 g	10g	1000	1	<2	9.5 – 10.5	• Fe (99.9 %), Mg (0 %), Mn (99.9 %), K (0 %), Na (0 %), Al (99.9 %), SO_4^{2-} (6.3 %), TSP (0 %) and Hardness (0 %).	Masindi, et al. (2017)

Table 2.3: Various Neutralizing Agents Used in AMD Treatment (continued).

Neutralizing Agent	Amount	Optimum Amount	Volume of AMD (mL)	Contact Time (h)	Initial pH	Final pH	Removal Efficiency	References
Brucite	0 – 20 g	10g	1000	1	<2	5.5 – 6.5	• Fe (74.6 %), Mg (0 %), Mn (0 %), K (0 %), Na (0 %), Al (99.9 %), SO_4^{2-} (11.3 %), TSP (0 %) and Hardness (0 %).	Masindi, et al. (2017)
Magnesite	0 – 20 g	10g	1000	1	<2	9	• Fe (99.9 %), Mg (0 %), Mn (99.9 %), K (0 %), Na (0 %), Al (99.9 %), SO_4^{2-} (12.5 %), TSP (0 %) and Hardness (0 %).	Masindi, et al. (2017)
Lime[2]	0 – 20 g	10g	1000	1	<2	6	• Fe (99.9 %), Mg (0 %), Mn (26.7 %), K (0 %), Na (0 %), Al (99.9 %), SO_4^{2-} (95.4 %), TSP (5.1 %) and Hardness (0 %).	Masindi, et al. (2017)
Hydrated lime	0 – 20 g	10g	1000	1	<2	11	• Fe (99.9 %), Mg (85.3 %), Mn (99.9 %), K (0 %), Na (0 %), Al (~98.2 %), SO_4^{2-} (96.2 %), TSP (15.8 %) and Hardness (11.6 %).	Masindi, et al. (2017)
Limestone	0 – 20 g	10g	1000	1	<2	6	• Fe (99.9 %), Mg (0 %), Mn (13.3 %), K (0 %), Na (0 %), Al (~99.9 %), SO_4^{2-} (88.8 %), TSP (5.5 %) and Hardness (0 %).	Masindi, et al. (2017)
Stainless steel (SS) slag	20 – 140 g	100 g	1000	4	2.5	6.0	• Fe (63.63 %) and SO_4^{2-} (40 %).	Name and Sheridan (2014)
Basic oxygen furnace (BOF) slag	20 – 140 g	100 g	1000	4	2.5	12.1	• Fe (99.7 %) and SO_4^{2-} (75 %).	Name and Sheridan (2014)
Eggshell powder (53 – 160 μm)	0.075 – 1.25 g	0.5 g	25	4	2.43	6.58	• Fe (99.9 %), Al (99.9 %), SO_4^{2-} (62.5 %); Mn (51.0 %), K (32.5 %), PO_4^{3-} (20.0 %) and NO_3^- (25.6 %).	Muliwa, Leswifi and Onyango (2018)

Note: [1] = Lime as a neutralizing agent by Kaur, et al. (2014); and
[2] = Lime as a neutralizing agent by Masindi, et al. (2017).

On the contrary, biological remediation technologies mainly involved the capture of metal ions by microorganisms as well as the generation of net alkalinity. Net alkalinity has been produced by the conversion of base and reductive microbiological processes such as denitrification, methanogenesis, reduction of SO_4^{2-}, Fe and manganese (Mn) (Johnson, and Hallberg, 2005). As seen from Figure 2.2, the main representative for active biological treatment was sulphidogenic bioreactors. Kennecott Bingham Canyon copper mine in Utah implemented this treatment and recovered >99 % copper from AMD solution of pH 2.6 (Johnson, and Hallberg, 2005).

Most of the biological remediation technologies have been classified as passive, and these have exhibited low maintenance cost and retention of solid products within the sediments for wetlands. Passive treatment systems included aerobic, anaerobic or compost wetlands, bioreactors and permeable reactive barriers (PRB). Kefeni, Msagati and Mamba (2017) stated that abandoned mines were more suitable to be treated by passive systems. In aerobic wetlands and bioreactors, microorganisms aided in the conversion of Fe^{2+} to Fe^{3+} ions. Another similar technology to compost bioreactor is known as reducing and alkalinity producing system (RAPS) which is shown in Figure 2.4. In Aznalcóllar of Spain, it was reported that the installed PRB which consisted of vegetal compost, sewage sludge, limestone and iron, successfully removed 50 – 98 % of metal ions and 0 – 43 % of SO_4^{2-} ions in the AMD with a rise of pH from 4 to 5 (Kefeni, Msagati and Mamba, 2017).

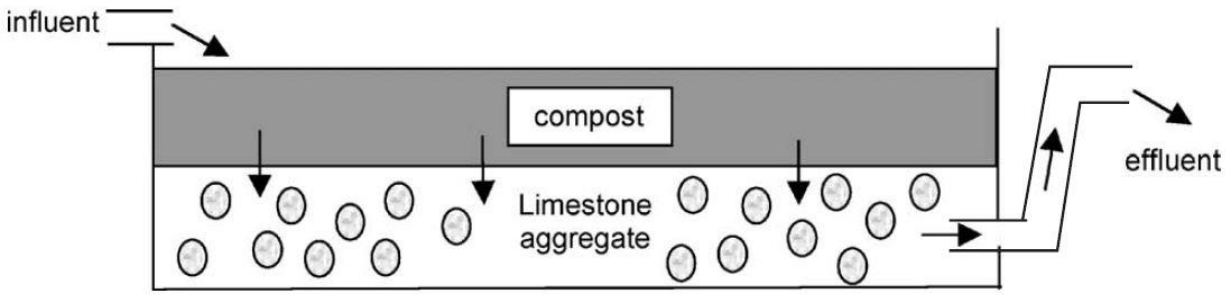

Figure 2.4: Reducing and Alkalinity System with Compost and Limestone Gravel Bed (Johnson and Hallberg, 2005).

Each of the technologies presents their own specialized benefits and limitations as well. For active system, high operating cost and sludge production need to be considered together with constant monitoring and maintenance. Passive treatment has often been emphasized on the requirement of a relatively bigger area of land, costly installation and was prone to the risk of system failure due to faulty designs, season change, and metal hydroxides accumulation. Active biological systems were prone to clogging and performance issues caused by metal precipitation (Bwapwa, Jaiyeola and Chetty, 2017). Meanwhile, passive biotic systems faced unstabilized fate of accumulated depositions (Johnson and Hallberg, 2005). Abiotic AMD treatment with basic mechanisms such as precipitation, adsorption and filtration resulted in small removal capacity and exhibited low selectivity, inability to handle organic substances and large production of waste (Bwapwa, Jaiyeola and Chetty, 2017). Both active and passive abiotic systems have consumed expensive neutralizing agents and caused depletion in natural resources (Moodley, et al., 2018).

2.3 Precipitated Calcium Carbonate as a Neutralizing Agent

Particulate calcium carbonate ($CaCO_3$) is divided into two classes, which are ground calcium carbonate (GCC) and precipitated calcium carbonate (PCC). The former is obtained from calcite deposit mining, on the other hand, the latter is formed by chemical reaction. The purer, refined or synthesized type of $CaCO_3$, PCC appears extremely white in colour and displays a uniform and narrow range of particle size with a smaller maximum size compared to GCC. For example, the difference in the performance of GCC and PCC can be observed in Light Weight Coating (LWC) Papers of the paper industry. The findings showed that PCC (light green line) displayed a higher performance in most of the fields as compared to GCC (medium green line), as shown in Figure 2.5. With a vast range of application, according to Business Wire (2017), PCC was forecasted to reach a target of 24 844.2 thousand metric tons by 2021, with a 6 % growth from 2017.

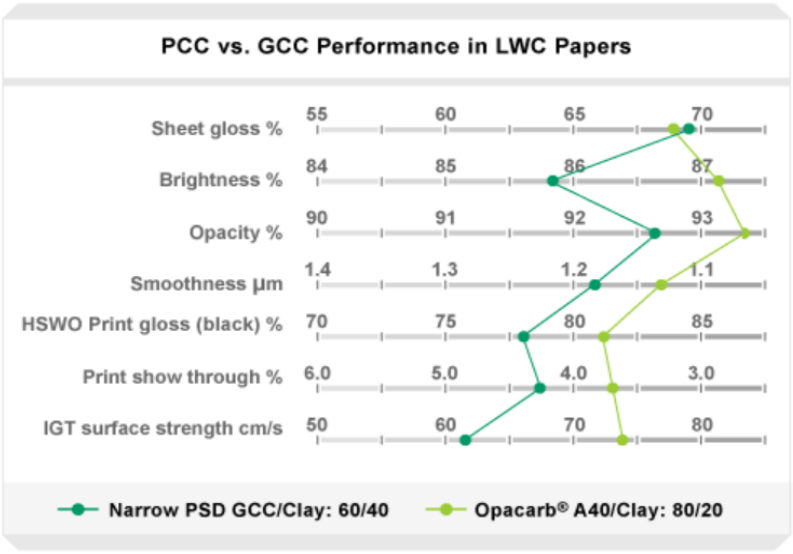

Figure 2.5: Difference Between the Performance of PCC and GCC in Light Weight Coating (LWC) (Minerals Technologies Inc., 2018).

Typically, three traditional approaches in PCC production comprised of carbonation, lime-soda and calcium chloride ($CaCl_2$)-sodium carbonate (Na_2CO_3) double salt decomposition processes. The former required bubbling of carbon dioxide (CO_2) gas into a calcium hydroxide ($Ca(OH)_2$) slurry as shown in Eq. (2.6). Meanwhile, the second approach was based on Eq. (2.7) whereby both sodium hydroxide (NaOH) and PCC were synthesized from the reaction of lime milk (aqueous $Ca(OH)_2$ slurry) with Na_2CO_3. Lastly, the third method generated sodium chloride and PCC through the reaction of calcium chloride with soda ash as shown in Eq. (2.8) (Said, et al., 2013; Kezuka, et al., 2018). Reaction in Eq. (2.6) also highlighted on the usage of CO_2 gas to be captured and incorporated into PCC (Said, et al., 2013). In contrast, the second and third methods were aqueous-based reactions using solutions to react and form $CaCO_3$ precipitates.

$$Ca(OH)_{2\,(aq)} + CO_{2\,(g)} \rightarrow CaCO_{3\,(s)} \quad (2.6)$$

$$Ca(OH)_{2\,(aq)} + Na_2CO_{3\,(aq)} \rightarrow 2NaOH_{(aq)} + CaCO_{3\,(s)} \quad (2.7)$$

$$CaCl_{2\,(aq)} + Na_2CO_{3\,(aq)} \rightarrow 2NaCl_{\,(aq)} + CaCO_{3\,(s)} \quad (2.8)$$

Other than the traditional approaches, literatures were found to provide alternative synthesis methods for PCC. These included the use of industrial by-products as alternative raw materials instead of conventional chemicals. Said, et al. (2013) utilized steel converter slag to produce PCC with the help of CO_2 fixation in a carbonation reactor. The study demonstrated Ca extraction from slag using the various extraction agents prior to the carbonation of salt and carbon dioxide gas. Meanwhile, De Crom et al. (2015) synthesized PCC from blast furnace (BF) slag via an indirect carbonation of calcium. These two studies could be classified as mineral carbonation whereby material with Ca content reacted with CO_2 to produce $CaCO_3$. These methods could potentially reduce CO_2 emission from iron and steel industries and divert significant amount of slags from the disposal areas.

In a study performed by De Beer, et al. (2015), they conducted PCC synthesis via direct aqueous calcium sulphide (CaS) carbonation using gypsum waste which resulted from limestone- or lime-incorporating AMD treatment system. This remediation method of gypsum waste could reduce airborne dust generation, possible surface and underground water contamination due to leakage, and high cost of maintenance of gypsum stacks at disposal sites. In contrast to carbonation processes, Zhan and Guo (2015) synthesized PCC in aqueous solution without introduction of CO_2 gas. The procedures consisted of leaching sintering dust of a steel industry with water and adding sodium carbonate (Na_2CO_3) precipitant to form PCC. All of these alternatives focused on technologies for transformation of industrial waste materials into commercial products which has aided in mitigating environmental burden and improving economic benefit by reusing the industrial by-products (De Beer, et al., 2015).

Due to the highly standardized particle size of PCC and crystalline forms, PCC has shown high demand from various types of industries. Mainly consumed by the paper industry, PCC has functioned to provide pigment coating, brightening, surface finishing, gloss enhancer and paper bonding as well as being a filler. The fine particle size contributed to an easy and controlled application. In the paints industry, PCC served as an extender agent to promote porosity and opacity, and as a finishing in paints and coatings

(Business Wire, 2017). The National Lime Association (2018) stated that in polymer applications, PCC has acted as a replacement for costly impact modifiers in rigid polyvinyl chloride (PVC), while nano-sized PCC helped to moderate automotive and construction sealants. Due to the acid neutralizing ability as well as high calcium content, PCC has been added to antacid tablets and liquids as well as supplements in the healthcare industry.

The polymorphs of PCC are classified into three different forms which are calcite, aragonite and vaterite (Gopi, Subramanian and Palanisamy, 2013; Kanoje, Patel and Kuperkar, 2017). Whereas, the morphologies of PCC range from chains, cubes, spheres, spindles, sheets, needles to amorphous. The various polymorphic forms of PCC render each form to be more suitable for different applications. Li, Li and Ma (2013) mentioned that the addition of cubic $CaCO_3$ in paints had helped to improve dispersion, while reinforcing effect was shown by acicular or rod-like $CaCO_3$ on rubber and plastics, and brightness and opacity of ink were influenced by spherical $CaCO_3$.

In another study performed by Nakamura, Kasuga and Sakka (2017), the usage of vaterite containing carbamate-functionalized siloxane with larger silicon content helped to increase the precipitation of strontium for wastewater treatment. Dang, et al. (2017) concluded that the usage of porous vaterite/chitosan oligosaccharide (COS) microspheres was shown to have a high and rapid maximum adsorption of 2066 mg/g for Pb^{2+} ions and 522 mg/g for Cd^{2+} ions. On the other hand, incorporation of aragonite into polyethersulfone hollow fibre (PES HF) membrane contributed to an efficiency of more than 99 % in oil filtration (Jimoh, et al., 2018). Hence, controlling the formation of PCC is an important factor to render it useful for its intended application.

2.3.1 Characterization of Precipitated Calcium Carbonate

Each of the PCC crystalline polymorphs exhibits its own distinguishable properties. The first property to be discussed is the thermodynamic stability in which calcite possesses the

highest followed by aragonite with moderate stability (metastable) and finally vaterite, the most unstable form. Secondly, the crystal system for calcite is rhombohedral, orthorhombic for aragonite, and hexagonal for vaterite (Matsumoto, Fukunaga and Onoe, 2010). Representing a part of PCC morphology, X-Ray Diffraction (XRD) can be employed for analysing the crystal phase and structure, whose function would be further discussed.

The phase composition and structure of PCC can be determined using XRD. Figure 2.6 demonstrates patterns of XRD result analysis for calcite, aragonite and vaterite. It was mentioned by Mori, Enomae and Isogai (2009) that calcite displayed high diffraction peak at 29.4^0, while the peaks for vaterite occurred at 24.8^0, 27.1^0 as well as 32.8^0. Aragonite was found to peak at around 26.0^0 as shown in Figure 2.7. The most diffraction peaks were observed for aragonite, followed by vaterite and calcite.

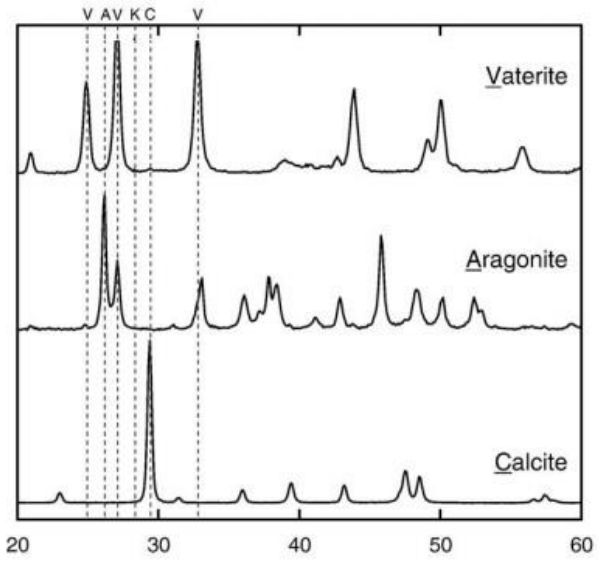

Figure 2.6: Various XRD Patterns of PCC Crystalline Structures (Mori, Enomae and Isogai, 2009).

Different functional groups react differently to influx of infrared light by absorbing only specific wavelength. At that characteristic wavelength, molecules of the functional group are excited, which drastically elevates their vibrational energy level without

influencing the rest of the structure, and this forms the basis for Fourier Transform Infrared Spectrometer (FTIR) analysis. Using this method, the polymorphs of PCC can be differentiated by their spectral transmittance peaks. Figure 2.7 shows the characteristic absorption bands for aragonite, vaterite, calcite, monohydrocalcite and ACC, whereby only the first three forms are focused on and will be further discussed.

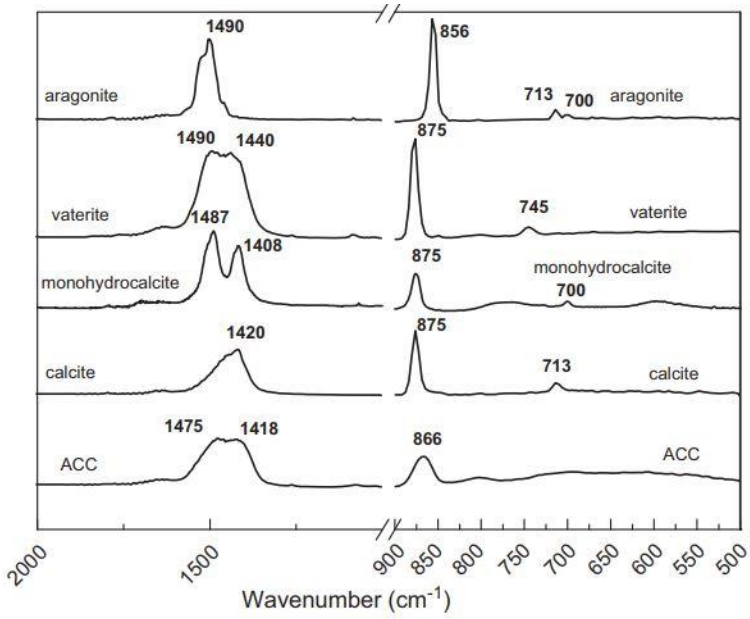

Figure 2.7: FTIR Spectra of Pure $CaCO_3$ Phase (Zhang, et al., 2012).

From the figure itself, three significant peaks for all three polymorphs can be observed. They have been classified as in-plane bending (v_4) mode, carbonate out-of-plane bending (v_2) mode, and asymmetric stretching (v_3) mode, with increasing wavelength peak (right to left). The characteristic transmittance peaks for calcite were observed as vibrational bands at around 713 cm^{-1} (v_4), 875 cm^{-1} (v_2) and a peak at 1420 cm^{-1} (v_3) (Zhang, et al., 2012) or about 1400 cm^{-1} (De Beer, et al., 2015). For aragonite, characteristic absorption bands were found to be at 700 cm^{-1} with a weak peaking, 713 cm^{-1} (v_4), 856 cm^{-1} (v_2) as well as a split peak at around 1490 cm^{-1} (v_3). Meanwhile, vibrational bands for vaterite were observed at 745 cm^{-1} (v_4), 875 cm^{-1} (v_2), with two peaks splitting at 1440 cm^{-1} and 1490 cm^{-1} (v_3). Another characteristic peak has been found to be symmetric carbonate stretching vibration (v_1), which occurred at 1090 cm^{-1} for vaterite,

whereas for calcite and aragonite, the peaks were found within the range of 1085 – 1087 cm^{-1} (Gopi, Subramanian and Palanisamy, 2013).

Another $CaCO_3$ characterization of utmost significance is represented by specific surface area which has largely impacted the properties of $CaCO_3$. It can be measured using Brunaeur, Emmett and Teller (BET) analysis via nitrogen gas (N_2) adsorption-desorption isotherms. Its importance was highlighted by Bang, et al. (2012), whereby among the vast application of $CaCO_3$, the usefulness of $CaCO_3$ in a specific field was governed by characteristics of $CaCO_3$ which comprised of morphology, polymorphs, specific surface area and particle size. In the field of chemisorption, specific surface area and reaction site represented significant surface properties of PCC which could influence its adsorption strength on other particles. Aragonite displayed higher adsorption capacity for phosphate than calcite which amounted to 10.5 µmol/g for aragonite and 3.5 µmol/g for calcite for one-day equilibrium (Millero, et al., 2001). Due to differing surface properties, $CaCO_3$ crystal structures exhibited varying adsorption performance.

Moreover, $CaCO_3$ can be characterized by particle size of its primary particles. Bang, et al. (2012) deduced an inverse proportion relation between specific surface area and particle size of primary particles whereby secondary particles could be formed via agglomeration. Considering specific surface area and particle size, both were affected by several factors which comprised of operating parameters such as pH, temperature and additive concentration. These parameters were observed to influence vaterite content of $CaCO_3$ as well (Polat, 2019). Individually, specific surface area was significantly influenced by individual effects of additive concentration, temperature and pH as well as the coupled impact of additive concentration and temperature. A reduction in particle size was exhibited in association with reduction in pH and temperature as well as a rise in additive concentration (Polat, 2019).

Apart from additive concentration, temperature and pH, other interrelated operating factors have been governing the crystallization process of $CaCO_3$ which encompassed type of additives, rate of reactants, content of solution, supersaturation,

mixing and hydrodynamic conditions (Matsumoto, Fukunaga and Onoe, 2010; Konopacka-Łyskawa, Kościelska and Karczewski, 2017). These factors on crystallization process led to variations in the characteristics of $CaCO_3$, not only amounting to specific surface area and particle size. For example, additives were found to pose an influence on the speed and steps of crystallization and resulted in alteration in nuclei formation, size distribution and morphology. A number of researches has been performed on $CaCO_3$ polymorphism. According to Konopacka-Łyskawa, Kościelska and Karczewski, (2017), the type of solvent governed the synthesis of $CaCO_3$ by forming more unstable polymorph in aqueous solutions which contained reacting ions and preventing the formation of metastable form in organic solvents. Hence, these factors characterized the resulting structure of the synthesized PCC.

For commercial $CaCO_3$, the BET specific surface area was determined to be around 2 m^2/g to 3 m^2/g and classified as non-porous (Galera Martínez, et al., 2019; Bang, et al., 2012). With the aid of microbubble generator, the specific surface area of calcite could increase to 30 m^2/g (Bang, et al., 2012). On the other hand, the formation of microcapsule of $CaCO_3$ was identified with specific surface area of 2.28 m^2/g to 18.43 m^2/g and classified as mesoporous with peak pore sizes of 50 nm to 60 nm (Fujuwara, et al., 2008). López-Periago, et al. (2010) stated that calcite could be obtained by using solutions of reduced concentration of CO_3^{2-} and Ca^{2+} ions which exhibited rhombohedral (approximately cubic) structure. The product of homogeneous solutions also presented rhombohedral calcite, however, industrial heterogeneous carbonation process resulted in the formation of scalenohedral calcite, which was observed to be thin and long with sharp edges.

In the case for aragonite, BET specific surface area of microcrystals was analysed as 4.07 m^2/g which was larger than calcite with 0.40 m^2/g (Rademaker and Launspach, 2011). Zhang, et al. (2012) concluded that in the presence of Mg^{2+} concentration, aragonite production was enhanced through the reaction of CO_3^{2-} and Ca^{2+} ions whereby low Mg^{2+} concentration resulted in direct formation. On the other hand, high Mg^{2+} concentration was prone to cause multi-step processes, which transformed amorphous $CaCO_3$ (ACC)

into aragonite. Guo, et al. (2011) mentioned that aragonite commonly appeared as rod or needle shape with a smooth surface (Zhang, et al., 2012), and has shown an aspect ratio (length to diameter) of approximately 5.7.

In contrast, vaterite demonstrated higher specific surface area in comparison with that of the two polymorphs (Guo, et al., 2017). Microspheres of vaterite demonstrated a BET specific surface area of 42.77 m^2/g and average pore size of 11.45 nm (Guo, et al., 2017). Other than spherical form, vaterite has also been presented as hexagonal (Mori, Enomae and Isogai, 2009; Yang and Nan, 2012; Trushina, et al., 2014). The spherical form with a large surface area (smaller than 1μm) represented the secondary structure of vaterite which was composed of 100 mm diameter primary vaterite particles (Mori, Enomae and Isogai, 2009) and this contributed to the relatively rougher surface observed. Moreover, the addition of surfactant or template has influenced the morphology of vaterite. Using sodium bis-2-ethylhexyl-sulfosuccinate (AOT) micelles as templates, star-shaped vaterite structures with centre holes were formed (Yang and Nan, 2012).

From the above findings, physico-chemical properties of PCC can be determined using XRD, FTIR and BET for its crystalline structure, functional group identification, specific surface area and porosity measurement respectively. Their distinct characteristics including that of each PCC polymorph will serve different results for them to be used as a treatment agent in remediating wastewater or AMD.

2.4 Operating Parameter Study

Various parameters were found to influence the performance of alkaline agents on treating AMD, such as concentration and oxidation state of metals present, pH of AMD, hydrolysis reactions and complex interactions between alkali and AMD (Kaur, et al., 2018). Other parameters to be considered included contact time as well as loading of neutralizing agent. In this study, only solution pH and loading of neutralizing agent will be focused. In

literature, the application of PCC in the treatment field has not been found to be extensively studied. Hence, $CaCO_3$ as a common neutralizing agent and other alkaline agents would be revealed in the following sections.

2.4.1 Initial pH Value

Seasonal changes resulting from precipitation, evaporation, flooding and others have influenced the chemical concentration and pH of AMD, which are both significant in determining the efficiency of contaminant removal (Muliwa, Leswifi and Onyango, 2018). Focusing on the latter, pH influences the solubility, mobility, lability, toxicity of heavy metal ions. These factors were enhanced due to low pH and had resulted in exceedingly high dissolved metal ion concentration in AMD (Masindi, et al., 2017). Moreover, the pH of AMD solution governs the metal ions precipitation. For example, Pavoni, et al. (2018) stated that a rise in pH has promoted the ionic species of Zn^{2+} and Tl^{+} ions to remain as aqueous in Zn – lead (Pb) mine of North-Eastern Italian Alps, whereby the latter species exhibited high mobility, low affinity for suspension and removal. By evaluating the initial pH of AMD, the existing degrees of dissolution and precipitation of metal ions can be approximated. Hence, this would aid in determining the amount of neutralizing agent to be added in the treatment.

Kaur, et al. (2018) mentioned that the order of precipitation to form the metal hydroxide and carbonate followed the sequence of $Fe^{3+} > Al^{3+} > Cu^{2+} > Zn^{2+} > Ni^{2+} > Mn^{2+}$ ions with increasing solution pH. It was stated that metal precipitation occurred at pH 3.5 to 4 for Fe^{3+} ions, at pH 9 for Mn^{2+} ions, at pH 5 to 9 for Al^{3+}, and finally, at pH 8 to 9 for divalent metal ions including Ni^{2+} and Zn^{2+} ions. In addition, oxygenated condition was found to have an influence over the pH precipitation. For instant, Fe^{3+} ion precipitated at pH 3.5 to 4.0 under oxygenated conditions, however, poorly oxygenated conditions only allowed precipitation at pH of 8.5. Co-precipitation of Mn^{2+} and Fe^{3+} ions may occurred at pH of 8 if the concentration of the former was found to be lower than that of

the latter. Hence, for a specific pH value, some metal ions may be dissolved, while others may undergo precipitation. For example, $Al(OH)_3$ re-dissolved as $Al(OH)_4^-$ ions while Mn^{2+} ions precipitated as $Mn(OH)_2$ at a pH of 9 (Kaur, et al., 2018).

A study was conducted by Name and Sheridan (2014) using metallurgical slags of basic oxygen furnace (BOF) and stainless steel (SS) to treat AMD. It was found that removal efficiencies of 99 % of the total Fe ionic species (Fe^{2+}, Fe^{3+} and $FeSO_4^+$ ions) and 75 % of SO_4^{2-} ions occurred at pH of 11.3 for BOF slag. For an equal slag-AMD ratio of 100g/L, SS slag resulted in removal efficiencies of 63.6 % of Fe ionic species and 40 % of SO_4^{2-} ions at pH of 5.9. The difference between the removal rates was claimed to be contributed by the difference in pH values. These stable Fe ionic forms could not be precipitated below pH values of 9, hence the removal of total ionic species of Fe was low for SS. However, before the specific pH of each metal precipitation was reached, removal may still be carried out in the form of adsorption other than precipitation and co-precipitation (Muliwa, Leswifi and Onyango, 2018; Masindi, et al., 2016).

On the other hand, the extent of hydrolysis can also be varied with solution pH. The rise in pH can stimulate the release of protons from hydration and promote olation and oxolation to produce Fe–OH–Fe bonds and Fe–O–Fe bonds (Muliwa, Leswifi and Onyango, 2018). Therefore, it was observed that the hydrolysis reactions of ionic species of Fe (Fe^{3+} and/or Fe^{2+} ions) and Al^{3+} ions improved with the alteration of pH from medium to neutral. The formation of the precipitates which included $Fe(OH)_3$, $Fe(OH)_4^-$, $Al(OH)_3$ and $Al(OH)_4^-$ exhibited increasing ease in removal (Muliwa, Leswifi and Onyango, 2018). In summary, a change in pH has influenced the efficiency of AMD treatment by metal ion precipitation and neutralization reaction.

2.4.2 Loading of Neutralizing Agent

High buffering capacity has been contributed by acid-buffering minerals which include calcite, dolomite, carbonate (CO_3^-) and bicarbonate (HCO_3^-), and has enhanced the neutralization of pore and surface water. In the abundance of calcite which is a polymorph of PCC, dissolution can occur to increase alkalinity in the form of CO_3^-, HCO_3^- as well as hydroxide (OH^-) ions, and exceed the acidity as contributed by forms such as carbonic acid (H_2CO_3) (Kastyuchik, Karam and Aïder, 2016). The specific 'abundance' is a crucial parameter controlling the overall degree of AMD neutralization. Moreover, the synthesis of PCC from calcium carbide sludge renders it important to evaluate the effectiveness of different loadings so as to produce an adequate amount of PCC for optimum AMD treatment.

In a finding by Kaur, et al. (2018), lime ($Ca(OH)_2$) was used as one of the neutralizing agent in AMD treatment with a dosage of 1.6 mmol to 3.3 mmol per 25 mL of AMD. The optimum loading was found to be 3.3 mmol in which metals present in AMD were removed at an efficiency of 99.9 % for Al^{3+}, 99.7 % for Mn^{2+}, 99.9 % for Cu^{2+}, 99.9 % for Zn^{2+}, 99.7 % for Fe^{3+} and 96.8 % for Ni^{2+} ions. The removal efficiency showed an increase with dosage, which was suggested to be caused by the formation of gypsum flocs with high surface area. The capture of metals by larger flocs of precipitations represented a significant metal removal mechanism. It was also observed that pH increased from 3.72 to 9.19.

In another study conducted by Othman, Sulaiman and Sulaiman (2017), calcium lime waste which mainly consisted of 94.3 % calcium oxide (CaO) was used as the neutralizing agent for AMD with a dosage of 0.5 g to 2.5 g per 1 L of AMD. A dosage of 1.5 g/L calcium lime waste represented the optimum dosage as the final concentrations of heavy metals such as Al, Cd, Cr, Cu, Fe, Pb, Zn and As were within the parameter limits of both Standards A and B of Malaysia Environmental Act 1974. Near-completion removal was observed for Al^{3+}, Cu^{2+} and Fe^{3+} ions. In addition, the pH value obtained was

around 7 to 8 at a contact time of 70 minutes and had fulfilled the requirement of pH 6 to 9 of Standard A and pH 5.5 to 9 of Standard B of Environmental Act 1974.

Masindi, et al. (2017) studied on the efficiencies of various alkaline agents on AMD neutralization, including caustic soda, soda ash, periclase, brucite, magnesite, lime ($Ca(OH)_2$), hydrated lime (Ca(OH)) and limestone ($CaCO_3$) with a dosage of 1g to 20 g per 1 L AMD. An optimum dosage of 10 g/L was applied for all neutralizing agents as it was deduced that the increase in alkalinity resulted in almost complete removal of ionic species of Fe and Al. The removal efficiencies for Fe ionic species (Fe^{3+} and Fe^{2+}) were 99.8 % for caustic soda, 97.6 % for soda ash, 74.6 % for brucite, and 99.9 % for all other reagents. For Al^{3+} ions, the removal efficiencies were 99.9 % for all reagents, except for caustic soda with 66.1 % and hydrated lime with 98.2 %. In addition, calcium-based reagents revealed a decrease in SO_4^{2-} ions and Ca^{2+} content which signified the generation of gypsum at 10 g/L. This was highlighted by the SO_4^{2-} ion removal efficiencies of 95.4 % for $Ca(OH)_2$, 96.2 % for Ca(OH) and 88.8 % for $CaCO_3$.

Heviánková, et al. (2013) studied the effectiveness of $CaCO_3$ and $Ca(OH)_2$ in AMD treatment with a dosage of 180 mg/L to 2000 mg/L. After a contact time of 30 minutes, $CaCO_3$ had shown an increase in the removal of ionic species of Fe (Fe^{2+} and Fe^{3+}) which was found to be 87.1 % for 150 mg/L, 89.8 % for 180 mg/L, 92.6 % for 200 mg/L, 94.9 % for 500 mg/L, 95.5 % for 1000 mg/L as well as 95.8 % for 2000 mg/L. From the above findings, the loading of neutralizing agent can be observed to influence the removal efficiency. Thus, it is important to determine the optimum dosage which would result in significant removal efficiency. All the above mentioned ranges of dosage could be taken into consideration for the determination of PCC dosage in this study.

2.5 Summary of Literature Review

Extensive reviews on AMD including its source, generation, characteristics as well as a brief description on its effects have been initially elucidated. Numerous conventional treatment methods for AMD based on their individual functions, benefits and limitations have been highlighted. These methods showed varying degrees of efficiency in remediating AMD. Among these, active abiotic treatment with addition of alkali was found to focus on pH neutralization and precipitation of heavy metal ions and anions present in AMD. Moreover, innovative materials have been introduced to incorporate the use of otherwise industry waste. In these treatment methods, PCC features as a promising alkaline neutralizing agent due to its derivation from calcium carbide sludge which could thereby potentially reuse and reduce the waste from acetylene gas production for the achievement of first objective in this study. The characteristics, applications, characterization and other synthesis methods of PCC have also been explained in this Chapter to provide a vast insight towards the expected characterization results of PCC in fulfillment of the second objectives.

Apart from that, operating parameters such as solution pH and loading of neutralizing agent have been revealed as they may influence the treatment of AMD. All of the reviews on AMD serve as a crucial precursor to understand the initial characteristics of AMD, emphasize the importance of remediation for achievement of the third objectives in this research project. In this study, the surfactant-polymer template precipitation method for PCC synthesis was adopted from Kanoje, Patel and Kuperkar (2017) which utilized dolomite as the calcium-based material. For AMD remediation, the use of industrial chemical calcium carbonate has been reported as a widely utilized neutralizing agent for AMD in literatures (Heviánková, et al., 2013; Masindi, et al., 2017). As a solution for both industrial wastes, calcium carbide sludge will be replacing dolomite, whereas, the industrial waste incorporated PCC will be applied for AMD treatment to reduce landfill burden and environmental constraint. To the best of our knowledge, PCC synthesis via surfactant-polymer template has not been performed using industrial waste calcium carbide sludge and the resulting PCC will studied for AMD remediation.

CHAPTER 3

METHODOLOGY

This chapter focuses on the methods used in the experiments conducted in this research study. Figure 3.1 represents the research flow chart of this work.

3.1 Materials and Chemicals

Table 3.1 lists the materials and chemicals that were used for this research study. All of the chemicals were analytical graded without further purification and used as-purchased.

Other than the chemicals listed in Table 3.1, industrial wastes in the form of calcium carbide sludge and acid mine drainage (AMD) were also used in this study. The calcium carbide sludge was collected as a by-product of acetylene gas production from MCB Industries Sdn. Bhd. The acetylene gas plant was located in Taiping, Perak. The sample was obtained using grab sampling method by collecting individual samples over a period of time to acquire a representative sample. It was stored in a desiccator for moisture absorption.

AMD was obtained from tin mining industry in the state of Perak, with a location as marked with a red cross in Figure 3.2. It was stored in a plastic container which was wrapped with aluminum foil and placed within the refrigerator at 4°C prior to usage.

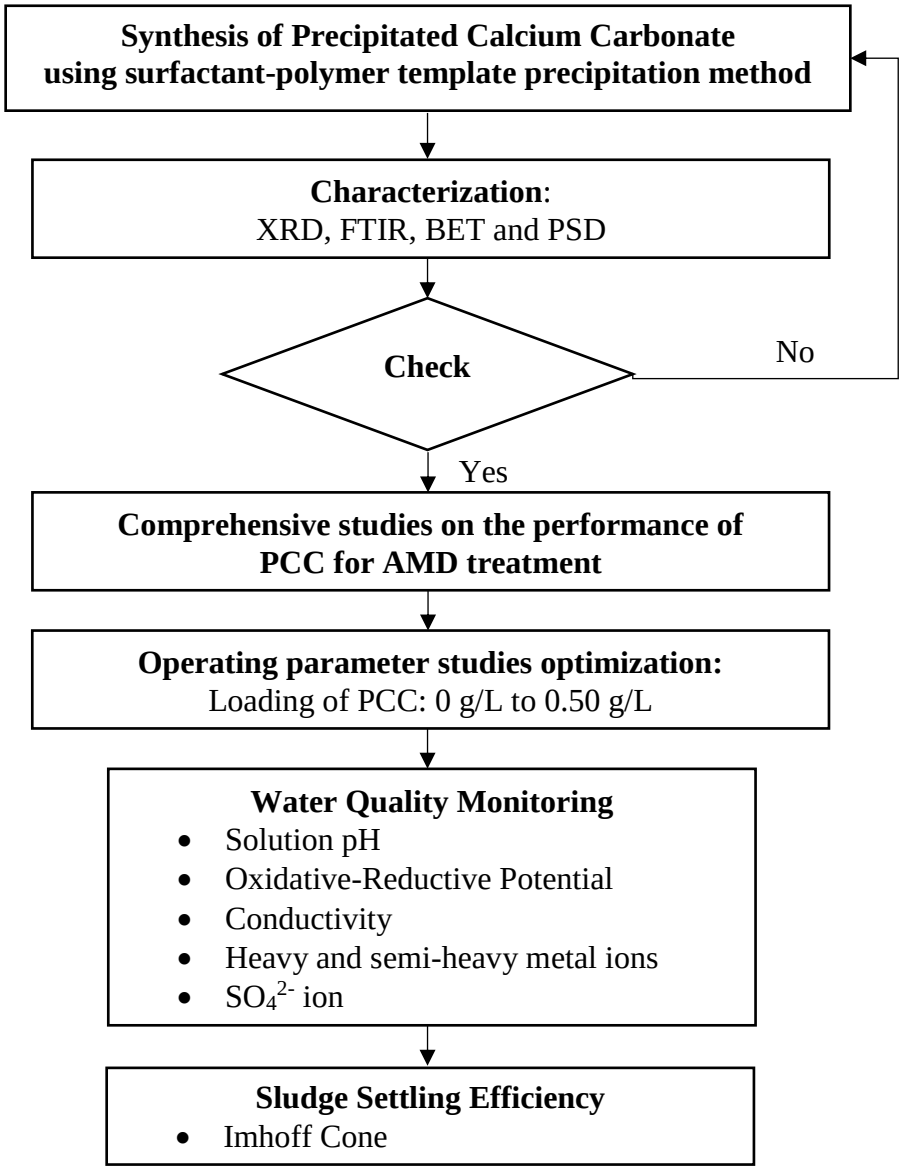

Figure 3.1: Flowchart of Experimental Work Involved in This Study.

Table 3.1: List of Materials and Chemicals Used.

Chemical/ Reagent	Purity	Supplier	Purpose of Use
Sucrose	99.9%	Chemical Solutions (Chemsol)	Used to prepare calcium sucrate solution
Polyethylene glycol (PEG)	-	Merck	Used as a polymer for the surfactant-polymer template
Polyvinyl alcohol (PVA)	>99.0% hydrolyzed	Sigma Aldrich	Used as a polymer for the surfactant-polymer template
Pluronics® P-123 (P123)	-	Sigma Aldrich	Used as a polymer for the surfactant-polymer template
Hexadecyl-trimethylammonium bromide (CTAB)	>99.0%	Acrōs Organics	Used as a cationic surfactant for surfactant-polymer template, served as a "control"
Sodium carbonate (Na_2CO_3) Anhydrous	>99.8%	SIME Scientific	Mixed with calcium sucrate solution to form PCC in the presence of surfactant-polymer template
Nitric Acid (HNO_3)	65%	R&M Chemicals	Used to acid digest aqueous solution for ICP-OES analysis
Distilled (DI) water (0.30 MΩ·cm)	-	Favorit	Used as an universal solvent for cleaning apparatus
Ultra-pure water (18.2 MΩ·cm)	-	Human Corporation	For the preparation of different aqueous and stock solutions for ICP-OES analysis
Deionized water (DIW) (>1 MΩ·cm)	-	Elga Veolia	Used to compare sludge settling efficiency of PCC

Figure 3.2: Location of Acquisition of AMD.

3.2 Apparatus

In this experimental procedure, the only apparatus employed was flocculator for AMD treatment process and synthesis of precipitated calcium carbonate (PCC).

3.2.1 Flocculator

The set-up of experimental apparatus and a representative schematic diagram are illustrated in Figures 3.3 and 3.4 respectively. The function of flocculator was to employ multiple stirrers for testing flocculation, coagulation or precipitation of chemical agents using *VELP® Scientifica JLT6 Flocculator*. The six stirring paddles were adjoined to stainless steel rods which were adjustable in height. The mixing speed and time of the test can be controlled by setting the mixing and time controls which were displayed on separate digital displays. The illumination switch enabled the back panel to be illuminated so as to provide sufficient lighting for better observation of the samples.

Figure 3.3: Flocculator in the Environmental Chemistry Laboratory.

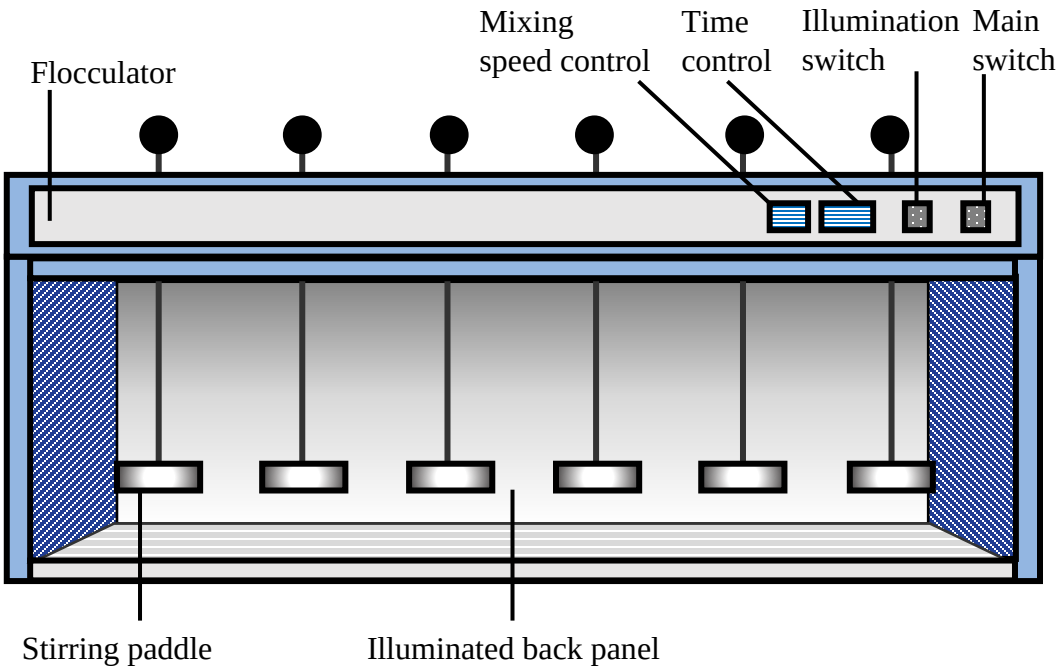

Figure 3.4: Schematic Diagram of Flocculator Set-up.

3.3 Analytical Procedures

Various parameters of AMD were analyzed prior to and during treatment which included pH, oxidation-reductive potential (ORP), conductivity, metal and sulphate (SO_4^{2-}) ion concentrations. Parameters of pH, ORP and conductivity were measured using a portable water quality meter. Aqueous samples were determined for various metal concentrations using Inductively Coupled Plasma Optical Emission Spectrometry (ICP-OES). Analysis for SO_4^{2-} ion was conducted by Ion Chromatography (IC).

3.3.1 Portable Water Quality Meter

The measurement of water quality parameters was performed by portable water quality meter which was *CyberScan PCD 650 Meter* by *Eutech Instruments*. It consisted of a waterproof handheld meter with digital display connected to three probes which were termed as pH probe, conductivity probe and DO probe. In total, eight parameters could be measured simultaneously by the water quality meter which comprised of pH, ion concentration, temperature, conductivity, ORP, total dissolved solids (TDS), salinity and dissolved oxygen (DO). For this study, water quality parameters which were measured included pH, ORP and conductivity. The units of measurement were expressed as mV for ORP and µS for conductivity. This analysis was performed at Faculty of Engineering and Green Technology, Universiti Tungku Abdul Rahman (FEGT, UTAR).

The pH probe was made up of a transparent plastic body which was filled with a storage solution. Prior to conducting the test, calibration of the pH probe was performed using standard pH buffer solutions obtained from the laboratory. The conductivity and DO probe were separately calibrated as well. After calibration was completed, the probes were rinsed with DI water and inserted into a 1 L glass beaker filled with 500 mL of diluted AMD, and fixed in position using a clamp stand. The probes were placed at an upright position without contacting the bottom face of the beaker. The readings of pH, ORP and conductivity were noted down for the raw AMD. During the treatment, measurements were obtained after the first 2 min which was then followed by every 5 min for a duration of 50 min. No further measurement was taken for pH with no more significant changes. Additional measurements were only taken for AMD with continual significant pH changes. In a similar manner, AMD was measured at an interval of 5 min until the pH reached an approximately constant value.

3.3.2 Inductively Coupled Plasma Optical Emission Spectrometry

ICP-OES was used to determine the metal concentrations of Mn, Fe, Ni, Cu, Zn, Al and As present in AMD. This analysis was performed by *Perkin Elmer® Optima^{TM} 7000 DV ICP-OES*. The equipment comprised of two main components, high-temperature ICP torch and charge-coupled device (CCD). The former was employed with argon gas to cause vaporization, atomization, excitation and ionization of elements. Following, the excited atoms and ions were isolated according to their emitted light wavelength by double monochromator prior to being detected via advanced detector technique of CCD (Boss and Fredeen, 2004). The unit of the measured metal concentrations was in µg/L. This analysis was conducted at Lee Kong Chain Faculty of Engineering and Science (LKC FES), UTAR.

The preparation of samples and calibration solutions was performed prior to ICP-OES analysis. For the sample preparation, the samples were diluted by a factor of 1000 using ultra-pure water before 1% HNO_3 was added to each sample. All samples were filtered using a syringe filter of pore size 0.22 µm. For the calibration solution preparation, 10 ppm multi-element calibration standard 3 (without Hg) was used to prepare stock solutions of 10 ppb, 25 ppb, 50 ppb, 100 ppb, 200 ppb and 400 ppb using ultra-pure water. The solutions were filtered using a syringe filter of pore size 0.22 µm. Calibration curves were plotted using the stock solutions to determine the concentration of these particular elements as shown in Appendix A1 to A7.

3.3.3 Ion Chromatography

IC functioned to separate, identify and quantify cations or anions presented in a sample, usually in liquid state (Kohli and Mittal, 2012; Moldoveanu and David, 2013). The concentration of the anion to be analyzed was SO_4^{2-} ion in AMD. Prior to analysis, sample preparation was required so as to protect analytical columns of IC. The preparation method

used was to filter the sample using a syringe equipped with a membrane filter. After preparation, the solution sample was introduced into IC by injection. The unit of concentration for IC analysis was measured in mg/L. This analysis was carried out at School of Chemical Sciences, Universiti Sains Malaysia (USM).

3.4 Preparation of Precipitated Calcium Carbonate

PCC was synthesized by mixing calcium sucrate and sodium carbonate in the presence of surfactant-polymer templates as reported by Kanoje, Patel and Kuperkar (2017). Three different polymers were utilized, i.e. PEG, PVA and P123, all in which were individually mixed with CTAB surfactant. Initially, calcium carbide sludge was pre-treated prior to the preparation of calcium sucrate solution. It was dried in the sun for 3 days and then grounded using pestle and mortar before being passed through an American Society for Testing and Materials (ASTM) No. 325 sieve (45 μm). An amount of 10 g pre-treated calcium carbide sludge was added to 100 mL of 1 M sucrose solution under constant stirring condition of 300 rpm for 1 h using a flocculator. After stirring, the mixture was centrifuged at a rate of 4000 rpm for 30 min to achieve a clearer mixture. The resulting supernatant was vacuum filtered to remove any precipitation and obtain calcium sucrate solution as the filtrate.

Following, the preparation of surfactant-polymer template was performed by mixing 1.3 mM CTAB and 1.0 g/L polymer concentration to prepare a volume of 80.0 mL solution under constant stirring condition for 1 h. A total of four different templates were prepared: PEG/CTAB, PVA/CTAB, P123/CTAB and CTAB only. The last template served as a control to compare the presence of polymer in influencing the synthesis of PCC. Equal volumes of 1.0 M calcium sucrate and 1.0 M sodium carbonate (Na_2CO_3) solutions, 10.0 mL each, were simultaneously poured into the surfactant-polymer template and stirred continuously for a further 30 min. The introduction of solutions to template caused instantaneous precipitation products to form. The reaction mixture was left for 24

h to settle down. After settling, the mixture was filtered to separate the precipitation using a vacuum filter before being rinsed with DI water and then dried in the oven at 50 °C for 1 h 30 min. Finally, the precipitation product was grounded and mixed to produce a powdered form. The flow of the surfactant/polymer-assisted synthesis of PCC was illustrated in Figure 3.5.

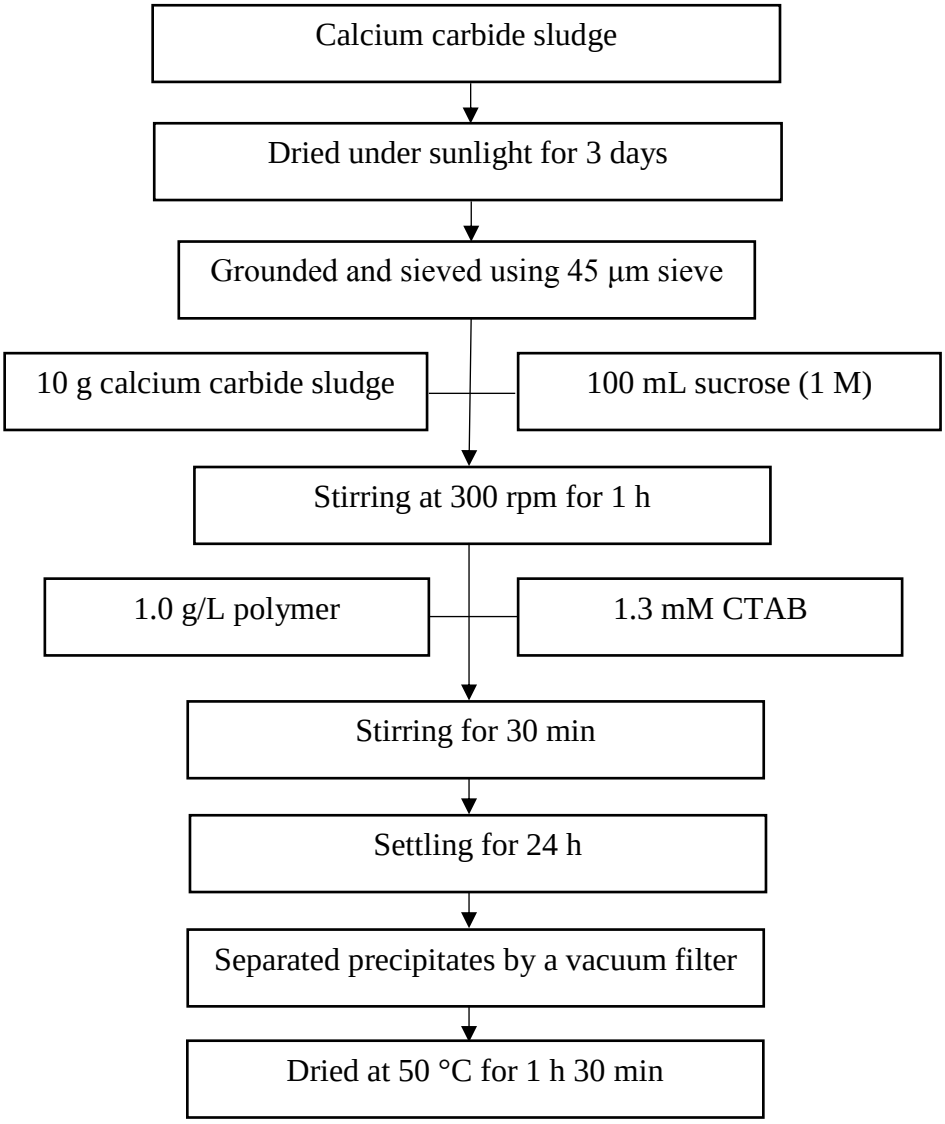

Figure 3.5: Flowchart of PCC Synthesis.

3.5 Characterization of Precipitated Calcium Carbonate

Various physical and chemical characterizations were conducted for the synthesized PCC products, which consisted of crystal phase, functional group, specific surface area and particle size distribution analyses.

3.5.1 Crystal Phase Analysis

The identification of crystal phase or structure of PCC samples was analyzed by X-Ray Diffraction (XRD). The instrument was installed with Cu Kα radiation in a range of 2θ under a scanning rate of 2 ° min^{-1} and settings of 20 ° to 70 °. This analysis was conducted using Quantum Skynet Extended Services.

3.5.2 Functional Group Analysis

The identification of functional group of PCC samples was performed by Fourier Transform Infrared Spectroscopy (FTIR) analysis. The formation of an infrared adsorption spectrum aided in identifying the functional groups presented in the sample. *Spectrum RX 1* FTIR Spectrometer was the instrument used to carry out the analysis. For the sample preparation, FTIR accessory kits were cleaned with absolute ethanol to remove impurities on FTIR sample holder, evacuable die set and grinder. The analysis was conducted at UTAR.

3.5.3 Specific Surface Area Analysis

Specific surface area and porosimetry measurements were examined using Brunauer, Emmett and Teller (BET) surface area analysis. The instrument utilized for this analysis was *Micromeritics ASAP^{TM} 2020* with *Accelerated Surface Area and Porosimetry System*. Adsorption-desorption isotherms of PCC products were determined with the use of nitrogen gas as an adsorbate at a degassing condition of -196 °C. As a preparation for the samples, vacuum preconditioning was performed at 90 °C for 1 h and subsequently, at 100 °C for 2 h at 10 mm Hg for the removal of excess humidity and adsorbed contaminants. This analysis was carried out using Quantum Skynet Extended Services.

3.5.4 Particle Size Distribution Analysis

Distribution of particle sizes in PCC samples was determined using a particle size analyzer via *Malvern Mastersizer 2000*. The optical bench was used to capture the actual scattering pattern from a field of particles. The size of particles which resulted in the pattern was then calculated using theories related to beam or light scattering pattern and the spectra was documented by a recorder. Prior to the analysis, the sample was prepared by mixing well in order to distribute the particles in deionized water evenly. The analysis was carried out at UTAR.

3.6 Activity of Acid Mine Drainage Treatment

The neutralizing performance of PCC in AMD treatment was carried out in a flocculator. In this study, 500 mL of diluted AMD and a specific weight of PCC were poured and added into a 1 L beaker. AMD solutions were diluted with DI water by a dilution factor of 10 and acidified with 0.31% of HNO_3 to retrieve the original pH readings. One of the component of jar test, paddle blades rotated with a revolution equivalent to the speed of

mixing. The mixing speed ranged from 10 rpm to 300 rpm. The beaker was fitted into the illuminated body of the flocculator by lifting the stirring rod to a sufficient height. Power and illumination switches were switched on. Initially, the speed was set to 200 rpm at a timing of 2 min using the mixing speed and time control. After the first stirring was completed, it was followed by a subsequent slow mixing set at 100 rpm for 50 min. The selection of mixing rate and sequence was based on literatures with alterations (Masindi, et al., 2017; Tolonen, et al, 2014). During the stirring, water quality parameter measurements were taken every 5 min using the portable water quality meter. The AMD was allowed 30 min to settle. The parameters consisted of pH, oxidation reduction potential (ORP) and conductivity. The readings for the parameters of AMD were recorded. A general removal efficiency equation applicable for each water quality parameter was shown in Eq. (3.1).

$$\text{Removal efficiency} = \frac{X_o - X_i}{X_o} \times 100\% \qquad (3.1)$$

whereby removal efficiency is expressed in percentage (%), X_o is the initial results of AMD and X_i is the final reading of a particular parameter of AMD after reaction time.

3.7 Process Parameters Studies

The process parameters such as type of polymers and loading of PCC were investigated based on their effect on AMD treatment with or without prior influence on the synthesis of PCC. In this study, one process parameter was varied, while other process parameters were kept constant. During the experiment, water quality parameters which included pH, ORP and conductivity were measured using portable water quality meter. The determination of other parameters included heavy metals of Al, Cu, Fe, Mn, Ni, Zn and As by an ICP-OES analysis as well as SO_4^{2-} anion using an IC test.

3.7.1 Effect of Polymer Type

Surfactants have been investigated to control the crystal size, growth and aggregation of PCC with significant assistance of additives for example, polymers. The coupled interaction between polymer and surfactant was reported to govern the crystallization of PCC by affecting the kinetics of precipitation of the mixture of calcium sucrate and Na_2CO_3 solution (Kanoje, Parikh and Kuperkar, 2018). This was due to the self-assembly and self-arrangement of surfactant-polymer templates which influenced the formation of precipitates on the templates (Mantilaka, et al., 2014). For this study, the types of polymer used were PEG, PVA and P123. Previously, the usage and influence of PEG on PCC precipitation was documented by Kanoje, Patel, and Kuperkar (2017). A fourth template consisting only of CTAB with no polymer served as a control for the experiment. For all four of these templates, the growth mechanism of PCC was studied by determining the effect of interaction between various polymer types and surfactant on the crystallization of PCC.

3.7.2 Effect of Dosage of Precipitated Calcium Carbonate

The effect of loading of PCC on AMD treatment was investigated using dosages of 0.10 g/L, 0.20 g/L, 0.30 g/L, 0.40 g/L and 0.50 g/L. The selection of this range of dosage was based on the loadings of neutralizing agents used as reported by Othman, Sulaiman and Sulaiman (2017). Their study directly utilized waste product in the form of calcium lime waste with a dosage of 0.5 g/L to 2.5 g/L. Since conversion of waste material was performed, the neutralizing agent product may be of higher purity, and hence a lower range of dosages was selected for this study. The evaluation of effect was based on the ability of a particular loading to neutralize pH and precipitate heavy and semi-heavy metal ions as well as anion. Thereby, the water quality parameters, metal and anion concentrations were measured for all loadings. The experiments were performed with a constant diluted AMD volume of 500 mL under natural pH of the AMD solution.

3.8 Settling of Sludge

The efficiency of sludge settling was determined by observing the volume of AMD sludge settling to the bottom of an Imhoff cone periodically. This was performed by using two mixtures in which the former consisted of treated AMD and PCC (AMD-PCC), while the latter consisted of deionized water and PCC (DIW-PCC). The latter served as a comparison to observe the settling of PCC without the presence of ions. The previous activity using flocculator was also applied to the DIW-PCC mixture in order to ensure valid comparison.

The two mixtures were introduced into individual 1-L graduated Imhoff cones. Prior to sedimentation, the sludge was distributed by inverting the cylinder three times with a cork plugged into the top (American Public Health Association, American Water Works Association, and Water Environment Federation, 2005). The Imhoff cone was then placed in an upright position within an Imhoff cone stand. The volume of sludge blanket was observed and recorded at a frequency which was dependent on the change in sludge settling rate. The time interval between observations was increased with sedimentation time until a constant final reading was obtained for both cones respectively. The sludge volume was equal to the final reading (Muliwa, Leswifi and Onyango. 2018). The units of measurement for the sludge blanket volume was in mL/L. The cork at the bottom of Imhoff cone was unscrewed to allow bottom settled sludge to flow out and be collected.

CHAPTER 4

RESULTS AND DISCUSSION

This chapter reviews the results of experiment described in this research work. The first section of this chapter focuses on the characterization studies of precipitated calcium carbonate (PCC). In the second section, the effect of PCC synthesized by various surfactant-polymer template on acid mine drainage (AMD) treatment is discussed in terms of neutralization and removal of heavy metal ions and anions. Consecutively, a further evaluation of AMD treatment by varying dosages of PCC synthesized by the best surfactant-polymer template is described in the third section. The fourth section is comprised of sludge settling efficiency of AMD with the addition of optimized PCC. Lastly, a comparison study is performed between developed PCC and literature works.

4.1 Characterization of PCC

The synthesized PCC was undertaken to perform various characterizations in order to examine their effectiveness or ineffectiveness in AMD treatment. The crystal phase structure was assessed using X-Ray Diffraction (XRD) analysis, while functional groups were identified by Fourier Transform Infrared Radiation (FTIR) analysis. On the other hand, specific surface area of PCC samples was measured using Brunauer, Emmett and

Teller (BET) analysis. Finally, the distribution of particle sizes of PCC samples was determined by particle size distribution analyzer.

4.1.1 Crystal Phase Analysis

Figure 4.1 exhibits XRD pattern of PCC products synthesized by CTAB, P123/CTAB, PEG/CTAB and PVA/CTAB surfactant-polymer templates. XRD patterns consisted of major diffraction peaks with values of 2θ = 23.0°, 29.4°, 36.0°, 39.4°, 43.1°, 47.4°, 48.5°, 56.5° and 57.3° which corresponded to basal planes of (012), (104), (110), (113), (202), (018), (116), (211) and (122). These peaks coincided with the characteristic peaks of calcite crystalline structure of PCC with a Joint Committee on Powder Diffraction Standards (JCPDS) card number of 25-0127. Both characteristic peaks of other PCC crystalline formations (vaterite and aragonite) and other diffraction peaks of impurities were not observed. Each of the PCC products displayed sharp and narrow diffraction peaks which signified high crystallinity.

It was found that the intensity of the peak pattern increased in the order of PEG/CTAB, CTAB, P123/CTAB and finally PVA/CTAB. The peak patterns of PCC synthesized on different surfactant-polymer templates have shown similar trends to the characteristic peaks of calcite. Diffraction peaks which more closely approached the characteristic peaks resided with P123/CTAB, followed by PVA/CTAB, PEG/CTAB and CTAB which exhibited the most deviated peaks. This deduced that the use of surfactant solely did not significantly influenced $CaCO_3$ as supported by literatures (Kanoje, Parikh and Kuperkar, 2018). Zhao and Wang (2012) mentioned that polymers contributed to the presence of an organic-inorganic interface as a chemical microenvironment for $CaCO_3$ nucleation in surfactant-polymer complexes. Overall, the peak patterns of PCC complexes coincided with the XRD patterns of calcite as shown in the literature report (Mantilaka, et al., 2014; Yang and Nan, 2012; Zhao, et al., 2012). Hence, the results ratified that the

synthesized PCC crystals comprised primarily of calcite which represented the most thermodynamically stable structure of calcium carbonate ($CaCO_3$) (Yang, et al., 2014).

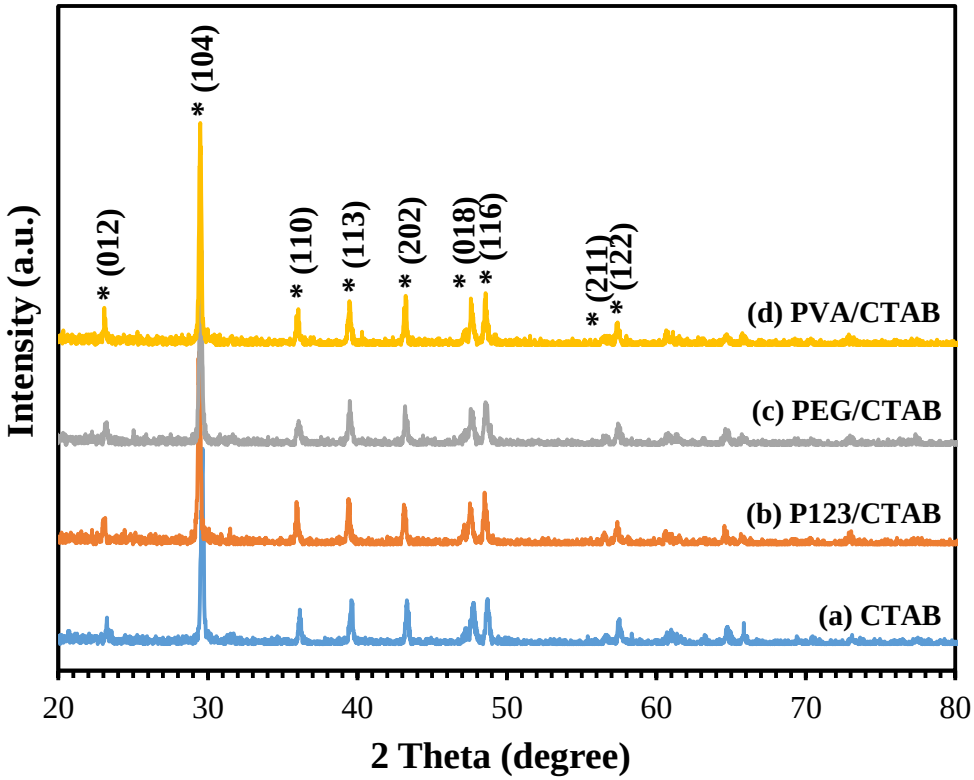

Figure 4.1: XRD Patterns of PCC Synthesized by (a) CTAB (b) P123/CTAB (c) PEG/CTAB and (d) PVA/CTAB Surfactant-Polymer Templates.

4.1.2 Functional Group Analysis

Figure 4.2 represents the FTIR spectra of PCC products synthesized by various surfactant-polymer templates. The presence of three characteristic absorption peaks in all PCC products indicated the crystal formation of calcite, which supported the XRD results. These were situated around wavelengths of 712 cm^{-1}, 872 – 873 cm^{-1} and 1420 cm^{-1} or 1400 cm^{-1} and were categorized as in-plane bending (v_4) mode of O – C – O bond, out-of-plane bending (v_2) mode of CO_3^{2-} as well as asymmetric stretching (v_3) mode of C – O

respectively (Li, Li and Ma, 2013; Gopi, Subramanian and Palanisamy, 2013). A minor peak which appeared at around 2515 cm^{-1} could reassure the presence of calcite in PEG/CTAB, PVA/CTAB as well as P123/CTAB synthesized PCC products. Zhao, et al. (2012) reported that temperature and the resulting energy of reaction environment determined the crystalline formation of $CaCO_3$. In their research, the nucleation growth observed produced vaterite and calcite under mediate temperature of 40°C, followed by a mixture of all three polymorphs at 60°C, and finally vaterite and aragonite at higher temperature of 80°C. Higher surface energy particles of vaterite and aragonite could be formed at higher reaction environment energy. Therefore, the nucleation growth of PCC resulted in calcite at room temperature.

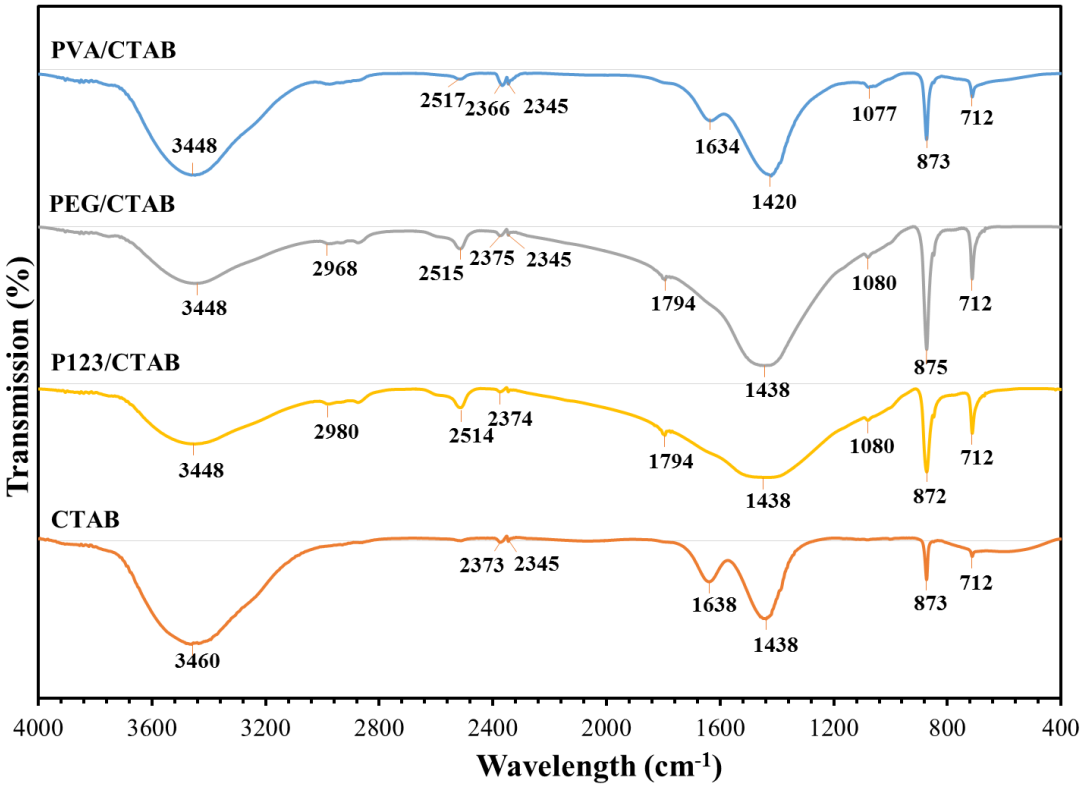

Figure 4.2: FTIR Spectra of PCC Synthesized by (a) CTAB (b) P123/CTAB (c) PEG/CTAB and (d) PVA/CTAB Surfactant-Polymer Templates.

All PCC samples synthesized by various surfactant-polymer templates were characterized with vibrational bands of 1638 cm^{-1}, 1794 cm^{-1} and 1634 cm^{-1} which could mark the presence of C=O bond vibration stretching. The occurrence of weak bands at 2979 cm^{-1} and 2984 cm^{-1} could indicate stretching of asymmetric and symmetric methyl and ethylene C-H bonds. It could be attributed to the representation of calcite crystals being strongly incorporated with surfactant molecules. Additionally, vibration bands of 3448 cm^{-1} and 3460 cm^{-1} could be referring to the presence of O-H stretching which was an indication of alcohol group. These crystal phase results were similar with the research work conducted by Kanoje, Patel and Kuperkar (2018) and (2017). The detection of different peaks corresponding to each developed PCC products proved that there was significant chemical adsorption of individual surfactant-polymer templates (Guo, et al., 2011).

4.1.3 Specific Surface Area Analysis

Figures 4.3 a – d illustrate the adsorption-desorption isotherms of nitrogen on PCC synthesized by various surfactant-polymer templates. For all templates, the desorption curves looped back earlier than the adsorption curves to form narrow hysteresis loops. Additions of surfactant-polymer templates were found to synthesize PCC of different BET surface areas. The BET surface areas were determined as 17.850 m^2/g, 25.0417 m^2/g, 8.2487 m^2/g and 10.637 m^2/g for PCC synthesized by CTAB, P123/CTAB, PEG/CTAB and PVA/CTAB surfactant-polymer templates respectively. For PCC, BET surface areas of above 20 m^2/g were classified as relatively high (Donate-Robles and Martín-Martínez, 2011). Variations in the BET surface area may be contributed by the hydrophobicity of polymer as well as the specific chemical interactions, which have been demonstrated to alter the morphology of PCC (Kanoje, Patel and Kuperkar, 2017). The PCC nucleation by surfactant-polymer complex micelles demonstrated incorporation of small molecules and may affect the amount of void space to influence the BET surface area (Jamrunroj, et al., 2019).

Based on Figure 4.3, all of the nitrogen (N_2) adsorption and desorption isotherms could be classified as reversible type II with narrow hysteresis loop of type H2 in accordance to IUPAC classification (Thommes, et al, 2015). This classification represented physisorption of most gases subjected to non-porous or macroporous adsorbents in which latter consisted pore size of more than 50 nm (Tan, et al., 2012). In a study conducted by Donate-Robles and Martin-Martinez (2011), the same characterization of type II with non-porous or macroporous was reported for PCC filler as well. Adsorption was characterized by monolayer-multilayer in an uncontrolled manner until the attainment of high partial pressure (P/P_o). From the front end of the graph, a gradual curvature was observed which could be signifying high overlapping monolayer coverage to induce multilayer adsorption. Adsorbed multilayer was found to build up infinitely with the attainment of P/P_o of 1 (Thommes, et al, 2015). The presence of narrow hysteresis loops indicated the existence of less narrow constrictions in the pores which allowed easier desorption (Pastorino, Canal and Ginebra, 2015).

For the same increment in P/P_o, PCC synthesized by P123/CTAB exhibited the highest rise in N_2 adsorption which was followed by CTAB, PVA/CTAB and finally PEG/CTAB. This signified that the presence of polymer modified the porosity of PCC, whereby P123/CTAB template could represent a possible candidate for better removal efficiency due to its higher surface area to yield higher adsorption capability. Salaudeen, et al. (2018) reported that the use of macroporous eggshell of Type II isotherm which represented a source of $CaCO_3$ demonstrated high initial CO_2 absorbance of 76.41 % conversion during gasification of biomass. In another study, Ma, et al. (2012) stated that specific surface area and meso/macroporous structure induced rapid heavy metal ions removal due to interaction between $CaCO_3$–maltose adsorbent and metal ions.

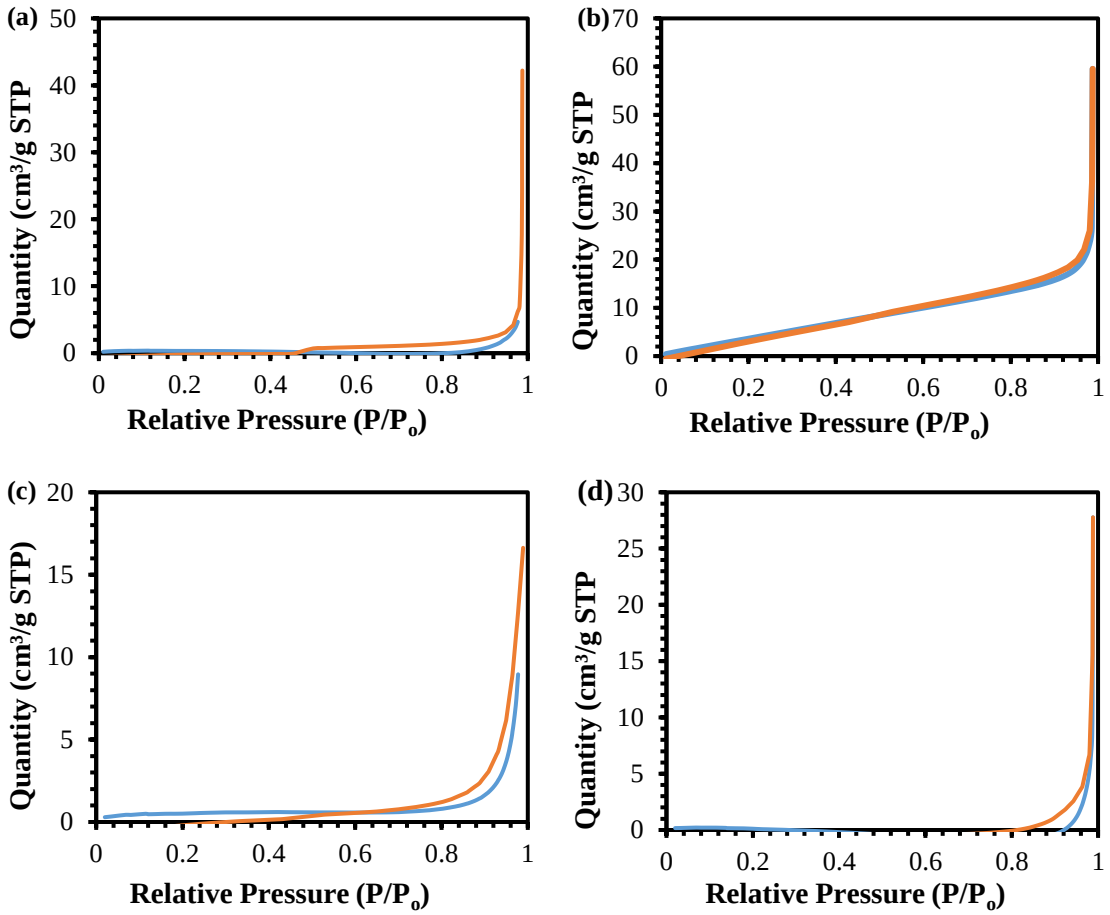

Figure 4.3: Adsorption and Desorption Isotherms of Nitrogen on PCC Synthesized by (a) CTAB (b) P123/CTAB (c) PEG/CTAB and (d) PVA/CTAB Surfactant-Polymer Templates.

4.1.4 Particle Size Analysis

Figure 4.4 presents the size distributions of PCC particles synthesized by various surfactant-polymer templates. Prior to the analysis, PCC samples were transferred to a compact benchtop digital refractometer, *Sper Scientific 300034 Digital Refractometer* to examine their refractive indices. The refractive indices were found to be 1.3346, 1.3344, 1.3333 and 1.3338 for PCC synthesized by CTAB, P123/CTAB, PEG/CTAB and PVA/CTAB respectively. An average value of 1.334 was computed as the refractive index

for these PCC products. All PCC complexes exhibited a uniform mean particle size of 0.158 μm with a narrow size distribution of 0.046 – 0.316 μm.

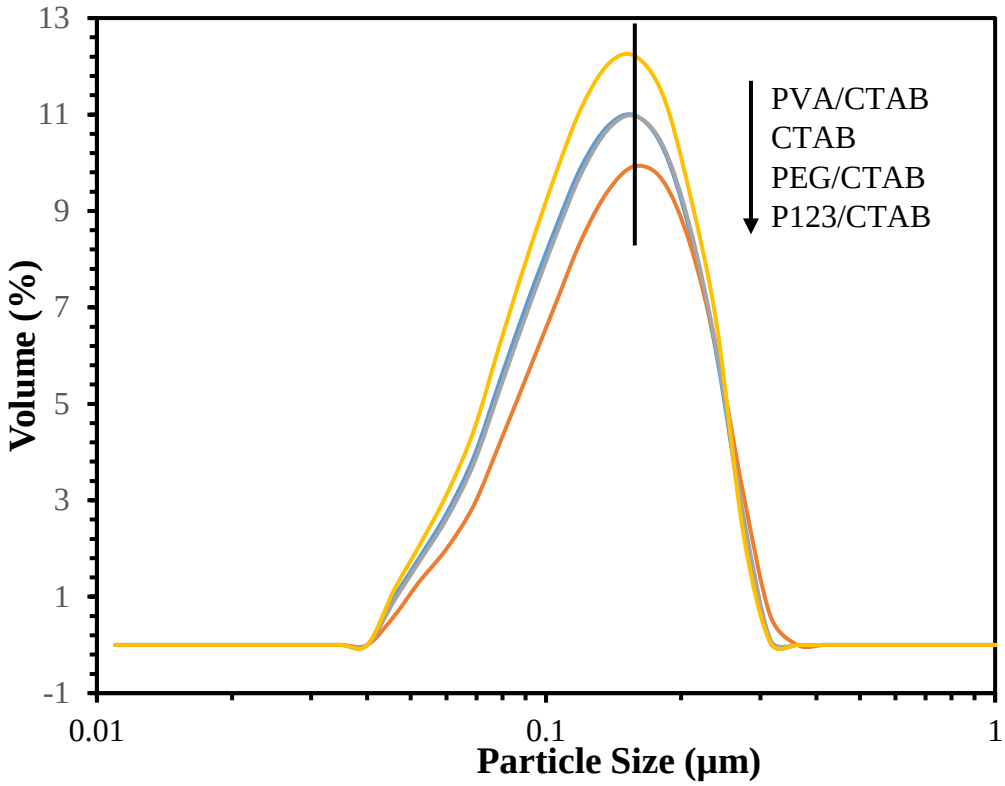

Figure 4.4: Particle Size Distribution of PCC Synthesized by (a) CTAB (b) P123/CTAB (c) PEG/CTAB and (d) PVA/CTAB Surfactant-Polymer Templates.

Studies had reported an average particle size of 1.6 μm and 2.0 μm for PCC modified by 1.2 mM and 0.05 mM of CTAB (Yang, et al., 2014). Meanwhile, the use of Pluronic F68 had resulted in PCC particle sizes of 5.0 μm, 3.5 μm, 2.5 μm and 1.8 μm in 0 g/L, 0.1 g/L, 3 g/L and 10 g/L concentrations of the crystal modifier (Zhao, et al., 2012). The literatures demonstrated particle size decreased with increasing concentrations of additives. It signified that the concentration of 1.0 g/L for polymer and 1.3 mM for surfactant used in this study was efficient in producing smaller particles which had been documented with a range of applications. Teir, Eloneva and Zevenhoven (2005) mentioned that PCC particles suited for use as printing filler pigments were less than 2

μm in size. Meanwhile, PCC particles with a diameter smaller than 1 μm were appropriate for industrial usage.

The uniformity of the particle size distribution was in accordance with studies conducted by Kanoje, Patel and Kuperkar (2017) and Mantilaka, et al. (2014). The use of polymer chains alone manifested wider variation in particle size distribution curves due to its non-rigidity which induced formation of varying shapes. No wide variation was demonstrated in the presence of CTAB alone. In a surfactant-polymer complex, opposite charges interacted between soft polymer chains with rigid surfactant micelles. As a result, well uniform particle size distributions were produced, together with variations due to the different lengths and shapes of each polymer.

4.2 Effect of PCC Synthesized by Different Surfactant-Polymer Templates on AMD Treatment

The efficiency of AMD treatment was evaluated based on the effect of PCC synthesized by various surfactant-polymer templates on different parameters of AMD. These parameters included pH, oxidative-reductive potential (ORP), conductivity and removal of heavy metal ions as well as anion. All of the relevant parameters were compared with limit values of several national and international standards and guidelines in order to assess their compliances. Depending on its source, AMD may be classified as natural or effluent discharge from mining industry. Hence, both water quality standards and regulations for industrial effluent discharge were utilized for compliance evaluation of AMD. The national standards included Department of Environment (DOE) National Water Quality Standards (NWQS) for Malaysia Class IIA on water quality as well as Standards A and B of Environmental Quality Act 1974 (EQA) Environmental Quality (Industrial Effluent) Regulations 2009 on industrial effluent. Whereas, international standards comprised of World Health Organization (WHO) 4th edition on Guidelines for Drinking Water Quality on water quality and United States Environmental Protection

Agency (EPA) Ore Mining and Dressing Effluent Guidelines 1975 for Iron Ore on industrial effluent.

4.2.1 Effect of PCC on pH of AMD

Addition of neutralizing agent in AMD attributed to a change in pH, metal content and oxidation state as well as a series of hydrolysis reactions. Figure 4.5 represents the change of pH of AMD subjected to treatment by PCC synthesized by various surfactant-polymer templates. It was observed that pH increased with contact time at different neutralization rates for PCC synthesized by various templates. Overall, a drastic increase was initially encountered and followed by a gradual decline in the rise in pH of AMD until a steady state had been reached. These readings were recorded during the flocculation process which lasted for 52 min and was subsequently followed by 30-min sedimentation. After sedimentation, the settled pH values obtained were 7.02, 8.22, 8.20, 8.16 for AMD treated with PCC synthesized by CTAB, P123/CTAB, PEG/CTAB and PVA/CTAB polymer surfactant template respectively. From the results, it can be deduced that PCC synthesized by P123/CTAB had attained the highest pH rise and complied with all applicable standards at a faster rate. All of the pH values were within the limits of Standards A (pH 6.0 – 9.0) and B (pH 5.5 – 9.0) as well as DOE NWQS Class IIA (pH 6.0 – 9.0). These values had also complied with international standards to the limits of EPA Ore Mining and Dressing Effluent Guidelines (pH 6.0 – 9.0) and WHO Guidelines on Drinking Water Quality (pH 6.5 – 8.5).

Each of the AMD treatments produced constant readings upon attainment of the previously mentioned pH values, with an exception for PCC synthesized by CTAB. This findings hypothesized the role of polymer in the configuration of PCC particles which may influenced AMD neutralization process. All of which, the mechanism behind pH elevation may be contributed by the dissolution of $CaCO_3$ due to reaction with acid which had been studied to occur up to pH 8.3. Following, another reaction may have occurred

between bicarbonate ion (HCO_3^-) and acid in order to produce carbonic acid (H_2CO_3). The end product could disintegrate to form water (H_2O) and carbon dioxide (CO_2). The overall reactions had been summarized as the substitution of cation constituents of AMD such as hydrogen, ferrous and ferric ions (H^+, Fe^{2+} and Fe^{3+}) with calcium (Ca^{2+}) ions of PCC, as shown in Eqs. (4.1) – (4.3) (Kaur, Couperthwaite and Millar, 2018; Mulopo, Mashego and Zvimba, 2012).

$$CaCO_3 + H^+ \rightarrow Ca^{2+} + HCO_3^- \quad (4.1)$$

$$HCO_3^- + H^+ \rightarrow H_2CO_3 \quad (4.2)$$

$$H_2CO_3 \rightarrow H_2O + CO_2 \quad (4.3)$$

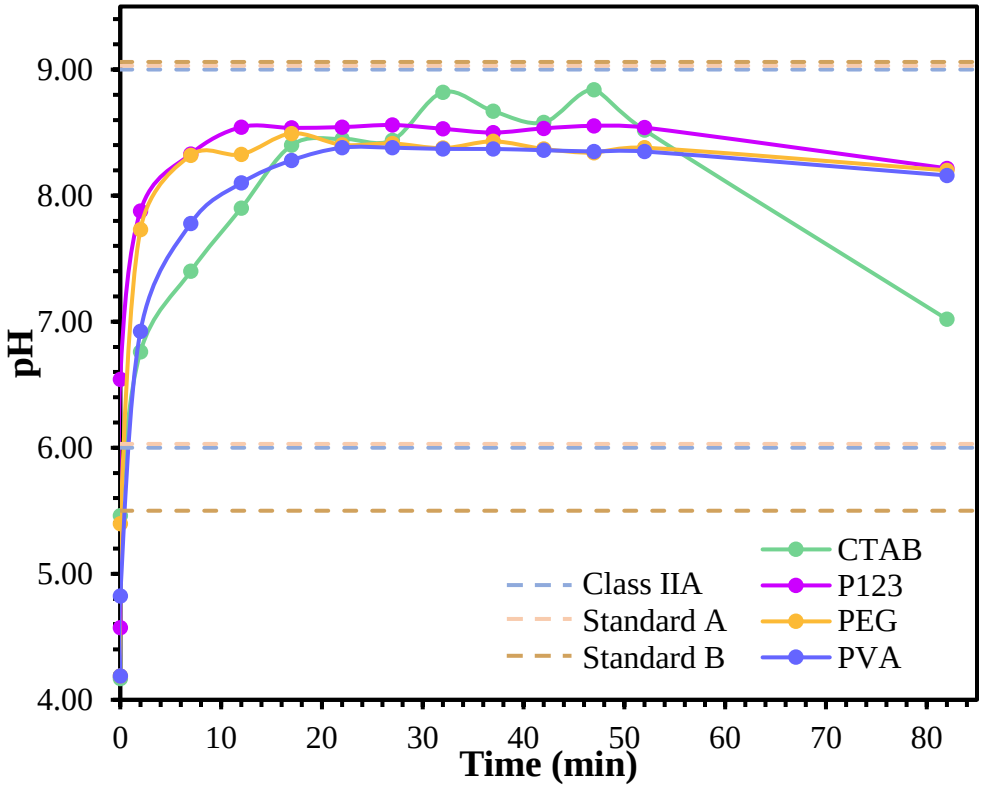

Figure 4.5: Variation of pH of AMD Treated Using PCC Synthesized by Various Surfactant-Polymer Templates.

Other possible reasons for the obtained pH values could be due to armour effect of precipitation coating the PCC particles. Formation of precipitates in AMD solution due to pH rise resulted in metal hydroxide precipitate such as ferric hydroxide ($Fe(OH)_3$) or gypsum ($CaSO_4.2H_2O$) deposition which formed a coating or armour on PCC particles (Skousen, Ziemkiewicz and McDonald, 2019; Sulaiman, Othman and Ibrahim , 2018; Potgieter-Vermaak, et al., 2006; De Beer, 2005). This armour induced passivation and hindered any further dissolution of the remaining PCC particles. Thus, the reactivity of PCC may be retarded to result in lower effectiveness. Another hypothesis for the decline in pH rise was the buffering effect of $CaCO_3$ whereby an increase in pH had caused difficulty in the dissolution of $CaCO_3$ (Skousen, Ziemkiewicz and McDonald, 2019). Kaur, Couperthwaite and Millar (2018) mentioned that the solution pH faced difficulty in increasing to a value more than 8 due to the elevated pH as well as high concentration of Ca^{2+} and HCO_3^- ions.

Generally, PCC synthesized by P123/CTAB surfactant-polymer template exhibited remarkable neutralization efficacy compared to PCC synthesized by other templates in terms of pH readings. This may be attributed by its specific surface area (25.0417 m^2/g), which was the highest among other synthesized PCC. In a study performed by Muliwa, Leswifi and Onyango (2018), eggshell (ES) was utilized as a neutralizing agent for AMD treatment, in which a dosage of 20 g/L of ES showed an increase in pH from 3.17 to 6.81 for particle size ranging from 850 – 1000 μm to < 53 μm. It was concluded that ES particles of smaller size and larger physical surface area resulted in better $CaCO_3$ dissolution, followed by enhanced acid neutralization and metal hydroxide precipitation. In another study, Potgieter-Vermaak, et al. (2006) had also confirmed the directly proportional relationship between surface area and neutralization rate. Thus, PCC synthesized by P123/CTAB surfactant-polymer template could be hypothesized to dissolute increased amount of $CaCO_3$ as supported by its fastest initial pH rise, and resulted in a superior overall treatment efficiency as justified by its highest final pH reading.

4.2.2 Effect of PCC on ORP of AMD

Figure 4.6 shows the change in oxidation-reductive potential (ORP) of AMD treated using PCC synthesized by various surfactant-polymer templates with time. The ORP represented the effect to which a substance would cause oxidation or reduction of another substance (Wang, et al., 2018). With the addition of PCC synthesized by various surfactant-polymer template, ORP instantaneously decreased which lasted up to 32 min before gradually decreasing to reach approximately constant readings. The final ORP readings obtained were 5.8 mV, -60.4 mV, -61.1 mV and -59.2 mV for AMD treated with PCC synthesized by CTAB, P123/CTAB, PEG/CTAB and PVA/CTAB surfactant-polymer templates respectively upon completion of 30 min sedimentation. During the decline, ORP readings transformed from positive to negative values. Positive ORP values denoted oxidizing state of AMD while negative ORP values represented reducing state of AMD. After 30 min sedimentation, all of the treated AMD showed a final state of reduction, except for treatment using PCC synthesized by CTAB template, which had transformed into a state of slight oxidation.

Initially, high positive ORP readings may signified the presence of high concentration of metal ions and anions, as supported in literature (Li, et al., 2014). The shift of reduction in oxidizing state to an increment in reducing state suggested that oxidized metal species present in AMD had experienced a net reduction (Jones and Cetin, 2017). Moreover, it could be amplified with the reduction of sulphate (SO_4^{2-}) ions to form gypsum. These findings indicated mass removal of heavy metal ions and SO_4^{2-} ions during this stage. On the other hand, the following slight reduction of ORP may be contributed by the exhaust of PCC dissolution (Gang, et al., 2019). It was discerned that the variation of ORP exhibited inversely proportional trend to the change in pH over the same period of time as reported in literatures (Jones and Cetin, 2017). The PCC synthesized by CTAB template depicted a similar trend with its pH counterpart whereby fluctuation in ORP was observed after reaching a steady state. This signified the role of polymer in surfactant-polymer template to assist the synthesis of PCC. A study conducted by Tajik, et al. (2013)

found that morphology of aggregates resulting from equimolar mixtures of cationic-anionic surfactants could be drastically influence by the application of polymers.

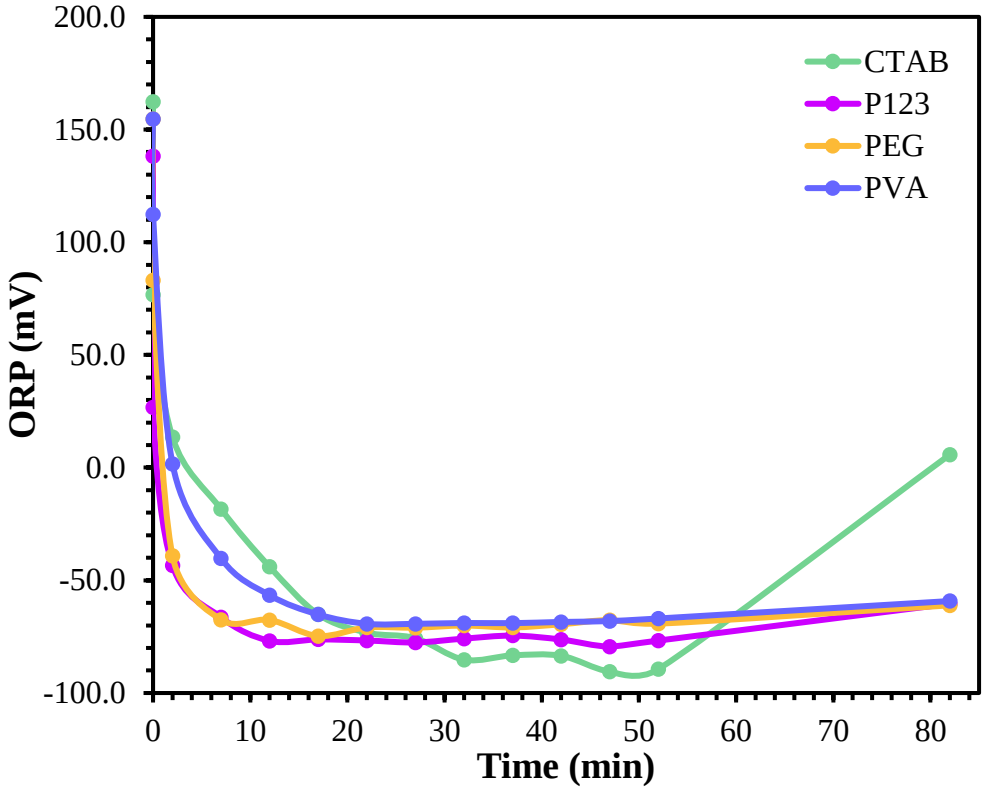

Figure 4.6: Variation of ORP of AMD Treated Using PCC Synthesized by Various Surfactant-Polymer Templates.

Several studies demonstrated similar trends in the change of ORP in various wastewater subjected to treatment. Li, et al. (2017) stated that the presence of Cu^{2+} ions in wastewater from wet hydrometallurgical copper extraction resulted in a surge in ORP which was converted to an electrode potential (E_h) readings, whereas a removal of Cu^{2+} ions by nanoscale zero-valent iron (nZVI) had shown a decrease in E_h of below -400 mV. Lizama Allende, et al. (2012) demonstrated that the use of limestone column had decreased the ORP readings from 453 mV to 198 mV associated with a removal of dissolved Fe from 105 mg/L to 0.11 mg/L in simulated mining-contaminated acidic wastewater. The AMD treated with PCC synthesized by P123/CTAB surfactant-polymer

template in this study achieved the most rapid change in ORP and highest steady ORP readings. Hence, this concluded that PCC synthesized by P123/CTAB template possessed high dissolution capacity and was able to impose high reduction power on oxidized metal and SO_4^{2-} ions.

4.2.3 Effect of PCC on Conductivity of AMD

Conductivity represented current being transferred by cations and anions present in AMD solution. Factors influencing conductivity comprised of concentration, mobility of ions, valence of ions as well as temperature (Radiometer Analytical SAS, 2004). Figure 4.7 represents the variation of conductivity of AMD treated using PCC synthesized by various surfactant-polymer templates with time. The initial conductivity of raw AMD was measured as 171.8 to 193.5 µS. A sudden decline was recorded upon the addition of PCC synthesized by various surfactant-polymer templates into individual beakers. Afterwards, no further decrease was measured before conductivity increased steeply which was then followed by a gradual increment in conductivity throughout the remaining contact time. After subjecting to 52 min flocculation and further 30 min sedimentation, the final conductivity readings obtained were 197.8 µS, 238.4 µS, 225.4 µS and 222.4 µS for AMD treated with PCC synthesized by CTAB, P123/CTAB, PEG/CTAB and PVA/CTAB surfactant-polymer templates, respectively. Throughout the entire flocculation and sedimentation, all of the conductivity readings were in compliance with the limit of 1000 µS established by NWQS Class IIA.

An increase in electrical conductivity and solution pH could be contributed by the release of light metal ions which included Ca^{2+}, Na^{+}, K^{+} and Mg^{2+} ions (Rangabhashiyam and Balasubramanian, 2019). This findings was supported by the dissolution of PCC to form Ca^{2+} ions (Kaur, Couperthwaite and Millar, 2018). It was suggested that an increase in ionic strength would cause a decline in the adsorption removal of heavy metal ions and enhanced the solubility of metal hydroxide precipitation (Ben Ali, et al., 2019). The

removal efficiency of heavy metal ions might have decrease possibly owing to the saturation of sites on surface of PCC for adsorption. On the contrary, solubility of metal hydroxide precipitation was also governed by solution pH and hence, the effect of ionic strength on it may not be pronounced.

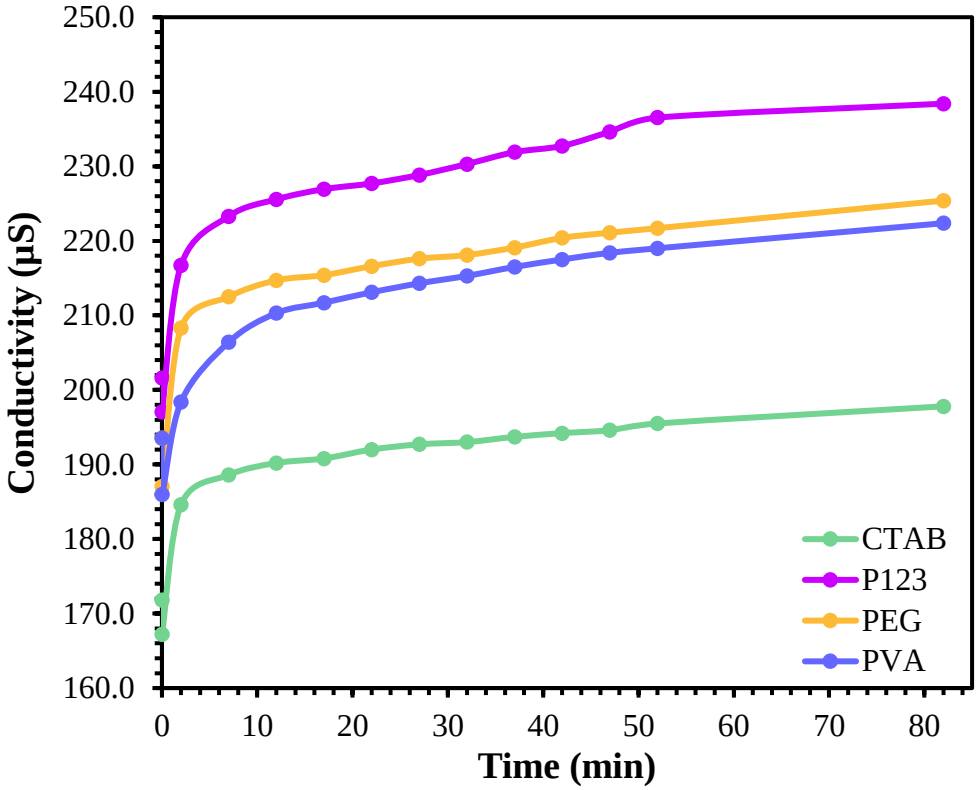

Figure 4.7: Variation of Conductivity of AMD Treated Using PCC Synthesized by Various Surfactant-Polymer Templates.

In a study performed by Türker (2018), electrical conductivity was observed to decrease in the outflow of duckweed-based wastewater treatment systems coupled with microbial fuel cell (DWWT-MFC) reactor compared to the inflow due to a removal of several cationic and anionic ions in the reactors matrix, which was possibly associated with precipitation. Throughout the entire contact time of 82 min, PCC synthesized by P123/CTAB template attained the highest conductivity and thus, this reinforced its high dissolution of PCC to yield more Ca^{2+} ions for better treatment efficiency.

4.2.4 Effect of PCC on Heavy Metal Ion Removal

Concentrations of various metal elements were analyzed for AMD solution before and after subjected to treatment using PCC synthesized by various surfactant-polymer templates to determine the removal efficiency of heavy metal ions. The elements of heavy metals selected for analysis were manganese (Mn), iron (Fe), nickel (Ni), copper (Cu), zinc (Zn), aluminum (Al) and arsenic (As). Figure 4.8 depicts the overall concentration of heavy metals present in AMD solutions which were treated with PCC synthesized by various surfactant-polymer templates. Prior to treatment, raw AMD was characterized with a concentration of 29.46 mg/L of Mn, 76.46 mg/L of Fe, 4.76 mg/L of Ni, 4.07 mg/L of Cu, 9.74 mg/L of Zn, 14.24 mg/L of Al and no detectable trace of As. The order of heavy metal ions present in AMD was Fe, Mn, Al, Zn, Ni and Cu. Due to the absence of As, no explanation shall be made on its removal mechanism.

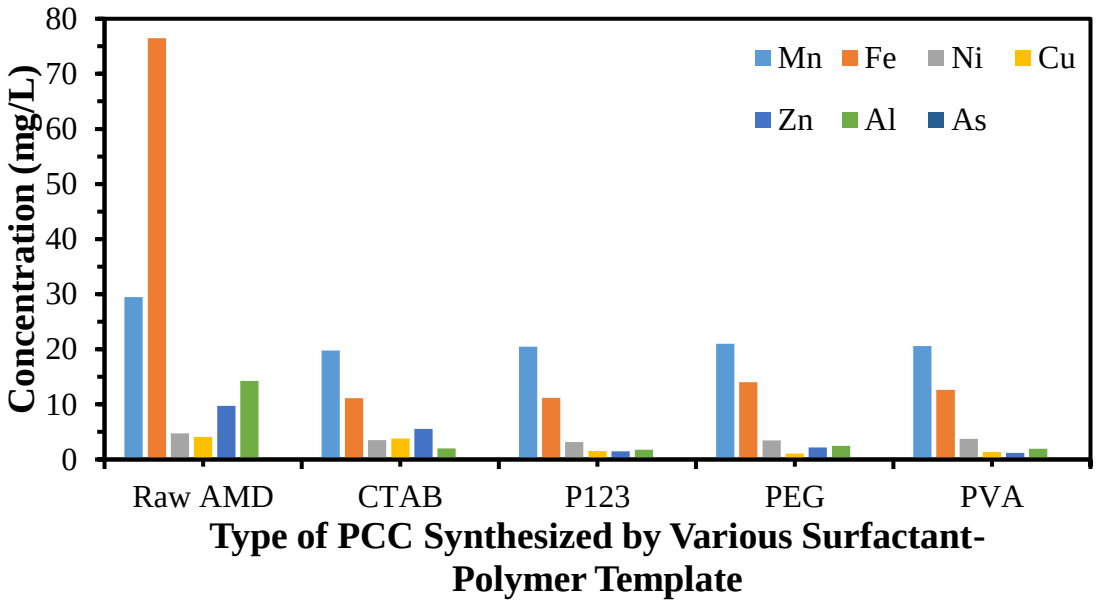

Figure 4.8: Overall Concentrations of Heavy Metals in AMD Solutions Treated Using PCC Synthesized by Various Surfactant-Polymer Templates.

After AMD treatment using PCC products, the final concentrations for Al was observed to be 2.02 mg/L with 85.83 %, 1.76 mg/L with 87.63 %, 2.49 mg/L with 82.51 %

and 1.92 mg/L with 86.50 % removal efficiency for PCC synthesized by CTAB, P123/CTAB, PEG/CTAB and PVA/CTAB surfactant-polymer template, respectively. In terms of Ni, the final concentrations were measured to be 3.54 mg/L (25.69 %), 3.18 mg/L (33.21 %), 3.47 mg/L (27.22 %) and 3.76 mg/L (21.09 %) for AMD treated using PCC synthesized by CTAB, P123/CTAB, PEG/CTAB and PVA/CTAB surfactant-polymer templates, respectively. Among these metal ions, the removal efficiencies of metal ions decreased by the order of Al, Fe, Zn, Cu, Mn and finally Ni. From the above findings, it can be concluded that PCC synthesized by P123/CTAB template showed the highest removal efficiencies for both metal ions. This was also achieved by CTAB with highest percentage removal for two metal ions (32.86 % Mn and 85.47 % Fe). The sequence was then followed by PCC synthesized by PVA/CTAB and finally PEG/CTAB.

The resulting Zn concentrations from the AMD treatment using PCC synthesized by P123/CTAB and PVA/CTAB did meet the acceptable conditions of Class IIA (5.0 mg/L), Standards A (2.0 mg/L) and B (2.0 mg/L), but not WHO (0.01 mg/L). All of the above mentioned Al concentrations complied with the acceptable conditions of Standards A (10 mg/L) and B (15 mg/L), but not WHO (0.2 mg/L). None compliance was observed for all Mn, Fe, Ni and Cu concentrations to limits of any applicable standard, including NWQS Class IIA (0.1 mg/L Mn, 1.0 mg/L Fe, 0.05 mg/L Ni and 0.02 mg/L Cu), Standards A (0.2 mg/L Mn, 1.0 mg/L Fe, 0.2 mg/L Ni, 0.2 and mg/L Cu) and B (1.0 mg/L Mn, 5.0 mg/L Fe, 1.0 mg/L Ni, 1.0 and mg/L Cu), WHO (0.1 mg/L Mn, 0.3 mg/L Fe, 0.07 mg/L Ni, 2 mg/L of Cu, 0.01 mg/L Zn and 0.2 mg/L Al) and EPA (2.0 mg/L Fe). The details of these metal concentrations are displayed in Appendix A8 to A12.

Principle removal mechanism of heavy metal ions involved precipitation whereby heavy metal ions combined with the dissolution products of PCC, hydroxyl (OH^-) ions and other anions, to produce less soluble metal hydroxide precipitate (Kaur, et al., 2018). Sorption or co-precipitation mechanism may occur along with FeO(OH) formation to remove other metal ions such as Mn (Kaur, et al., 2017). These two represented another removal mechanism which could occur if the solution pH fell below the precipitation pH of that particular heavy metal ion (Muliwa, Leswifi and Onyango, 2018). The equations

of heavy metal ion removal mechanism were as shown in Eqs. (4.4) – (4.14) (Kaur, et al., 2018; Muliwa, Leswifi and Onyango, 2018; Othman, Sulaiman and Sulaiman, 2017; Seo, et al., 2017; Name and Sheridan, 2014).

$$Mn^{2+} + 2OH^- \rightarrow Mn(OH)_2 \quad (4.4)$$

$$Fe^{3+} + 2OH^- \rightarrow Fe(OH)_2 \quad (4.5)$$

$$Fe^{3+} + 2OH^- \rightarrow FeOOH + H^+ \quad (4.6)$$

$$Ni^{2+} + CO_3^{2-} \rightarrow NiCO_3 \quad (4.7)$$

$$Ni^{2+} + SO_4^{2-} \rightarrow NiSO_4 \quad (4.8)$$

$$Cu^{2+} + SO_4^{2-} + 6OH^- \rightarrow Cu(SO_4)(OH)_6 \quad (4.9)$$

$$CuSO_4 + 2OH^- \rightarrow CuO + SO_4^{2-} + H_2O \quad (4.10)$$

$$Zn^{2+} + 2CO_3^{2-} + 6OH^- \rightarrow Zn_5(CO_3)_2(OH)_6 \quad (4.11)$$

$$Zn^{2+} + SO_4^{2-} \rightarrow ZnSO_4 \quad (4.12)$$

$$Al^{3+} + 3OH^- \rightarrow Al(OH)_3 \quad (4.13)$$

$$Al(OH)_3 + OH^- \rightarrow (Al(OH)_4)^- \quad (4.14)$$

Several reasons could contribute to the order of metal ion removal efficiencies. Selective precipitation occurred due to influence by pH with a sequence as follows: (pH > 6) Fe^{3+}, Al^{3+}, Fe^{2+}, Cu^{2+}, Zn^{2+}, Ni^{2+} to Mn^{2+} (pH > 9) (Kaur, et al., 2018; Masindi, et al., 2017). In a study conducted by Masindi, et al. (2017), the effect of pH precipitation was supported whereby pH was raised to above 6 and achieved removal efficiencies of 99 % Al and 20 % Mn for limestone. For this current study, the results showed similar trend whereby the final pH ranging from 7.02 to 8.22 supported Al precipitation, however, was insufficient for complete Mn removal in AMD solutions subjected to treatment using PCC synthesized by various polymer-surfactant templates. Another factor affecting metal ion removal could be the surface area of precipitates produced during AMD treatment. The removal of Ni, Cu and Zn could be performed through adsorption onto surface area of gypsum floc (Kaur, et al., 2018). Due to the low concentration of Cu, its removal could be conducted in this manner, which was supported by the high percentage removal of SO_4^{2-} ions (69.58 %) possibly leading to gypsum formation for PCC synthesized by PEG/CTAB.

Overall, PCC synthesized by CTAB and P123/CTAB surfactant-polymer template exhibited the highest removal efficiency for most elements. In literature work conducted by Hashemi, Eslami and Karimzadeh (2019), zeolites modified by cationic surfactant had been commonly applied in removal of heavy metal ions such as Pb^{2+} ion. The introduction of surfactant aided in altering the surface charge of zeolite to adsorb wastewater pollutants (Palmer and Hatley, 2018). Being a cationic surfactant, this results proposed the significance of the role of CTAB in PCC for heavy metal ion removal. However, due to the non-compliance of Zn in PCC synthesized by CTAB, PCC synthesized by P123/CTAB was opted as the optimum surfactant-polymer templates for PCC synthesis in heavy metal ion removal.

4.2.5 Effect of PCC on Sulphate Ion Removal

Figure 4.9 depicts both initial and final SO_4^{2-} ion concentration of AMD solutions which were treated using PCC synthesized by various surfactant-polymer templates. Prior to treatment, SO_4^{2-} ion concentration of raw AMD was analyzed as 2510.27 mg/L. After being subjected to neutralizing agent PCC, concentrations of SO_4^{2-} ion in AMD exhibited an increasing sequence of 763.69 mg/L (69.58 %), 793.51 mg/L (68.39 %), 1057.12 mg/L (57.89 %) and 1357.90 mg/L (45.91 %) for treatment using PCC synthesized by PEG/CTAB, P123/CTAB, CTAB and PVA/CTAB surfactant-polymer templates respectively. The results signified that each type of synthesized PCC was able to significantly remove SO_4^{2-} ion in which PEG/CTAB demonstrated the best removal efficiency.

It was elucidated that raw AMD contained pyrite which upon exposure to air and moisture resulted in pyrite oxidation to produce a high yield of SO_4^{2-} ions and sulphuric acid (H_2SO_4) (Potgieter-Vermaak, et al., 2006). The removal mechanism of SO_4^{2-} ion was initiated by dissolution of PCC in AMD to form Ca^{2+} ions as shown in the previous equation Eq. (4.1). As a result of PCC dissolution, AMD was saturated with Ca^{2+} as well

as SO_4^{2-} ions whereby both ions reacted via precipitation to yield partially soluble gypsum, which could represented the dominant species as well as other sulphate precipitates, for example, nickel sulphate ($NiSO_4$), bronchantite ($Cu_4SO_4(OH)_6$) and zinc sulphate ($ZnSO_4$) (Muliwa, Leswifi and Onyango, 2018; Kaur, et al., 2018; Name and Sheridan, 2014) Crystallization of gypsum immobilized SO_4^{2-} ions, however, this precipitation mechanism could only be applied to SO_4^{2-} ions associated with free acids, therefore, only partial reduction of sulphates was performed (Muliwa, Leswifi and Onyango, 2018). The removal mechanism can be expressed as shown in Eq. (4.15).

$$Ca^{2+} + SO_4^{2-} + 2H_2O \rightarrow CaSO_4.2H_2O \qquad (4.15)$$

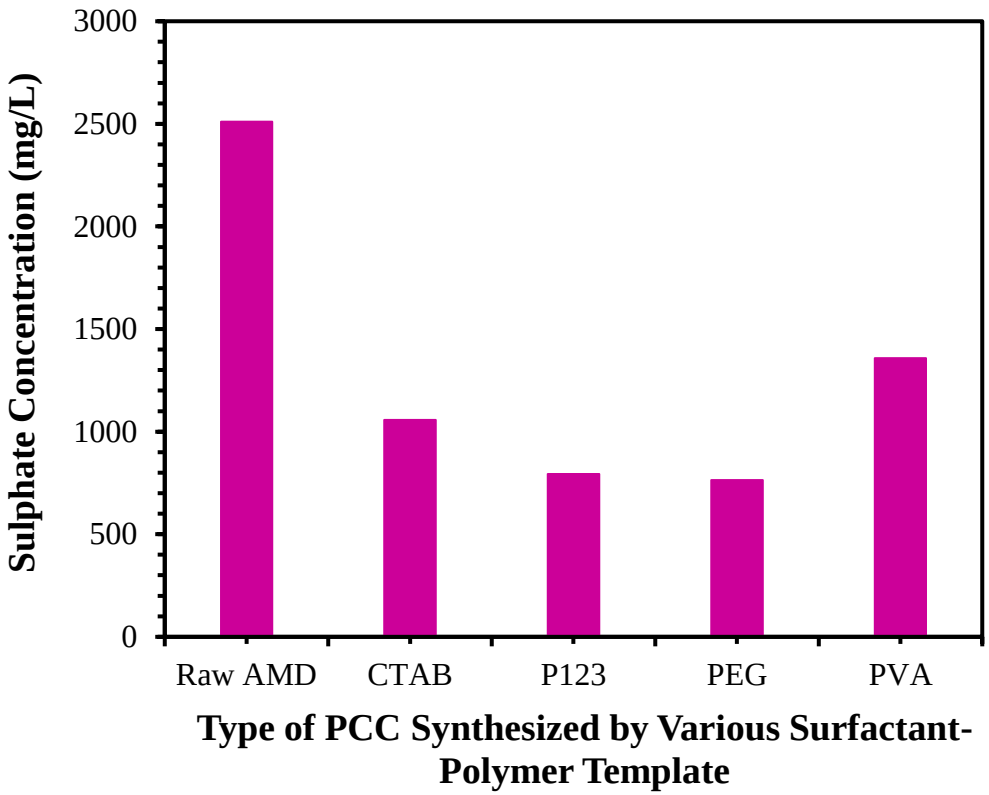

Figure 4.9: Variation of Sulphate Concentration with PCC Synthesized by Various Surfactant-Polymer Templates.

Literatures revealed the removal efficiencies of SO_4^{2-} ion subjected to similar neutralizing agents as compared to PCC (Masindi, et al., 2017; Potgieter-Vermaak, et al., 2006). In a study performed by Masindi, et al. (2017), the addition of various Ca-based neutralizing agents into AMD solutions demonstrated varying degrees of removal efficiencies of SO_4^{2-} ion. Under a fixed dosage of 10 g/L, SO_4^{2-} ion concentration was reduced from 80,000 mg/L to 9000 mg/L, 3005 mg/L and 3705 mg/L with the addition of limestone, hydrated lime and lime respectively. Potgieter-Vermaak, et al. (2006) studied the effectiveness of pre-treatment agents in AMD whereby limestone had removed SO_4^{2-} ion from 6000 mg/L to 1869 mg/L. From the findings, Ca-derived agents were found to provide saturation of Ca^{2+} ions in solution for effective SO_4^{2-} ion removal performance. In this study, PCC synthesized by various surfactant-polymer template could be hypothesized to dissolute and produce varying saturation of Ca^{2+} ions. SO_4^{2-} ion precipitation was also affected by the effective removal of other metal ions such as Ni, Cu and Zn (Kaur, et al., 2018). Overall, PCC synthesized by PEG/CTAB surfactant-polymer template displayed the optimum SO_4^{2-} ion removal, and was closely followed by P123/CTAB which may be associated with highest removal of Ni ions.

4.3 Effect of Different Dosages of PCC Synthesized by P123/CTAB Template on AMD Treatment

4.3.1 Effect of PCC Dosages on pH of AMD

The neutralization rate of AMD was monitored by examining the variation in pH of AMD subjected to various dosages of PCC synthesized by P123/CTAB. Figure 4.10 illustrates the variation in pH of AMD which was treated using various dosages of PCC synthesized by P123/CTAB surfactant-polymer template. Upon addition of various dosages, pH of AMD was immediately increased before gradually flattening to produce constant readings. After subjecting to 30 min sedimentation, the end point pH values were measured as 7.94, 7.67, 8.22, 8.36, 8.58 for dosages of 0.10 g/L, 0.20 g/L, 0.30 g/L, 0.40 g/L and 0.50 g/L,

respectively of PCC synthesized by P123/CTAB surfactant-polymer template. Each of the dosages except for 0.50 g/L conformed to acceptable conditions of Standards A (pH 6.0 – 9.0) and B (pH 5.5 – 9.0), DOE NWQS Class IIA (pH 6.0 – 9.0), Ore Mining Operations Effluent Guidelines (pH 6.0 – 9.0) and WHO Guidelines on Drinking Water Quality (pH 6.5 – 8.5).

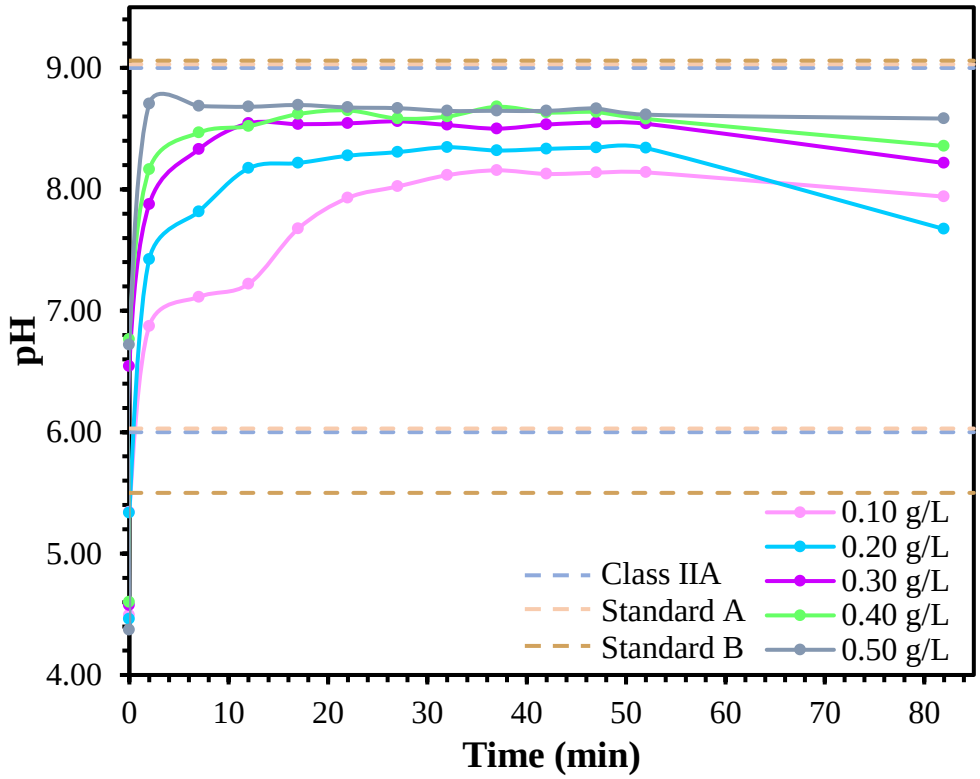

Figure 4.10: Variation of pH with Dosage of PCC Synthesized by P123/CTAB Surfactant-Polymer Template.

Overall, higher dosages resulted in more pronounced increase in pH values. The reason was due to high acidity content of raw AMD which inundated low dosages of PCC synthesized by P123/CTAB template (Muliwa, Leswifi and Onyango, 2018). Lower concentration of $CaCO_3$ could not manage to react with much H^+ ions and yield Ca^{2+} and HCO_3^- ions via dissolution of PCC. Therefore, low PCC dosages could not achieve high neutralizing rate. In addition to complete PCC dissolution, partial dissolution of PCC

could also occur in the presence of water to form $Ca(OH)^+$ and $Ca(OH)_2$. in which the latter product split into Ca^{2+} ion and hydroxide ion (OH^-) as shown in Eq. (4.16) (Kastyuchik, Karam and Aïder, 2016).

$$Ca(OH)_2 \rightarrow Ca^{2+} + 2OH^- \quad (4.16)$$

The OH^- ion represented a strong base, whereby pH increased with its concentration. Depending on the dosage of PCC, the dissolution rate was found to differ. Under high concentration of PCC, dissolution of $CaCO_3$ yielded more alkalinity in the forms of CO_3^{2-}, HCO_3^- and OH^- ions rather than acidity which could be present as H_2CO_3 (Kastyuchik, Karam and Aïder, 2016). Hence, the net alkalinity produced in higher dosages induced a rise in pH, Ca^{2+} and HCO_3^- ion activities and reduction in partial pressure of CO_2 (Muliwa, Leswifi and Onyango, 2018). This could be accompanied by a decrease in the rate of PCC dissolution which may be due to the saturation of AMD with Ca^{2+} ions. Another reason could be the reaction of Ca^{2+} ions with SO_4^{2-} ions in which the latter immobilized Ca^{2+} and hindered any further yield of alkalinity (Masindi, et al., 2017).

In other research works, similar trends in pH have been observed with varying dosages. Sulaiman, Othman and Ibrahim (2018) utilized magnesium oxide (MgO) as a neutralizing agent whereby an increment in dosage from 2.0 g/L, 3.0 g/L to 4.0 g/L resulted in a pH rise from 6.68, 8.48 to 8.58 under a contact time of 30 min. The dosage of 3.0 g/L was chosen as the optimum dosage due to its compliance with Standards A and B. Kaur, et al. (2017) showed that an increase in the amount of lime from 1.6 mmol to 3.3 mmol had increased the pH readings from 3.72 to 9.19. For Ca-based agents, each mole of Ca^{2+} ion present in the solution was capable of neutralizing 2 mol of H^+ ion (Sephton, Webb and McKnight, 2019). Thus, an increment in dosage elevated the number of Ca^{2+} ion moles which in turn strengthened the AMD neutralizing performance of that particular dosage. For this current study, although the dosage of 0.50 g/L PCC synthesized by P123/CTAB template showed the highest neutralizing power, its pH readings were critically near the upper limits of most standards after a short contact time of 2 min.

Moreover, due to economic reasons, dosage of 0.40 g/L was selected as the optimum dosage for PCC synthesized by P123/CTAB surfactant-polymer template.

4.3.2 Effect of PCC Dosages on ORP of AMD

Figure 4.11 presents the variation of ORP of AMD being subjected to various dosages of PCC synthesized by P123/CTAB template. After the addition of PCC, ORP was observed to decline from positive to negative readings and reached a steady state. After 30-min sedimentation, the final ORP readings were -35.2 mV, -35.9 mV, -60.4 mV, -61.4 mV and -69.1 mV for a dosage of 0.10 g/L, 0.20 g/L, 0.30 g/L, 0.40 g/L and 0.50 g/L respectively. It indicated that all AMD solutions were in reduction state. Overall, there was a reduction in ORP as dosage increased, which indicated net reduction of the oxidized metal ions.

Higher ORP denoted a restriction for reducible metals to be released (Dai, et al., 2019). This was observed in the initial ORP readings, whereby dissolution of PCC was insufficient and thus, oxidized metals were the dominant species. It could be elucidated that higher dosages allowed shorter contact time to achieve steady neutralization rate as supported by literatures (Name and Sheridan, 2014; Heviánková, et al., 2013; Potgieter-Vermaak, et al., 2006). The contact time represented a factor for the rate of contaminant removal from a solution (Muliwa, Leswifi and Onyango, 2018). This signified that higher dosages imposed faster reducing power on oxidized metals and might be able to generate higher metal ion removal efficiencies (Jones and Cetin, 2017).

Guo, et al. (2019) reported that with an increase in dosages of zero-valent iron (ZVI) powder from 0 mg/L to 1000 mg/L caused ORP readings within two separate reactors decreased from 89 – 261 mV to 75 – 176 mV due to the high reducibility powers of ZVI. In another study by Li, et al. (2018), it was observed that the addition of a slight amount of oxidants was not able to alter the ORP readings significantly as well as its property of reduction or oxidation. These findings hinted the importance of dosage on

affecting the solution ORP. The dosage of 0.50 g/L represented the best selection for optimization due to its lowest ORP reading. However, dosage of 0.40 g/L could be opted as the optimum loading owing to economic considerations as well as the close resemblance of ORP readings.

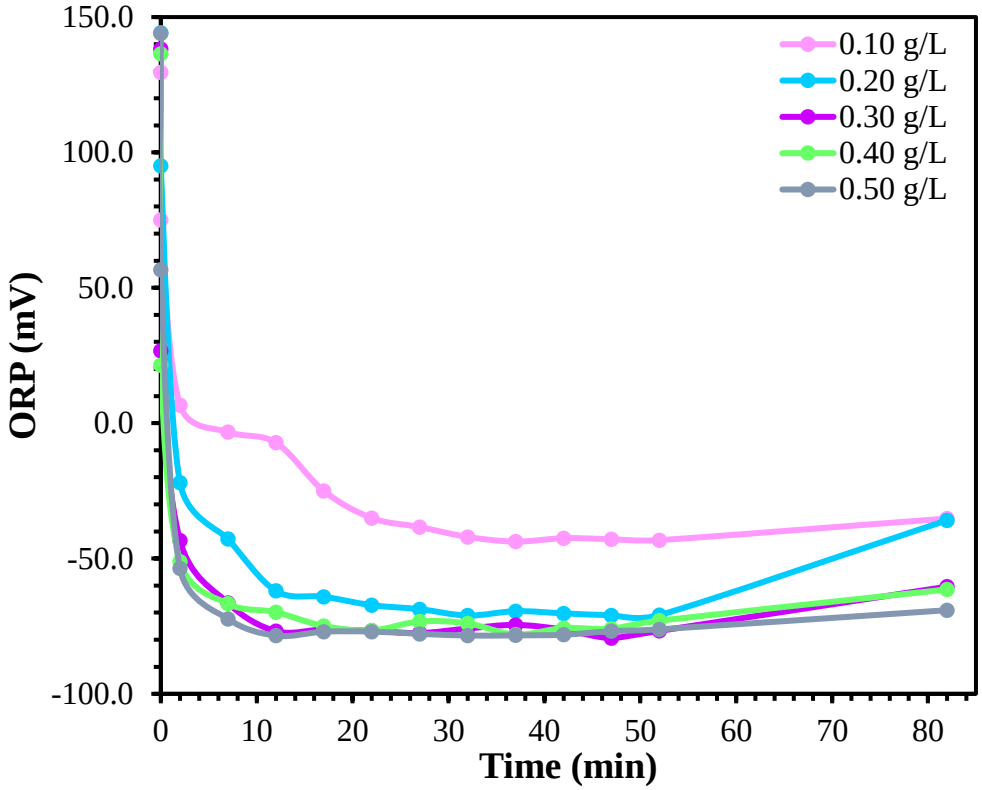

Figure 4.11: Variation of ORP with Dosage of PCC Synthesized by P123/CTAB Surfactant-Polymer Template.

4.3.3 Effect of PCC Dosages on Conductivity of AMD

Figure 4.12 shows the change in conductivity of AMD with respect to various dosages of PCC synthesized by P123/CTAB surfactant-polymer template. Conductivity ranged from 198.0 µS to 216.0 µS which immediately decreased upon introduction of various dosages of PCC. Afterwards, there was a constant rise in conductivity to yield end conductivity

readings of 221.5 µS, 237.6 µS, 238.4 µS, 230.1 µS and 249.7 µS for AMD treatment using PCC synthesized by P123/CTAB of dosages 0.10 g/L, 0.20 g/L, 0.30 g/L, 0.40 g/L and 0.50 g/L, respectively. Overall, an increment in conductivity was found to be associated with an increase in dosage. All conductivity readings were in compliance with NWQS Class IIA limit of 1000 µS.

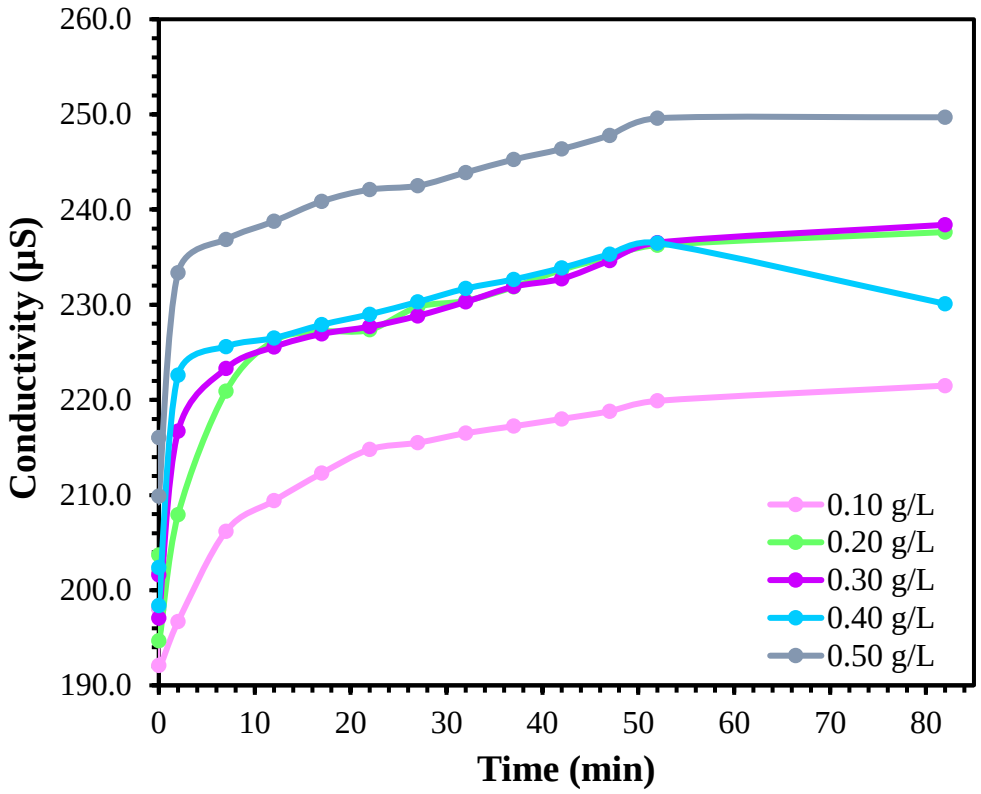

Figure 4.12: Variation of Conductivity with Dosage of PCC Synthesized by P123/CTAB Surfactant-Polymer Template.

The relationship between conductivity and dosage could be explained by the dissolution of soluble minerals present in PCC occurred upon mixture of PCC into AMD. The resulting mixture could be expected to exhibit high conductivity values as a result of greater dissolution due to higher dosages (Mackie and Walsh, 2015). An increment in conductivity with time was also observed and this could be a result of increase in calcite dissolution with reaction time as supported by Kastyuchik, Karam and Aïder (2016). Xu,

et al. (2018) hypothesized another reason owing to the increase in conductivity with time which was due to the release of significant amount of electrolytes. This reinforced the occurrence of PCC dissolution which introduced more ionic species in the form of Ca^{2+} ions into AMD.

The conductivity served as a representation of ionic strength of a solution. Mackie and Walsh (2015) mentioned that elevated ionic strength would provide better compression of electrical double layer of colloids, which in turn lowered repulsive electrostatic forces. Consequently, collisions of colloids would be increased for aggregation to occur. This was supported by literature work whereby an improvement in the removal efficiency of Zn^{2+} ions from 76.7 % to 88.0 % was correlated with an elevation in solution conductivity from 0.15 mS/cm to 9.72 mS/cm (Chen, et al., 2018). For this current study, a slight decrease in the change of conductivity at the end of the 30-min sedimentation may signified a reduction in the ionic strength due to precipitation of cations and anions. Overall, dosage of 0.50 g/L which exhibited the highest conductivity readings may be hypothesized to possess higher heavy metal ion removals and high release of light metal ions such as Ca^{2+} ions due to its high dissolution abilities.

4.3.4 Effect of PCC Dosages on Heavy Metal Ion Removal

Figure 4.13 depicts the overall metal concentrations present in AMD after being subjected to various dosages of PCC synthesized by P123/CTAB surfactant-polymer template. In terms of Al, the concentrations achieved 2.25 mg/L (84.21 %), 2.02 mg/L (85.81 %), 1.76 mg/L (87.63 %), 1.68 g/L (88.21 %) and 1.67 mg/L (88.98 %) after being subjected to dosages of 0.10 g/L, 0.20 g/L, 0.30 g/L, 0.40 g/L and 0.50 g/L, respectively. The least removal efficiency resided with Mn whereby the concentrations were measured as 22.87 mg/L (22.37 %), 21.93 mg/L (25.56 %), 20.48 mg/L (30.48 %), 19.88 mg/L (32.52 %) and 16.60 mg/L (43.65 %) for dosages of 0.10 g/L, 0.20 g/L, 0.30 g/L, 0.40 g/L and 0.50 g/L, respectively of PCC synthesized by P123/CTAB template. As a conclusion, the

sequence of removal efficiencies was arranged as Al, Fe, Zn, Cu, Ni and Mn. For all metal elements, a decrease in heavy metal ion concentration was observed with a rise in the dosage. The dosage of 0.50 g/L represented the dosage with the highest removal efficiency for all metal ions, with dosage of 0.10 g/L being the least.

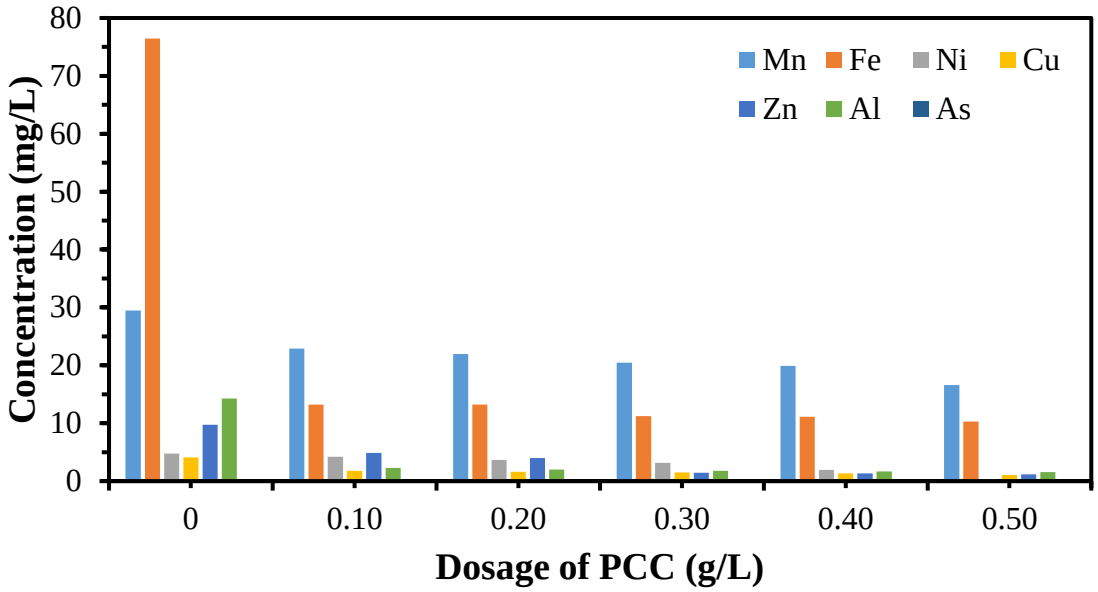

Figure 4.13: Overall Concentrations of Heavy Metals in AMD Treated Using Various Dosages of PCC Synthesized P123/CTAB Surfactant-Polymer Template.

All of the AMD solutions treated by high dosages of 0.30 g/L, 0.40 g/L and 0.50 g/L were able to meet the limits of NWQS Class IIA (5.0 mg/L Zn), Standards A (10 mg/L Al and 2.0 mg/L Zn) and B (15 mg/L Al and 2.0 mg/L Zn) for metal concentrations of Al and Zn. The dosage of 0.50 g/L was able to comply with limit of Standard B for Ni (1.0 mg/L) as well. The exception was dosage of 0.10 g/L and 0.20 g/L which did not fulfilled limits of Zn (Standards A and B). None of the dosages conformed to the limits of NWQS Class IIA (0.1 mg/L Mn, 1.0 mg/L Fe, 0.05 mg/L Ni and 0.02 mg/L Cu), Standards A (0.2 mg/L Mn, 1.0 mg/L Fe, 0.2 mg/L Ni and 0.2 mg/L Cu) and B (1.0 mg/L Mn, 5.0 mg/L Fe and 1.0 mg/L Cu), WHO (0.1 mg/L Mn, 0.3 mg/L Fe, 0.01 mg/L Zn and 0.1 mg/L Al) and USEPA (2.0 mg/L Fe) for Mn, Fe, Ni, Cu, Zn and Al. The details of these metal concentrations due to various PCC dosages are shown in Appendix A13 to A17.

There were several reasons for the observed order of removal efficiencies. The relationship between dosages and removal ability could be reinforced by the findings whereby limited active sites of neutralizing agents deterred the removal efficiency of heavy metal ions. An increase in dosage would yield more active sites to promote adsorption as well as precipitation and thus enabling better removal efficiency (Muliwa, Leswifi and Onyango, 2018). In addition, percentage removal of Ni was correlated to the concentration of SO_4^{2-} ions due to the formation of $NiSO_4$ precipitate (Kaur, et al., 2018). It was observed that both concentrations of Ni and SO_4^{2-} ions decreased with increasing dosages, whereby the percentage removal of Ni increased drastically due to its original concentration being very low (4.76 mg/L). High removal efficiencies of Al ions could be contributed by the production of calcium aluminium hydroxide co-precipitates which increased with increment in Ca^{2+} concentration and PCC dosage, as shown in Eq. (4.17) (Kaur, et al., 2018).

$$2Ca^{2+} + 2OH^- + 2[Al(OH)_4]^- + nH_2O \rightarrow Ca_2(H_2O)_n[Al_2(OH)_{10}] \quad (4.17)$$

Moreover, it was observed that different dosages achieved different pH readings which may impose selective precipitation. Seo, et al. (2017) reported that the recovery rates of metal concentrations were 93.5 % – 97.9 % of Al for a pH of 5.5, and 52.8 % – 79.9 % of Fe for a pH of 7.5, 72.3 % – 87.5 % of Mn for a pH of 10.5 when treated by NaOH, $Ca(OH)_2$ and Na_2CO_3. In another study, the addition of Bayer precipitates caused an elevation in pH from 3.72 to 6.05 with removal efficiencies of 99.79 % Al and 58.39 % Mn for a dosage of 20.1 g/L and a pH elevation to 8.00 with removal efficiencies of 99.9 % Al, 82.82 % Mn for a dosage of 60 g/L (Kaur, et al., 2018). These findings signified the induction of selective precipitation by pH rise. It was further supported by Seo, et al. (2017) that the order of removal was Al, Fe and Mn, whereby the type of neutralizing agents utilized had no influence on this sequence. From both findings, Mn was found to achieve better removal percentages in the presence of high dosage and thus high pH as supported by the results of dosage 0.50 g/L in this research work. This study revealed similar pH readings for both dosage of 0.40 g/L and 0.50 g/L with significant difference in the metal removal efficiencies, especially for Ni due to its low concentration. Otherwise, dosage of

0.40 g/L would be supported as the optimum dosage as concentrations of other heavy metal ions closely resembled that of dosage 0.50 g/L.

4.3.5 Effect of PCC Dosages on Sulphate Ion Removal

Figure 4.14 illustrates the concentration of SO_4^{2-} ion in AMD before and after being treated by various dosages of PCC synthesized by P123/CTAB surfactant-polymer template. The initial SO_4^{2-} ion concentration of 2510.27 mg/L of raw AMD was reduced to 1252.24 mg/L (50.12 %), 964.50 mg/L (61.58 %), 793.51 mg/L (68.39 %), 683.65 mg/L (72.77 %) and 605.16 mg/L (75.89 %) as a result of being subjected to dosages of 0.10 g/L, 0.20 g/L, 0.30 g/L, 0.40 g/L and 0.50 g/L of PCC synthesized by P123/CTAB template. The concentration of SO_4^{2-} ion was found to be inversely proportional to the dosage of PCC, as revealed by Masindi, et al. (2017).

The trend of concentration of SO_4^{2-} ion could be explained by factors influencing the removal efficiency of SO_4^{2-} ion which included contact time as well as availability of Ca^{2+} ion. Higher dosages of PCC exhibited a larger total surface area for enhanced dissolution of PCC (Muliwa, Leswifi and Onyango, 2018). With higher concentration of Ca^{2+} ion, an increase of SO_4^{2-} ions could be precipitated to form gypsum. Potgieter-Vermaak, et al. (2006) concluded that precipitation represented the main mechanism for SO_4^{2-} ion removal by neutralizing agents which were found to be rich in Ca. Other than precipitation, sorption of SO_4^{2-} ion could also be induced to occupy the surface of PCC (Fernando, et al., 2018). However, as the concentration of gypsum in AMD solution neared the saturation point, dissolution of PCC may be reduced or completely hindered which could be supported by similar SO_4^{2-} ion removal efficiencies between higher PCC dosages.

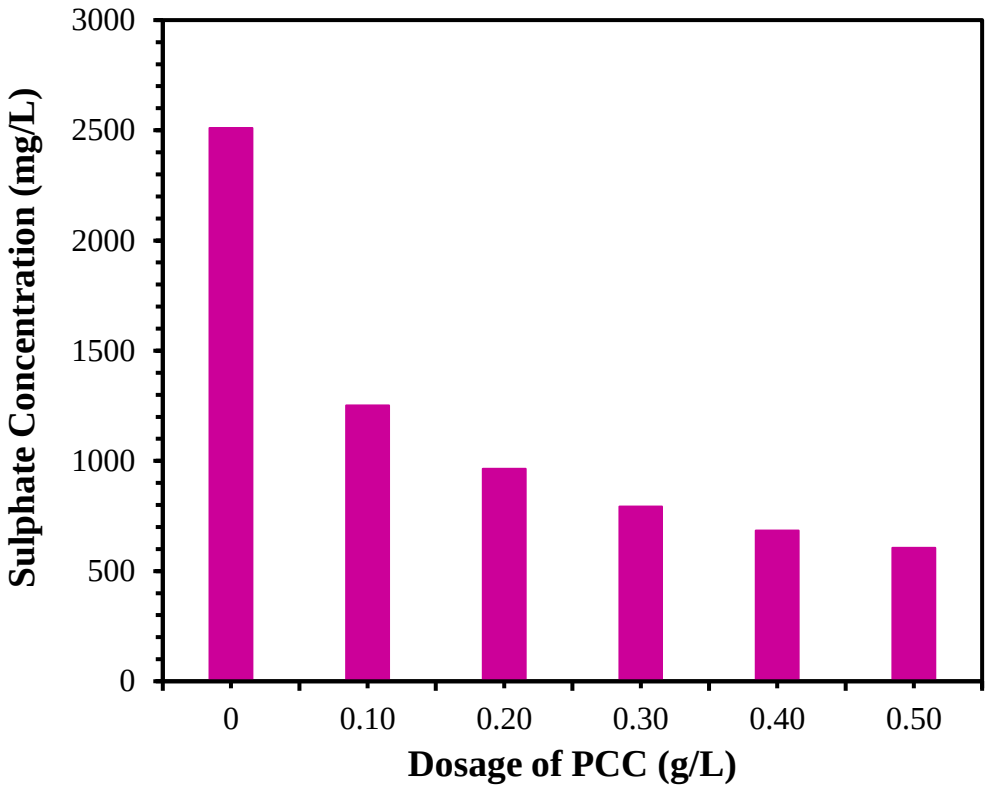

Figure 4.14: Variation of Sulphate Concentration with Dosage of PCC Synthesized by P123/CTAB Surfactant-Polymer Templates.

Literature works reported similar relationship between dosage and SO_4^{2-} ion removal efficiency. Sulaiman, Othman and Ibrahim (2018) mentioned that an increase in dosage of MgO from 1.0 g/L, 2.0 g/L to 3.0 g/L showed a reduction in sulphur content of AMD from 3.03 %, 1.87 % to 1.53 %. In another research, Potgieter-Vermaak, et al. (2006) stated SO_4^{2-} ion decreased from 6000 mg/L to 1869 mg/L and 1827 mg/L in AMD when subjected to a dosage of 50 g/L and 100 g/L of limestone. This current findings revealed higher percentage removal were achieved with dosages 0.40 g/L and 0.50 g/L when compared to that of other dosages of PCC synthesized from P123/CTAB template. Both exhibited similar removal percentages (~70 %), therefore, dosage of 0.40 g/L was selected as the optimum dosage due to economic reasons.

4.4 Sludge Settling Test

From the previous section, it was concluded that P123/CTAB represented the best surfactant-polymer template with an optimum dosage of 0.40 g/L PCC. The addition of optimized PCC sample into AMD and deionized water (DIW) were used to evaluate the effect of optimized PCC on settling efficiency of sludge. Figure 4.15 illustrates the sludge settling curve of AMD and DIW treated by optimized PCC, (AMD-PCC) and (DIW-PCC), for a sedimentation time of 24 h. Both AMD-PCC and DIW-PCC demonstrated drastic drops in height of sludge interface before gradually decreasing to reach constant final sludge volumes of 6.50 mL/L for AMD-PCC and 1.50 mL/L for DIW-PCC. AMD-PCC displayed longer settling as compared to that of DIW-PCC. Both initial settling rate and final sediment volume had been reported to be significant in settling and compaction performance (Yan, et al, 2013). Figures 4.16a and b shows the apparatus set-up of Imhoff cones filled with AMD-PCC and DIW-PCC respectively at a settling time of 100 min. It was observed that both mixtures produced flocs of different sizes. The AMD-PCC exhibited larger, denser and rounder flocs which had initially been observed to settle rapidly (Figure 4.16a), as compared to DIW-PCC which displayed lighter and smaller flocs with smaller settling rate (Figure 4.16b).

Difference of settling rate in both AMD-PCC and DIW-PCC could be contributed by the precipitation of metal ions (Seo, et al., 2017). Addition of neutralizing agents attributed to the formation of sludge with efficient removal of heavy metal ions in AMD-PCC via the settling and sedimentation (Seo, et al, 2017; Marcello, et al., 2008; Sheoran and Sheoran, 2006). Significant flocs could be observed as a result of adequate residence time of the solutions as associated with size and depth of container as well as water quality and quantity (Skousen, Ziembiewicz and McDonald, 2019). The low settling rate of AMD-PCC could be also influenced by the presence of SO_4^{2-} ions which was found to generate and cause slow sedimentation of large amounts of secondary precipitates including $CaSO_4.2H_2O$ (Pozo, et al., 2017). The effect of floc size on the rate of sedimentation was influenced by water content. As a result, higher water content in DIW-PCC resulted in the formation of lighter flocs as compared to AMD-PCC flocs (Mackie

and Walsh, 2015). The final sludge volume of both mixtures in the presence and absence of ions proved that PCC particles represented suitable weighting materials to be used in sedimentation.

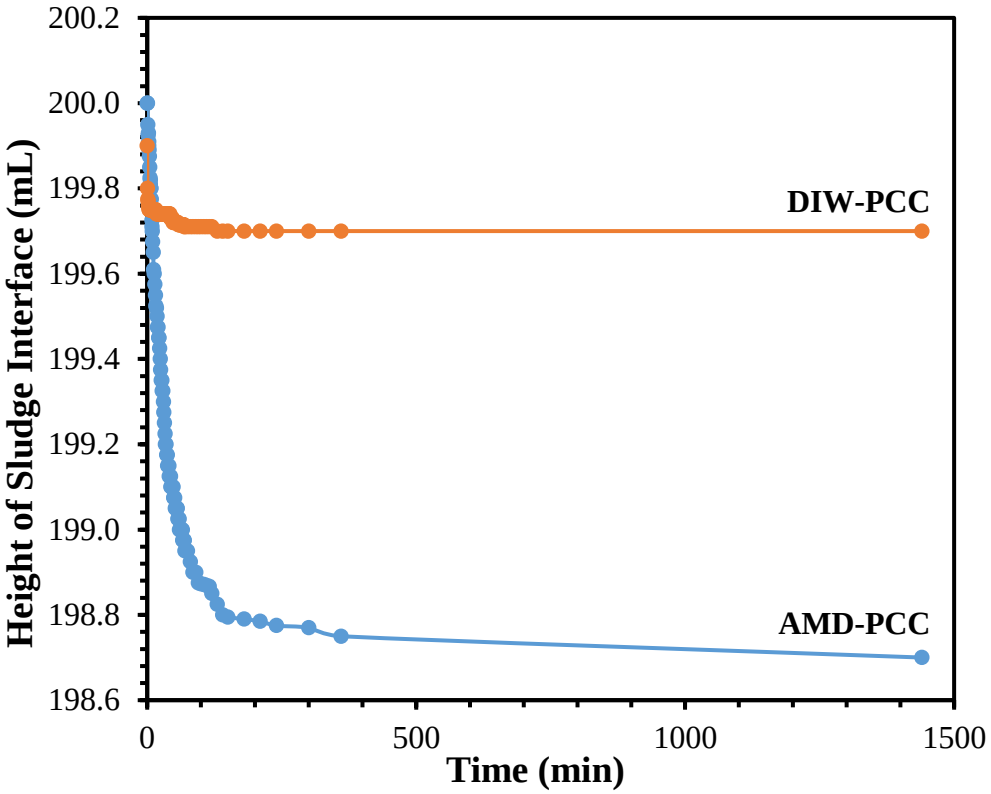

Figure 4.15: Sludge Settling Curves of (a) AMD-PCC and (b) DIW-PCC.

From the above findings, it could be interpreted that 0.65 % of sludge was generated per volume of AMD-PCC. With reference to other findings, Seo, et al. (2017) deduced a 10 % of sludge amount generated per 1 L of AMD as a result as of pH neutralization via 0.5 M sodium carbonate (Na_2CO_3) addition. As a comparison, the use of PCC with lower yield of sludge could signify cost savings in terms of reduced capital costs with smaller and lesser number of sedimentation ponds to be utilized in treatment plants (Muliwa, Leswifi and Onyango, 2018; Seo, et al., 2017). It can be concluded that addition of 0.40 g/L PCC synthesized by P123/CTAB template was sufficient for high settling rate, yet managed not to decrease the compressibility of sludge blanket as there

was no increase in volume over time. These two factors resulted from the high density of the produced sludge and represented important characteristics to be considered for the dosage of AMD weighing materials (Muliwa, Leswifi and Onyango, 2018; Demers, Finch and El-Ammouri, 2009).

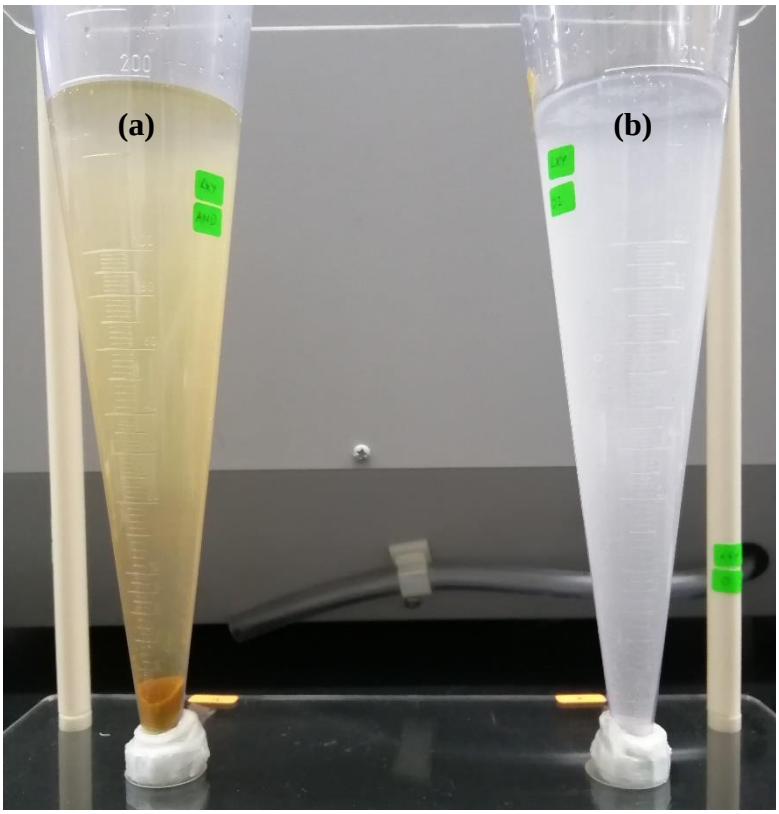

Figure 4.16: Settling Test of AMD Treatment with (a) AMD-PCC and (b) DIW-PCC after 100 Minutes.

4.5 Comparison between PCC and Literature Works

The use of PCC synthesized by various surfactant-polymer templates as a neutralizing agent for AMD treatment exhibited comparable results with literature works. Table 4.1 represents the comparison between neutralizing performance of PCC and other neutralizing agents towards AMD with respect to their neutralizing conditions. Othman,

Sulaiman and Sulaiman (2017) had utilized calcium lime waste with an optimum dosage of 1.5 g/L to neutralize AMD from a pH value of ~2.75 to ~8 within a contact time of 1 h 10 min. The neutralizing capacity of calcium lime waste achieved heavy metal ion removal efficiencies of ~40 % for Mn, ~99.9 % for Fe, ~90 % for Ni, >90 % for Cu, ~90 % for Zn, >90 % for Al and ~98 % for As. In another study, Masindi, et al. (2017) conducted a research on the effectiveness of soda ash in AMD treatment, whereby an optimum dosage of 10 g/L attained an increase in pH from <2 to 7, as well as conductivity from 5470 mS/m to 9590 mS/m. This was accompanied by percentage removal efficiencies of 33.3 % for Mn, 97.6 % for Fe, 99.9 % for Al and 0.4 % for SO_4^{2-} ions.

In this study, the results obtained were comparable with the above mentioned literature works. It was demonstrated that the use of 0.40 g/L PCC synthesized by P123/CTAB surfactant-polymer template had been capable in exhibiting similar Mn removal efficiency despite of its comparatively lower dosage. In addition, similar removal efficiencies in Fe and Cu were also observed between 0.40 g/L of optimized PCC and 1.5 g/L of calcium lime waste. The calcium lime waste was reported to contain 94.3 % calcium oxide (CaO) and the remaining being other impurities which could generate contaminant ionic compounds and limit the full potential of calcium lime waste (Othman, Sulaiman and Sulaiman, 2017; Mulopo, Mashego and Zvimba, 2012). The current study had conducted a conversion of calcium carbide sludge to PCC in order to optimize full content of $CaCO_3$ and therefore permitted the addition of a lower dosage to achieve comparable neutralizing performance.

In terms of SO_4^{2-} ions, PCC synthesized by P123/CTAB template was able to provide excellent removal percentage as compared to soda ash. This reason was due to the generation of sodium sulphate (Na_2SO_4) in solution as a result of soda ash dissolution to yield Na^+ ions which reacted with SO_4^{2-} ions in AMD (Masindi, et al., 2017). This complex was highly soluble and not effective in precipitating SO_4^{2-} ions for removal. For the removal of other metal ions, the difference in removal efficiencies may be contributed by the pronounced difference in dosage as well as different neutralizing conditions.

Table 4.1: Comparison of AMD Neutralizing Performance of PCC with Literature Works.

Neutralizing Agent	Dosage	Optimum Dosage	Contact Time (h)	pH	ORP (mV)	Conductivity (µS)	Removal Efficiency	References
PCC synthesized by various templates	0.10 – 0.50 g/L	0.40 g/L	1 h 12 min	4.60 to 8.36	136. 4 to -61.4	202.4 to 230.1	• Mn (32.52 %), Fe (85.47 %), Ni (59.67 %), Cu (67.99 %), Zn (85.07 %), Al (87.63 %) and SO_4^{2-} (72.77 %).	Current Study
Bayer precipitate	20.1 – 60.0 g/L	60 g/L	24	3.74 to 8.00	-	-	• Mn (82.82 %), Fe (99.7 %), Ni (96.8 %), Cu (99.9 %), Zn (99.9 %), and Al (99.9 %).	Kaur, et al. (2018)
Calcium lime waste	0.5 – 2.5 g/L	1.5 g/L	1 h 10 min	~2.75 to ~8	-	-	• Mn (~40 %), Fe (~99.9 %), Ni (~90 %), Cu (>90 %), Zn (~90 %), Al (>90 %) and As (~98 %).	Othman, Sulaiman and Sulaiman (2017)
Soda ash	0 – 20 g/L	10 g/L	1	<2 to 7	-	5470 mS/m to 9590 mS/m	• Mn (33.3 %), Fe (97.6 %), Al (99.9 %) and SO_4^{2-} (0.4 %).	Masindi, et al. (2017)
Brucite	0 – 20 g/L	10 g/L	1	<2 to 5.5 – 6.5	-	5470 mS/m to 6460 mS/m	• Mn (0 %), Fe (74.6 %), Al (99.9 %) and SO_4^{2-} (11.3 %).	
Lime[2]	0 – 20 g/L	10 g/L	1	<2 to 6	-	5470 mS/m to 4410 mS/m	• Mn (26.7 %), Fe (99.9 %), Al (99.9 %) and SO_4^{2-} (95.4 %).	
Limestone	0 – 20 g/L	10 g/L	1	<2 to 6	-	5470 mS/m to 4330 mS/m	• Mn (13.3 %), Fe (99.9 %), Al (~99.9 %) and SO_4^{2-} (88.8 %).	
Stainless steel (SS) slag	20 – 140 g/L	100 g/L	4	2.5 to 6.0	-	-	• Fe (63.63 %) and SO_4^{2-} (40 %).	Name and Sheridan (2014)
Basic oxygen furnace (BOF) slag	20 – 140 g	100 g/L	4	2.5 to 12.1	-	-	• Fe (99.7 %) and SO_4^{2-} (75 %).	Name and Sheridan (2014)
Eggshell powder (53 – 160 µm)	3 – 50 g/L	20 g/L	4	2.43 to 6.58	-	-	• Mn (51.0 %), Fe (99.9 %), Al (99.9 %) and SO_4^{2-} (62.5 %).	Muliwa, Leswifi and Onyango (2018)

CHAPTER 5

CONCLUSION AND RECOMMENDATIONS

5.1 Conclusion

The precipitated calcium carbonate (PCC) has been successfully synthesized by various surfactant-polymer templates to be applied as a neutralizing agent for active acid mine drainage (AMD) treatment. The characterization of PCC synthesized by CTAB, P123/CTAB, PEG/CTAB and PVA/CTAB templates was performed via XRD, FTIR, PSD and BET analyses. Results of XRD analysis had confirmed that all PCC products consisted primarily of high thermodynamically stable calcite with high crystallinity. FTIR spectra reassured the formation of calcite and could signify the presence of C=O and O-H bonds in PCC synthesized by various surfactant-polymer templates. On the other hand, BET analysis affirmed that PCC products exhibited varying BET surface areas from 8.2487 m^2/g to 25.0417 m^2/g. Additionally, based on nitrogen adsorption and desorption isotherms, PCC products were demonstrated as a reversible type II with H2 hysteresis loop and classified as macroporous with pore size exceeding 50 nm. The PSD analysis reported a uniform mean particle size of 0.158 µm with a narrow size distribution of 0.046 – 0.316 µm for all PCC synthesized by various surfactant-polymer templates. As a result, the first two objectives of this study have been achieved by the synthesis of PCC using calcium carbide sludge and subsequent characterizations of the PCC products.

The PCC synthesized by various surfactant-polymer templates was evaluated for its neutralizing efficiency for AMD treatment in terms of pH, oxidative reductive potential (ORP), conductivity and removal of heavy metal ions as well as anions. Firstly, pH of AMD solution was found to increase to 7.02, 8.22, 8.20 and 8.16 with the addition of PCC synthesized by CTAB, P123/CTAB, PEG/CTAB and PVA/CTAB, respectively in which all of them complied to every applicable national (Standards A and B as well as NWQS Class IIA) and international (WHO Guidelines for Drinking Water Quality and EPA Ore Mining and Dressing Effluent Guidelines) standards and guidelines. In terms of other effects, PCC synthesized by various surfactant-polymer templates had shown reduction in ORP with time which indicated a net reduction of oxidized heavy metal species. On the contrary, an increase in conductivity and thus ionic strength was demonstrated with time.

The concentrations of heavy metal ions were analyzed which included Manganese (Mn), Iron (Fe), Nickel (Ni), Copper (Cu), Zinc (Zn), Aluminum (Al) and Arsenic (As). It was observed that Al reflected the highest removal efficiency of 85.83 %, 87.63 %, 82.51 % and 86.50 % with the addition of PCC synthesized by CTAB, P123/CTAB, PEG/CTAB and PVA/CTAB, respectively. By considering standard compliances, the findings demonstrated that only PCC synthesized by P123/CTAB and PVA/CTAB were able to comply with national Standards A and B (2.0 mg/L) as well as NWQS Class IIA (5.0 mg/L) for Zn. In terms of anions, all of the PCC products synthesized by various surfactant-polymer template resulted in removal efficiencies exceeding 50 % of initial SO_4^{2-} ion concentration. High removal of SO_4^{2-} ion was exhibited by PCC synthesized by P123/CTAB with a percentage efficiency of 68.39 %. PCC synthesized by P123/CTAB template selected as the optimized type of PCC as it displayed the highest overall neutralizing performance due to the achievement of highest pH of 8.22 within standard compliances, lowest ORP of -60.4 mV, highest conductivity of 238.4 µS, high removal efficiency of 87.63 % Al and other heavy metal ions as well as anion. These enhancements may be due to PCC synthesized by P123/CTAB exhibiting the highest BET surface area, nitrogen adsorption capacity as well as high thermodynamically stable calcite crystallinity.

Subsequently, the effect of PCC synthesized by P123/CTAB at varied dosages was conducted in order to evaluate their individual neutralizing capacities in treating AMD with the same parameters being measured. An increase in dosage was found to be correlated to an increase in pH with readings of 7.94, 7.67, 8.22, 8.36 and 8.58 for dosages of 0.10 g/L, 0.20 g/L, 0.30 g/L, 0.40 g/L and 0.50 g/L PCC, respectively. All pH readings were in within the acceptable conditions for every national and international standards and guidelines with the exception of dosage 0.50 g/L, which exceeded the upper limit of WHO. Similarly, a reduction in ORP was observed with time as well as higher dosages due to higher reducing power towards oxidized metals. The conductivity was observed to increase with increasing dosages which could be attributed by the dissolution of PCC synthesized by P123/CTAB template.

In terms of heavy metal ions, Fe revealed a decrease in concentration as dosage increased with removal efficiencies of 82.68 %, 82.75 %, 85.34 % and 85.47 % for 0.10 g/L, 0.20 g/L, 0.30 g/L, 0.40 g/L and 0.50 g/L of PCC, respectively. For standard compliances, only dosages 0.30 g/L, 0.40 g/L and 0.50 g/L showed full compliance to national Standards A and B (2.0 mg/L) as well as NWQS Class IIA (5.0 mg/L) for Zn. Higher dosages with more active sites enhanced adsorption, precipitation and removal efficiency. Similarly, this trend was observed for other ionic species including SO_4^{2-} ion. The reason owing to the decrease in concentration of SO_4^{2-} ion may be due to a total larger surface area and enhanced dissolution of PCC which yield higher concentrations of Ca^{2+} ion to react with and form additional gypsum. The findings verified that PCC synthesized by P123/CTAB template with a dosage of 0.40 g/L represented the optimum dosage due to its close proximity with the high neutralizing performance of 0.50 g/L dosage and yet would be more economical for use in large-scaled treatment of AMD.

Under optimized conditions of PCC, sludge settling was performed which induced the formation of larger, denser and rounder flocs in AMD treated by PCC (AMD-PCC) with high settling rate and a final sludge volume for 6.5 mL/L. In the absence of ions, deionized water (DIW) treated by PCC (DIW-PCC) was observed to produce lighter and smaller flocs with lower settling rate to produce a final sludge volume of 1.50 mL/L. The

above findings supported PCC synthesized by P123/CTAB template as a weighing material for AMD treatment with lower sludge yield as compared to literatures. With these findings, the third objective has been fulfilled whereby evaluation of AMD treatment was conducted using PCC. In summary, the application of PCC synthesized by P123/CTAB template with an optimum dosage of 0.40 g/L was manifested as a useful method to divert calcium carbide sludge – a form of acetylene gas production waste, which was conventionally disposed to landfills and to produce effective neutralizing agent for AMD treatment.

As a conclusion, all of the above findings have satisfied the specific objectives mentioned in this study. The first objective has been accomplished by modification of surfactant-polymer template precipitation method using calcium carbide sludge to recover useful constituents of the industrial waste and successfully synthesized PCC in the presence of various surfactant-polymer templates. The confirmation of PCC products was performed by various characterizations as stated in the second objectives, whereby all synthesized products were revealed as calcite, a crystalline structure of calcium carbonate. Although PCC synthesized by different surfactant-polymer template showed variations in functional group and specific surface area, PSD results have reinforced that general characteristics of PCC were still exhibited by all PCC products in terms of uniformity and narrow distribution of particle size. All of these characteristics exhibited their respective significance in the effects of PCC synthesized by different surfactant-polymer template and different dosages of PCC on AMD treatment. The evaluation of these effects on various parameters has been determined and justified the compatibility of PCC for AMD remediation in fulfillment of the third and final objective.

5.2 Recommendations

Prior to the completion of this research, the fundamentals and technical aspects as listed below could be considered to be applied in future research studies.

i. The effects of other parameters which were not covered in this research for example heavy metal ions of potassium (K) and sodium (Na), anions of nitrate (NO_3^-) and phosphate (PO_4^{3-}), total suspended particles (TSP), turbidity, hardness and presence of impurities in synthesized PCC, sludge volume index (SVI) could be incorporated into future studies for the purpose of providing better evaluation of neutralizing performance of synthesized PCC in AMD treatment.
ii. In the presence of sufficient AMD, PCC synthesized by various surfactant-polymer templates could be compared with commercialized calcium carbonate ($CaCO_3$) to verify the difference in characterization, neutralizing performance as well as their contributing effects of parameters towards AMD.
iii. Column leaching test could be introduced to provide a simulation of AMD being leached from surface water into groundwater and to determine the neutralization performance of PCC synthesized by surfactant-polymer templates as well as to monitor geochemical changes of the collected leachate over a period of time.
iv. Function of microorganisms such as SO_4^{2-} reducing bacteria present in AMD could be investigated to further enhance AMD neutralization.

REFERENCES

Aguiar, A., Andrade, L., Ricci, B., Pires, W., Miranda, G. and Amaral, M., 2016. Gold acid mine drainage treatment by membrane separation processes: An evaluation of the main operational conditions. *Separation and Purification Technology*, 170, pp. 360-369.

Ahmad, S. and Jones, D., 2013. Investigating the mining heritage significance for Kinta District, the industrial heritage legacy of Malaysia. *Procedia - Social and Behavioral Sciences*, 105, pp. 445-457.

American Public Health Association, American Water Works Association, and Water Environment Federation, 2005. *Standard Methods for the Examination of Water and Wastewater*. 21st ed. New York: APHA, AWWA, WEF.

Bang, J., Jang, Y.N., Kim W., Song, K.S., Jeon, C.W., Chae, S.C., Lee, S., Park, S. and Lee, M.G., 2012. Specific surface area and particle size of calcium carbonate precipitated by carbon dioxide microbubbles. *Chemical Engineering Journal*, 198-199, pp. 254-260.

Ben Ali, H.E., Neculita, C.M., Molson, J.W., Maqsoud, A. and Zagury, G.J., 2019. Efficiency of batch biochemical reactors for mine drainage treatment at low temperature and high salinity. *Applied Geochemistry*, 103, pp. 40-49.

Bier, R., Voss, K. and Bernhardt, E., 2015. Bacterial community responses to a gradient of alkaline mountaintop mine drainage in Central Appalachian streams. *The ISME Journal*, 9, pp. 1378-1390.

Bigham, J. and Cravotta III, C., 2016. Acid Mine Drainage. *Encyclopedia of Soil Science, Third Edition*, [online] pp. 6-10. Available at: https://pubs.er.usgs.gov/publication/70182719 [Accessed 26 May 2018].

Bigham, J. and Cravotta III, C., 2016. Acid Mine Drainage. In: R. Lal, eds., *Encyclopedia of Soil Science*, 3rd ed. Boca Raton: CRC Press.

Boss, C.B. and Fredeen, K.J., 2004. *Concepts, instrumentation and techniques in inductively coupled plasma optical emission spectrometry*. 3rd ed. Shelton, USA: Perkin Elmer.

Business Wire, 2017. *Global precipitated calcium carbonate market - drivers and forecasts by Technavio.* [online] Businesswire.com. Available at: https://www.businesswire.com/news/home/20170727006325/en/Global-Precipitated-Calcium-Carbonate-Market---Drivers [Accessed 24 Jun. 2018].

Bwapwa, J., Jaiyeola, A. and Chetty, R., 2017. Bioremediation of acid mine drainage using algae strains: A review. *South African Journal of Chemical Engineering*, 24, pp. 62-70.

Byrne, P., Hudson-Edwards, K., Bird, G., Macklin, M., Brewer, P., Williams, R. and Jamieson, H., 2018. Water quality impacts and river system recovery following the 2014 Mount Polley mine tailings dam spill, British Columbia, Canada. *Applied Geochemistry*, 91, pp. 64-74.

Chen, X., Ren, P., Li, T., Trembly, J.P. and Liu, X., 2018. Zinc removal fom model wastewater by electrocoagulation: Processing, kinetics and mechanism. *Chemical Engineering Journal*, 349, pp. 358-367.

Dai, Q., Ma, L., Ren, N., Ning, P., Guo, Z. and Xie, L., 2019. Research on the variations of organics and heavy metals in municipal sludge with additive acetic acid and modified phospohgypsum. *Water Research*, 155, pp. 42-55.

Dang, H., Yuan, X., Xiao, Q., Xiao, W., Luo, Y., Wang, X., Song, F. and Wang, Y., 2017. Facile batch synthesis of porous vaterite microspheres for high efficient and fast removal of toxic heavy metal ions. *Journal of Environmental Chemical Engineering*, 5, pp. 4505-4515.

De Beer, M., 2005. *Treatment of acid mine drainage and acidic effluents*. MSc. North-West University.

De Beer, M., Doucet, F., Maree, J. and Liebenberg, L., 2015. Synthesis of high-purity precipitated calcium carbonate during the process of recovery of elemental sulphur from gypsum waste. *Waste Management*, 46, pp. 619-627.

De Crom, K., Chiang, Y., Van Gerven, T. and Santos, R., 2015. Purification of slag-derived leachate and selective carbonation for high-quality precipitated calcium carbonate synthesis. *Chemical Engineering Research and Design*, 104, pp. 180-190.

Demers, I., Finch, J. and El-Ammouri, E., 2009. Use of activated silica sol as a flocculant in the treatment of acid mine drainage to promote sludge stability. *Minerals Engineering*, 22, pp. 506-512.

Department of Environment Malaysia, 2015. *Environmental Quality Report*. Putrajaya: Department of Environment Malaysia.

Department of Environment, 2010. *Environmental Requirements: A Guide for Investors. 11th ed.* [online] Available at: http://www.doe.gov.my/eia/wp-content/uploads/2012/03/A-Guide-For-Investors1.pdf [Accessed 25 Jun. 2018].

Donate-Robles, J. and Martín-Martínez, J.M., 2011. Addition of precipitated calcium carbonate filler to thermoplastic polyurethane adhesives. *International Journal of Adhesion & Adhesives*, 31, pp. 795-804.

Feris, L. and Kotze, L., 2017. The regulation of acid mine drainage in South Africa: Law and governance perspectives. *Potchefstroom Electronic Law Journal/Potchefstroomse Elektroniese Regsblad*, 17, pp. 2105-2163.

Fernando, W.A.M., Ilankoon, I.M.S.K., Syed, T.H. and Yellishetty, M., 2018. Challenges and opportunities in the removal of sulphate ions in contaminated mine water: A review. *Minerals Engineering*, 117, pp. 74-90.

Fujiwara, M., Shiokawa, K., Morigaki, K., Zhu, Y. and Nakahara, Y., 2008. Calcium carbonate microcapsules encapsulating biomacromolecules. *Chemical Engineering Journal*, 137, pp. 14-22.

Galera Martínez, M, Minh, D.P., Nzihou, A. and Sharrock, P., 2019. Valorization of calcium carbonate-based solid wastes for the treatment of hydrogen sulfide in a semi-continuous reactor. *Chemical Engineering Journal*, 360, pp. 1167-1176.

Gang, X., Wang, Q., Qian, Y., Gao, P., Su, Y., Liu, Z., Chen, H., Li, X., Chen, J., 2019. Simulateneous removal of aniline, antimony and chromium by ZVI coupled with H_2O_2: Implication for textile wastewater treatment. *Journal of Hazardous Materials*, 368, pp. 840-848.

Gopi, S., Subramanian, V.K. and Palanisamy, K., 2013. Aragonite-calcite-vaterite: A temperature influenced sequential polymorphic transformation of $CaCO_3$ in the presence of DTPA, *Materials Research Bulletin*, 48, pp. 1906-1912.

Guo, B., Chen, Y., Lv, L., Ahmad, H.A., Ni, S., Ren, L., Cui, Z., Fang, X., Qian, Z. and Ding, S., 2019. Transformation of the zero valent iron dosage effect on anammox after long-tern culture: From inhibition to promotion. *Process Biochemistry*, 78, pp. 132-139.

Guo, B., Zhao, T., Sha, F., Zhang, F., Li, Q., Zhao, J. and Zhang, J., 2017. Synthesis of vaterite $CaCO_3$ micro-spheres by carbide slag and a novel CO_2 -storage material. *Journal of CO_2 Utilization*, 18, pp. 23-29.

Guo, H., Qin, Z., Qian, P., Yu, P., Cui, S. and Wang, W., 2011. Crystallization of aragonite CaCO3 with complex structures. *Advanced Powder Technology*, 22, pp. 777-783.

Hashemi, M.S.H., Eslami, F. and Karimzadeh, R., 2019. Organic contaminants removal from industrial wastewater by CTAB treated synthetic zeolite Y. *Journal of Environmental Management*, 233, pp. 785-792.

Heviánková, S., Bestová, I. and Kyncl, M., 2014. The application of wood ash as a reagent in acid mine drainage treatment. *Minerals Engineering*, 56, pp. 109-111.

Heviánková, S., Bestová, I., Kyncl, M., Šimková, L. and Zechner, M., 2013. Calcium carbonate as an agent in acid mine water neutralization. *Journal of the Polish Mineral Engineering Society*, 32, pp. 159-166.

Holban, A.M. Grumezescu, A.M. and Andronescu, E., 2016. Inorganic nanoarchitectonics designed for drug delivery and anti-infective surfaces. *Surface Chemistry of Nanobiomaterials*, 3, pp. 301-327.

International Organising Committee for the World Mining Congresses, 2018. *World Mining Data 2018*. World Mining Data. [online] Vienna: Federal Ministry of Sustainability and Tourism. Available at: http://www.wmc.org.pl/sites/default/files/WMD2018.pdf [Accessed 3 Jun. 2018].

Jamrunroj, P., Wongsakulphasatch, S., Maneedaeng, A., Cheng, C.K. and Assabumrungrat, S., 2019. Surfactant assisted CaO-based sorbent synthesis and their application to high-temperature CO_2 capture. *Powder Technology*, 344, pp. 208-221.

Jimoh, O., Okoye, P., Otitoju, T. and Ariffin, K., 2018. Aragonite precipitated calcium carbonate from magnesium rich carbonate rock for polyethersulfone hollow fibre membrane application. *Journal of Cleaner Production*, 195, pp. 79-92.

Johnson, D. and Hallberg, K., 2005. Acid mine drainage remediation options: A review. *Science of the Total Environment*, 338, pp. 3-14.

Jones, S.N. and Cetin, B., 2017. Evaluation of waste materials for acid mine drainage remediation. *Fuel*, 188, pp. 294-309.

Kanoje, B., Parikh, J. and Kuperkar, K., 2018. Crystallization study and morphology behaviour of calcium carbonate crystals in aqueous Surfactant-Pluronics ® prototype. *Journal of Materials Research and Technology*, 7, pp. 508-514.

Kanoje, B., Patel, D. and Kuperkar, K., 2017. Morphology modification in freshly precipitated calcium carbonate particles using surfactant-polymer template. *Materials Letters*, 187, pp. 44-48.

Kastyuchik, A., Karam, A. and Aïder, M., 2016. Effectiveness of alkaline amendments in acid mine drainage remediation. *Environmental Technology and Innovation*, 6, pp. 49-59.

Kastyuchik, A., Karam, A. and Aïder, M., 2016. Effectiveness of alkaline amendments in acid mine drainage remediation. *Environmental Technology & Innovation*, 6, pp. 49-59.

Kaur, G., Couperthwaite, S.J. and Millar, G.J., 2018. Performance of bauxite refinery residues for treating acid mine drainage. *Journal of Water Process Engineering*, 26, pp. 28-37.

Kaur, G., Couperthwaite, S.J., Hatton-Jones, B.W. and Millar G.J., 2018. Alternative neutralization materials for acid mine drainage treatment. *Journal of Water Process Engineering*, 22, pp. 46-58.

Kaur, M., 2013. Increase in tin mining activities. *The Star*. [online] Available at: https://www.thestar.com.my/news/community/2013/06/12/increase-in-tin-mining-activities/ [Accessed 11 Jun. 2018].

Kefeni, K., Msagati, T. and Mamba, B., 2017. Acid mine drainage: Prevention, treatment options, and resource recovery: A review. *Journal of Cleaner Production*, 151, pp. 475-493.

Kezuka, Y., Kuma, Y., Nakai, S., Matsubara, K. and Tajika, M., 2018. Calcium carbonate chain-like nanoparticles: Synthesis, structural characterization, and dewaterability. *Powder Technology*, 335, pp. 195-203.

Kohli, R. and Mittal, K., 2012. *Developments in surface contamination and cleaning - Detection, characterization, and analysis of contaminants*. Elsevier, pp. 107-178.

Konopacka-Łyskawa, D., Kościelska, B. and Karczewski, J., 2017. Controlling the size and morphology of precipitated calcite particles by the selection of solvent composition. *Journal of Crystal Growth*, 478, pp. 102-110.

Latif, M., Naganathan, S., Razak, H. and Mustapha, K., 2015. Evaluating the performance of calcium carbide kiln dust in mortar – Initial study. *Procedia Engineering*, 125, pp. 788-795.

Li, G., Li, Z. and Ma, H., 2013. Synthesis of aragonite by carbonization from dolomite without any additives. *International Journal of Mineral Processing*, 123, pp. 25-31.

Li, S., Wang, W., Liang, F. and Zhang, W., 2017. Heavy metal removal using nanoscale zero-valent iron (nZVI): Theory and application. *Journal of Hazardous Materials*, 322, pp. 163-171.

Li, S., Wang, W., Yan, W. and Zhang, W, 2014. Nanoscale zero-valent iron (nZVI) for the treatment of concentrated Cu(II) wastewater: A field demonstration. *Environ. Sci.: Processes Impacts*, 16, pp. 524-533.

Li, Y., Guo, X., Dong, H., Luo, X., Guan, X., Zhang, X. and Xia, X., 2018. Selenite removal from groundwater by zero-valent iron (ZVI) in combination with oxidants. *Chemical Engineering Journal*, 345, pp. 432-440.

Lizama Allende, K., Fletcher, T.D. and Sun, G., 2012. The effect of substrate media on the removal of arsenic, boron and iron from an acidic wastewater in planted column reactors. *Chemical Engineering Journal*, 179, pp. 119-130.

López-Periago, A., Pacciani, R., García-González, C., Vega, L. and Domingo, C., 2010. A breakthrough technique for the preparation of high-yield precipitated calcium carbonate. *The Journal of Supercritical Fluids*, 52, pp. 298-305.

Ma, X, Li, L., Yang, L., Su, C., Wang, K., Yuan, S. and Zhou, J., 2012. Adsorption of heavy metal ions using hierarchical $CaCO_3$–maltose meso/macroporous hybrid materials: Adsorption isotherms and kinetic studies. *Journal of Hazardous Materials*, 209-210, pp. 467-477.

Mackie, A.L. and Walsh, M.E., 2015. Investigation into the use of cement kiln dust in high density sludge (HDS) treatment of acid mine water. *Water Research*, 85, pp. 443-450.

Majzlan, J., Števko, M., Chovan, M., Luptáková, J., Milovská, S., Milovský, R., Jeleň, S., Sýkorová, M., Pollok, K., Göttlicher, J. and Kupka, D., 2018. Mineralogy and geochemistry of the copper-dominated neutral mine drainage at the Cu deposit Ľubietová-Podlipa (Slovakia). *Applied Geochemistry*, 92, pp. 59-70.

Mantilaka, M.M.M.G.P.G., Pitawala, H.M.T.G.A., Rajapakse, R.M.G., Karunaratne, D.G.G.P., and Upul Wijayantha, K.G., 2014. Formation of hollow bone-like morphology of calcium carbonate on surfactant/polymer templates. *Journal of Crystal Growth*, 392, pp. 52-59.

Marcello, R.R., Galato, S., Peterson, M., Riella, H.G. and Bernardin, A.M., 2008. Inorganic pigments made from the recycling of coal mine drainage treatment sludge. *Journal of Environmental Management*, 88, pp. 1280-1284.

Masindi, V., Akinwekomi, V., Maree, J. and Muedi, K., 2017. Comparison of mine water neutralisation efficiencies of different alkaline generating agents. *Journal of Environmental Chemical Engineering*, 5, pp. 3903-3913.

Masindi, V., Gitari, M., Tutu, H. and De Beer, M., 2016. Fate of inorganic contaminants post treatment of acid mine drainage by cryptocrystalline magnesite: Complimenting experimental results with a geochemical model. *Journal of Environmental Chemical Engineering*, 4, pp. 4846-4856.

Matsumoto, M., Fukunaga, T. and Onoe, K., 2010. Polymorph control of calcium carbonate by reactive crystallization using microbubble technique. *Chemical Engineering Research and Design*, 88, pp. 1624-1630.

Millero, F., Huang, F., Zhu, X., Liu, X. and Zhang, J., 2001. Adsorption and desorption of phosphate on calcite and aragonite in seawater. *Aquatic Geochemistry*, 7, pp. 33-56.

Mineral Development Act 1994, 1994. Laws of Malaysia. Act 525.

Minerals Technologies Inc, 2018. *Precipitated calcium carbonate (PCC)*. [online] Mineralstech.com. Available at: https://www.mineralstech.com/Pages/SMI/Precipitated-Calcium-Carbonate-(PCC).html [Accessed 24 Jun. 2018].

Moldoveanu, S. and David, V., 2013. *Essentials in modern HPLC separations*. Elsevier, pp. 191-362.

Moodley, I., Sheridan, C.M, Kappelmeyer, U. and Akcil, A., 2018. Environmentally sustainable acid mine drainage remediation: Research developments with a focus on waste/by-products. *Minerals Engineering*, 126, pp. 207-220.

Mori, Y., Enomae, T. and Isogai, A., 2009. Preparation of pure vaterite by simple mechanical mixing of two aqueous salt solutions. *Materials Science and Engineering: C*, 29, pp. 1409-1414.

Muliwa, A., Leswifi, T. and Onyango, M., 2018. Performance evaluation of eggshell waste material for remediation of acid mine drainage from coal dump leachate. *Minerals Engineering*, 122, pp. 241-250.

Mulopo, J., 2015. Continuous pilot scale assessment of the alkaline barium calcium desalination process for acid mine drainage treatment. *Journal of Environmental Chemical Engineering*, 3, pp. 1295-1302.

Mulopo, J., Mashego, M. and Zvimba, J.V., 2012. Recovery of calcium carbonate from steelmaking slag and utilization for acid mine drainage pre-treatment. *Water Science and Technology*, 65, pp. 2236-2241.

Nakamura, J., Kasuga, T. and Sakka, Y., 2017. Preparation of carbamate-containing vaterite particles for strontium removal in wastewater treatment. *Journal of Asian Ceramic Societies*, 5, pp. 364-369.

Name, T. and Sheridan, C., 2014. Remediation of acid mine drainage using metallurgical slags. *Minerals Engineering*, 64, pp. 15-22.

Othman, A., Sulaiman, A. and Sulaiman, S., 2017. Carbide lime in acid mine drainage treatment. *Journal of Water Process Engineering*, 15, pp. 31-36.

Ouakibi, O., Hakkou, R. and Benzaazoua, M., 2014. Phosphate carbonated wastes used as drains for acidic mine drainage passive treatment. *Procedia Engineering*, 83, pp. 407-414.

Palmer, M. and Hatley, H., 2018. The role of surfactants in wastewater treatment: Impact, removal and future techniques: A critical review. *Water Research*, 147, pp. 60-72.

Pastorino, D., Canal, C. and Ginebra, M., 2015. Multiple characterization study on porosity and pore structure of calcium phosphate cements. *Acta Biomaterialia*, 28, pp. 205-214.

Pavoni, E., Covelli, S., Adami, G., Baracchini, E., Cattelan, R., Crosera, M., Higueras, P., Lenaz, D. and Petranich, E., 2018. Mobility and fate of Thallium and other potentially harmful elements in drainage waters from a decommissioned Zn-Pb mine (North-Eastern Italian Alps). *Journal of Geochemical Exploration*, 188, pp. 1-10.

Pfitzner, K., Harford, A., Whiteside, T. and Bartolo, R., 2018. Mapping magnesium sulfate salts from saline mine discharge with airborne hyperspectral data. *Science of the Total Environment*, 640-641, pp. 1259-1271.

Polat, S., 2019. Evaluation of the effects of sodium laurate on calcium carbonate precipitation: Characterization and optimization studies. *Journal of Crystal Growth*, 508, pp. 8-18.

Potgieter-Vermaak, S.S., Ptogieter, J.H., Monama, P. and Van Gieken, R., 2006. Comparison of limestone, dolomite and fly ash as pre-treatment agents for acid mine drainage. *Minerals Engineering*, 19, pp. 454-462.

Pozo, G., Pongy, S., Keller, J., Ledezma, P. and Freguia, S., 2017. A novel bioelectrochemical system for chemical-free permanent treatment of acid mine drainage. *Water Research*, 126, pp. 411-420.

Radiometer Analytical SAS, 2004. *Conductivity theory and practice*. France: Radiometer Analytical SAS.

Rattanashotinunt, C., Thairit, P., Tangchirapat, W. and Jaturapitakkul, C., 2013. Use of calcium carbide residue and bagasse ash mixtures as a new cementitious material in concrete. *Materials & Design*, 46, pp. 106-111.

Said, A., Mattila, H., Järvinen, M. and Zevenhoven, R., 2013. Production of precipitated calcium carbonate (PCC) from steelmaking slag for fixation of CO_2. *Applied Energy*, 112, pp. 765-771.

Salaudeen, S.A., Tasnim, S.H., Heidari, M., Acharya, B. and Dutta, A., 2018. Eggshell as a potential CO_2 sorbent in the calcium looping gasification of biomass. *Waste Management*, 80, pp. 274-284.

Seo, E.Y., Cheong, Y.W., Yim, G.J., Min, K.W. and Geroni, J.N., 2017. Recovery of Fe, Al and Mn in acid coal mine drainage by sequential selective precipitation with control of pH. *Catena*, 148, pp. 11-16.

Sephton, M.G., Webb, J.A. and McKnight, S., 2019. Applications of Portland cement blended with fly ash and acid mine drainage treatment sludge to control acid mine drainage generation from waste rocks. *Applied Geochemistry*, 103, pp. 1-14.

Sheoran, A. and Sheoran, V., 2006. Heavy metal removal mechanism of acid mine drainage in wetlands: A critical review. *Minerals Engineering*, 19, pp. 105-116.

Simate, G. and Ndlovu, S., 2014. Acid mine drainage: Challenges and opportunities. *Journal of Environmental Chemical Engineering*, 2, pp. 1785-1803.

Škapin, S. and Sondi, I., 2010. Synthesis and characterization of calcite and aragonite in polyol liquids: Control over structure and morphology. *Journal of Colloid and Interface Science*, 347, pp. 221-226.

Skousen, J.G., Ziemkiewicz, P.F. and McDonald, L.M., 2019. Acid mine drainage formation, control and treatment: Approaches and strategies, *The Extractive Industries and Society*, 6, pp. 241-249.

Sulaiman, A., Othman, A. and Ibrahim, I., 2018. The use of magnesium oxide in acid mine drainage treatment. *Materials Today: Proceedings*, 5, pp. 21566-21573.

Tan, Y.H., Davis, J.A., Fujikawa, K., Ganesh, N.V., Demchenko, A.V. and Stine, K.J., 2012. Surface area and pore size characteristics of nanoporous gold subjected to thermal, mechanical, or surface modification studied using gas adsorption isotherms, cyclic voltammetry, thermogravimetric analysis, and scanning electron microscopy. *Journal of Materials Chemistry*, 22, pp. 6733-6745.

Tang, C., Hedegaard, M.J., Lopato, L. and Albrechtsen, H.J., 2019. Softening of drinking water by the pellet reactor - Effects of influent water composition on calcium carbonate pellet characteristics. *Science of the Total Environment*, 652, pp. 538-548.

Teir, S., Eloneva, S. and Zevenhoven, R., 2005. Production of precipitated calcium carbonate from calcium silicates and carbon dioxide. *Energy Conversion and Management*, 46, pp. 2954-2979.

The National Lime Association, 2018. *Precipitated calcium carbonate*. [online] Lime.org. Available at: https://www.lime.org/lime-basics/uses-of-lime/other-uses-of-lime/precipitated-calcium-carbonate/ [Accessed 24 Jun. 2018].

Thommes, M., Kaneko, K., Neimark, A.V., Olivier, J.P, Rodriguez-Reinoso, F., Rouquerol, J. and Sing, K.S.W., 2015. Physisorption of gases, with special reference to the evaluation of surface area and pore size distribution (IUPAC Technical Report). *Pure Applied Chemistry*, 87, pp. 1051-1069.

Tolonen, E., Sarpola, A., Hu, T., Rämö, J. and Lassi, U., 2014. Acid mine drainage treatment using by-products from quicklime manufacturing as neutralization chemicals. *Chemosphere*, 117, pp. 419-424.

Trushina, D., Bukreeva, T., Kovalchuk, M. and Antipina, M., 2014. $CaCO_3$ vaterite microparticles for biomedical and personal care applications. *Materials Science and Engineering: C*, 45, pp. 644-658.

Türker, O.C., Simultaneous boron (B) removal and electricity generation from domestic wastewater using duckweed-based wastewater treatment reactors coupled with microbial fuel cell. *Journal of Environmental Management*, 228, pp. 20-31.

United States Environmental Protection Agency, 2011. *Ore mining and dressing preliminary study report*. United States Environmental Protection Agency.

US EPA, 2017. *Secondary drinking water standards: Guidance for nuisance chemicals | US EPA*. [online] Available at: https://www.epa.gov/dwstandardsregulations/secondary-drinking-water-standards-guidance-nuisance-chemicals [Accessed 22 Jun. 2018].

Wan Zuhairi, W.Y., Syuhadah, P. and Hazwani, M., 2009. Acid mine drainage and heavy metals contamination at abandoned and active mine sites in Pahang. *Bulletin of the Geological Society of Malaysia*, 55, pp. 15-20.

Wang, J., Zhang, T., Mei, Y. and Pan, B., 2018. Treatment of reverse-osmosis concentrate of printing and dyeing wastewater by electro-oxidation process with controlled oxidation-reduction potential (ORP). *Chemosphere*, 201, pp. 621-626.

World Health Organization, 2011, *Guidelines for drinking water quality: fourth edition incorporating the first addendum*. Switzerland: World Health Organization.

Xu, L., Xu, X., Cao, G., Liu, S., Duan, Z., Song, S., Song, M. and Zhang, M., 2018. Optimization and assessment of Fe-electrocoagulation for the removal of potentially toxic metals from real smelting wastewater, *Journal of Environmental Management*, 218, pp. 129-138.

Yang, B. and Nan, Z., 2012. Abnormal polymorph conversion of calcium carbonate from calcite to vaterite. *Materials Research Bulletin*, 47, pp. 521-526.

Yang, X., Meng, H., Li, T., Shi, L., Li, Y. and Xu, G., 2014. $CaCO_3$ crystallization in HPCHS/CTAB mixed solutions. *Powder Technology*, 256, pp. 272-278.

Zhan, G. and Guo, Z., 2015. Preparation of potassium salt with joint production of spherical calcium carbonate from sintering dust. *Transactions of Nonferrous Metals Society of China*, 25, pp. 628-639.

Zhang, Z., Xie, Y., Xu, X., Pan, H. and Tang, R., 2012. Transformation of amorphous calcium carbonate into aragonite. *Journal of Crystal Growth*, 343, pp. 62-67.

Zhao, L., and Wang, J., 2012. Biomimetic synthesis of hollow microspheres of calcium carbonate crystals in the presence of polymer and surfactant. *Colloids and Surfaces A: Physicochemical and Engineering Aspects*, 393, pp. 139-143.

Zhao, Y., Wang, X., Jiao, J., Wang, R., and Yu, L., 2012. The preparation of calcium carbonate crystals in pluronic F68 solution. *Journal of Molecular Liquids*, 169, pp. 144-151.

APPENDICES

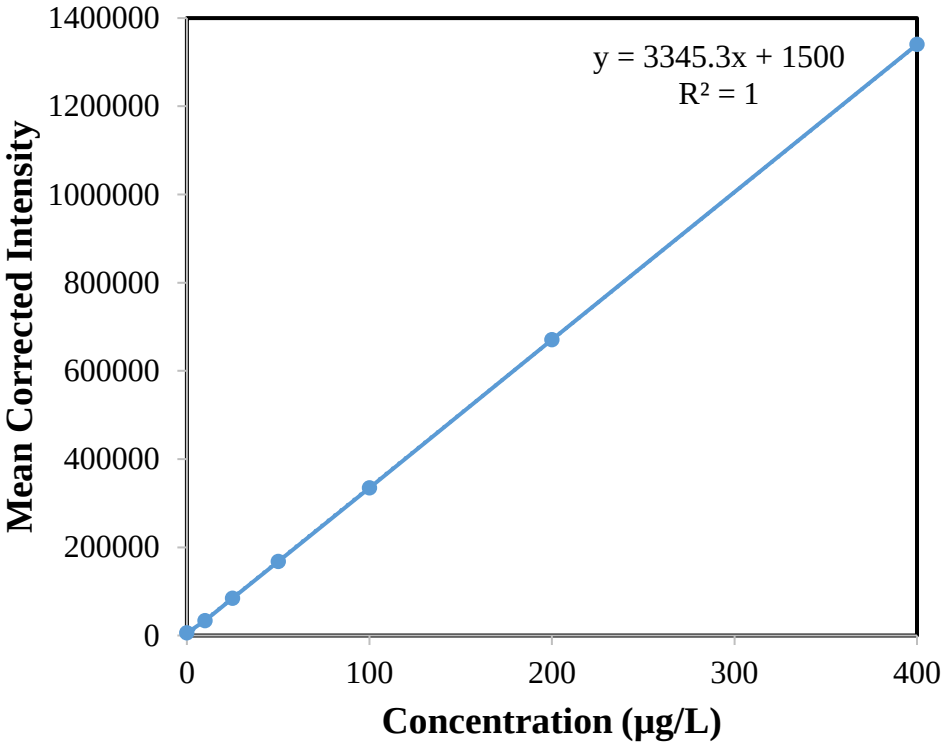

Appendix A1: Calibration Curve for Mn.

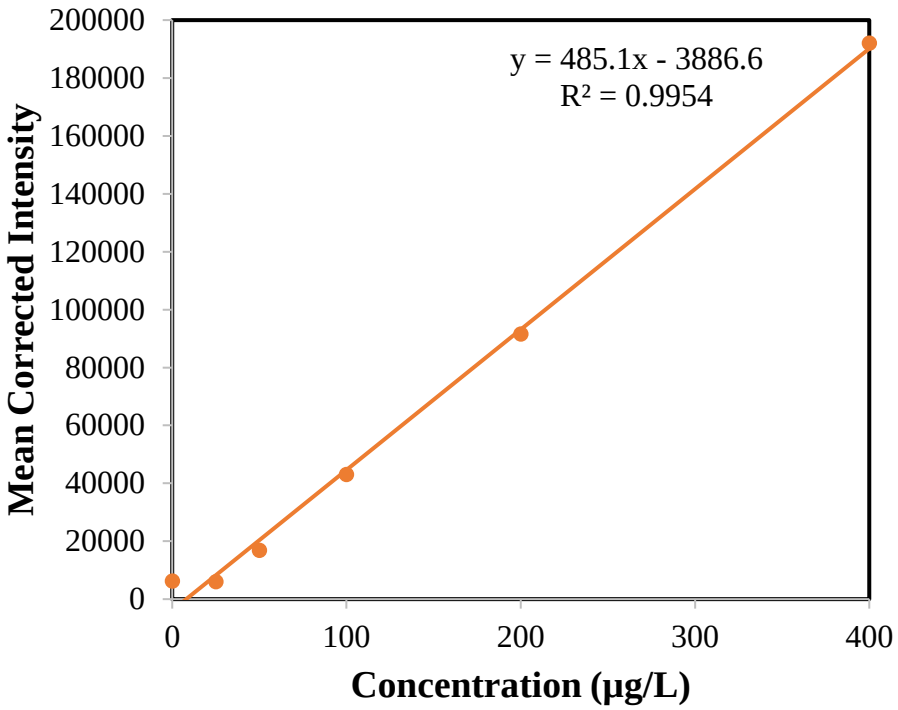

Appendix A2: Calibration Curve for Fe.

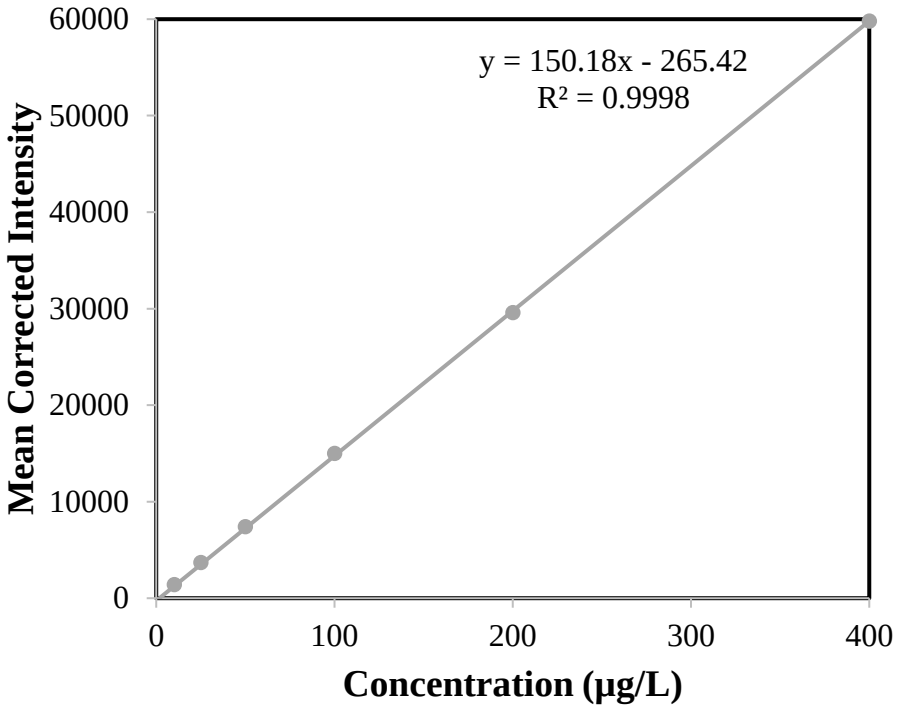

Appendix A3: Calibration Curve for Ni.

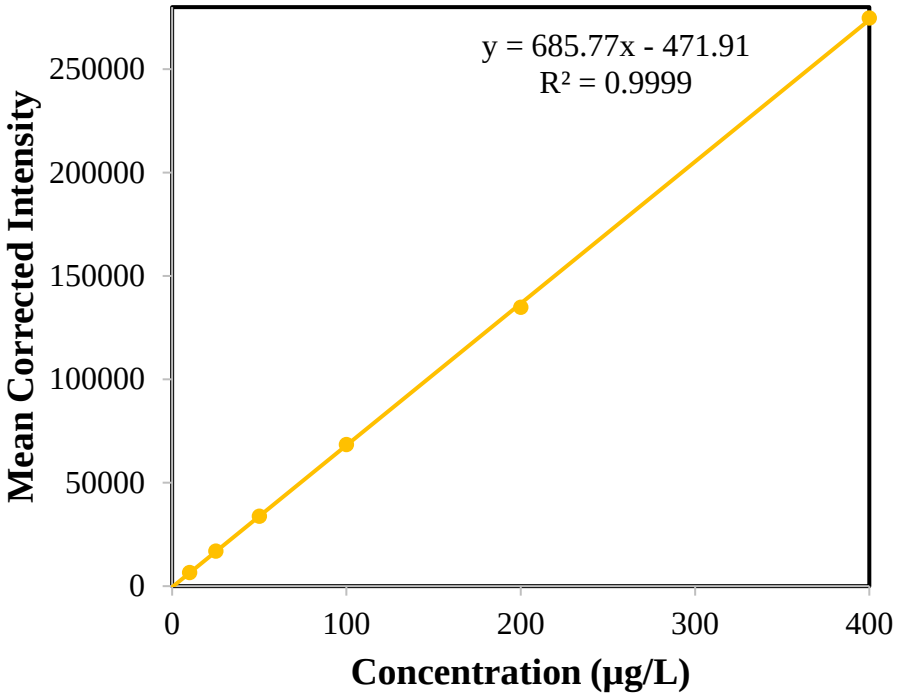

Appendix A4: Calibration Curve for Cu.

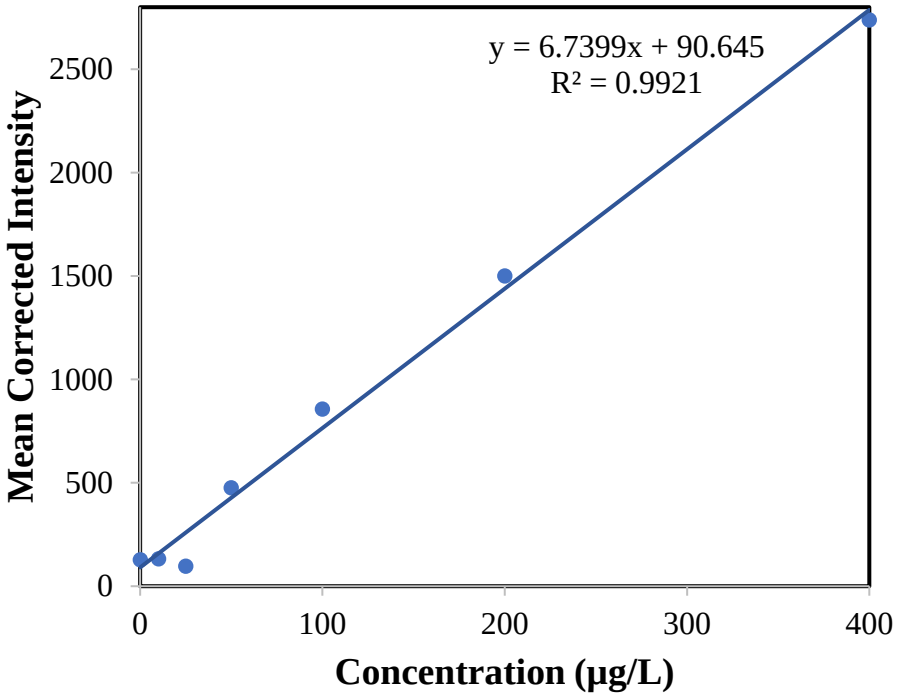

Appendix A5: Calibration Curve for Zn.

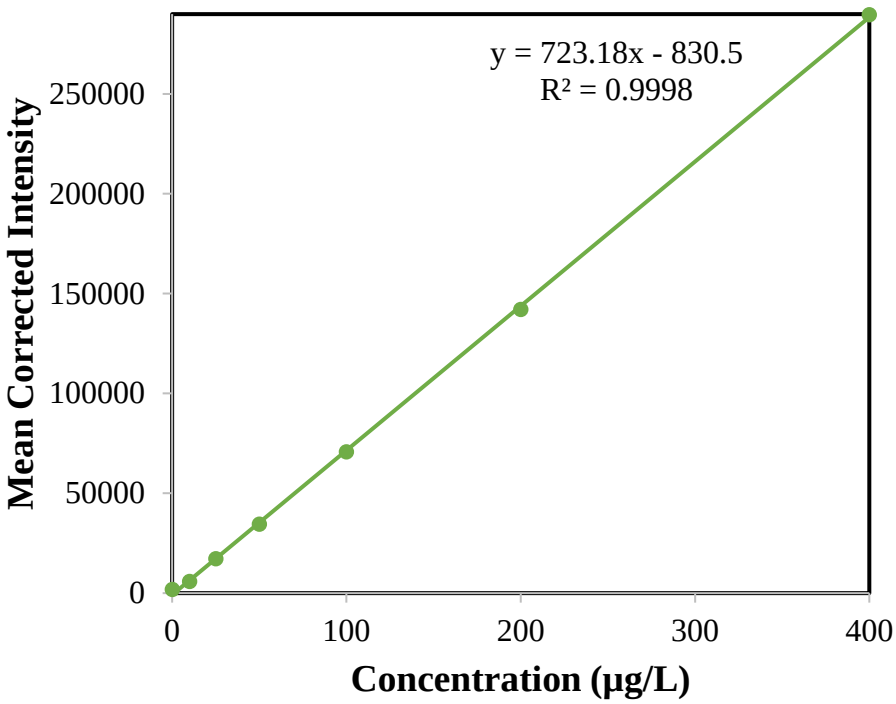

Appendix A6: Calibration Curve for Al.

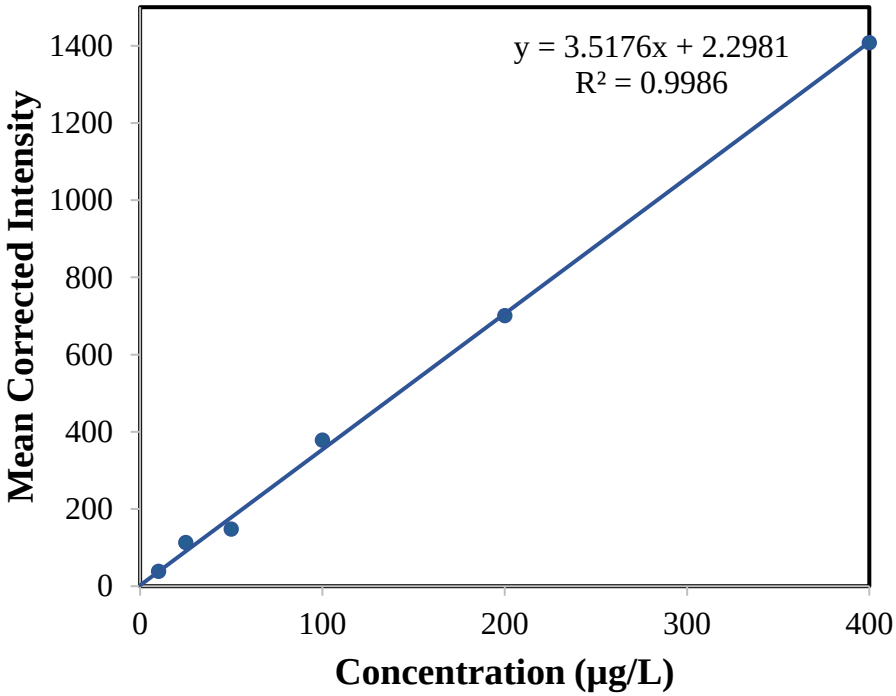

Appendix A7: Calibration Curve for As.

Appendix A8: Metal Concentrations of Raw AMD.

Elements	AMD						
	Results (mg/L)	NWQS		EQA Effluent Discharge Standard			
	Original	Class IIA	Comply	Standard A	Comply	Standard B	Comply
Mn	29.460	0.1	N	0.2	N	1.0	N
Fe	76.460	1.0	N	1.0	N	5.0	N
Ni	4.761	0.05	N	0.2	N	1.0	N
Cu	4.070	0.02	N	0.2	N	1.0	N
Zn	9.737	5.0	N	2.0	N	2.0	N
Al	14.240	-	N/A	10	N	15	Y
As	ND	0.05	Y	0.05	Y	0.1	Y

Appendix A9: Metal Concentrations of AMD Treated Using PCC Synthesized By CTAB Template.

Elements	CTAB							
	Original		NWQS		EQA Effluent Discharge Standard			
	Results (mg/L)	Removal (%)	Class IIA	Comply	Standard A	Comply	Standard B	Comply
Mn	19.780	32.86	0.1	N	0.2	N	1.0	N
Fe	11.110	85.47	1.0	N	1.0	N	5.0	N
Ni	3.538	25.69	0.05	N	0.2	N	1.0	N
Cu	3.791	6.86	0.02	N	0.2	N	1.0	N
Zn	5.561	42.89	5.0	N	2.0	N	2.0	N
Al	2.018	85.83	-	N/A	10	Y	15	Y
As	ND	-	0.05	N	0.05	Y	0.1	Y

Appendix A10: Metal Concentrations of AMD Treated Using PCC Synthesized By P123/CTAB Template.

Elements	P123							
	Original		NWQS		EQA Effluent Discharge Standard			
	Results (mg/L)	Removal (%)	Class IIA	Comply	Standard A	Comply	Standard B	Comply
Mn	20.480	30.48	0.1	N	0.2	N	1.0	N
Fe	11.210	85.34	1.0	N	1.0	N	5.0	N
Ni	3.180	33.21	0.05	N	0.2	N	1.0	N
Cu	1.517	62.73	0.02	N	0.2	N	1.0	N
Zn	1.454	85.07	5.0	Y	2.0	Y	2.0	Y
Al	1.762	87.63	-	N/A	10	Y	15	Y
As	ND	-	0.05	Y	0.05	Y	0.1	Y

Appendix A11: Metal Concentrations of AMD Treated Using PCC Synthesized By PEG/CTAB Template.

Elements	PEG							
	Original		NWQS		EQA Effluent Discharge Standard			
	Results (mg/L)	Removal (%)	Class IIA	Comply	Standard A	Comply	Standard B	Comply
Mn	20.970	28.82	0.1	N	0.2	N	1.0	N
Fe	14.030	81.65	1.0	N	1.0	N	5.0	N
Ni	3.465	27.22	0.05	N	0.2	N	1.0	N
Cu	1.086	73.32	0.02	N	0.2	N	1.0	N
Zn	2.157	77.85	5.0	Y	2.0	N	2.0	N
Al	2.490	82.51	-	N/A	10	Y	15	Y
As	ND	-	0.05	Y	0.05	Y	0.1	Y

Appendix A12: Metal Concentrations of AMD Treated Using PCC Synthesized By PVA/CTAB Template.

Elements	PVA							
	Original		NWQS		EQA Effluent Discharge Standard			
	Results (mg/L)	Removal (%)	Class IIA	Comply	Standard A	Comply	Standard B	Comply
Mn	20.620	30.01	0.1	N	0.2	N	1.0	N
Fe	12.610	83.51	1.0	N	1.0	N	5.0	N
Ni	3.757	21.09	0.05	N	0.2	N	1.0	N
Cu	1.359	66.61	0.02	N	0.2	N	1.0	N
Zn	1.187	87.81	5.0	Y	2.0	Y	2.0	Y
Al	1.923	86.50	-	N/A	10	Y	15	Y
As	ND	-	0.05	Y	0.05	Y	0.1	Y

Appendix A13: Metal Concentrations of AMD Treated Using Dosage of 0.10 g/L PCC Synthesized By P123/CTAB Template.

Elements	P123 0.10							
	Original		NWQS		EQA Effluent Discharge Standard			
	Results (mg/L)	Removal (%)	Class IIA	Comply	Standard A	Comply	Standard B	Comply
Mn	22.870	22.37	0.1	N	0.2	N	1.0	N
Fe	13.240	82.68	1.0	N	1.0	N	5.0	N
Ni	4.193	11.93	0.05	N	0.2	N	1.0	N
Cu	1.771	56.49	0.02	N	0.2	N	1.0	N
Zn	4.860	50.09	5.0	Y	2.0	N	2.0	N
Al	2.249	84.21	-	N/A	10	Y	15	Y
As	ND	-	0.05	Y	0.05	Y	0.1	Y

Appendix A14: Metal Concentrations of AMD Treated Using Dosage of 0.20 g/L PCC Synthesized By P123/CTAB Template.

Elements	P123 0.20							
	Original		NWQS		EQA Effluent Discharge Standard			
	Results (mg/L)	Removal (%)	Class IIA	Comply	Standard A	Comply	Standard B	Comply
Mn	21.930	25.56	0.1	N	0.2	N	1.0	N
Fe	13.190	82.75	1.0	N	1.0	N	5.0	N
Ni	3.665	23.02	0.05	N	0.2	N	1.0	N
Cu	1.584	61.08	0.02	N	0.2	N	1.0	N
Zn	3.996	58.96	5.0	Y	2.0	N	2.0	N
Al	2.020	85.81	-	N/A	10	Y	15	Y
As	ND	-	0.05	Y	0.05	Y	0.1	Y

Appendix A15: Metal Concentrations of AMD Treated Using Dosage of 0.30 g/L PCC Synthesized By P123/CTAB Template.

Elements	P123 0.30							
	Original		NWQS		EQA Effluent Discharge Standard			
	Results (mg/L)	Removal (%)	Class IIA	Comply	Standard A	Comply	Standard B	Comply
Mn	20.480	30.48	0.1	N	0.2	N	1.0	N
Fe	11.210	85.34	1.0	N	1.0	N	5.0	N
Ni	3.180	33.21	0.05	N	0.2	N	1.0	N
Cu	1.517	62.73	0.02	N	0.2	N	1.0	N
Zn	1.454	85.07	5.0	Y	2.0	Y	2.0	Y
Al	1.762	87.63	-	N/A	10	Y	15	Y
As	ND	-	0.05	Y	0.05	Y	0.1	Y

Appendix A16: Metal Concentrations of AMD Treated Using Dosage of 0.40 g/L PCC Synthesized By P123/CTAB Template.

Elements	P123 0.40							
	Original		NWQS		EQA Effluent Discharge Standard			
	Results (mg/L)	Removal (%)	Class IIA	Comply	Standard A	Comply	Standard B	Comply
Mn	19.880	32.52	0.1	N	0.2	N	1.0	N
Fe	11.110	85.47	1.0	N	1.0	N	5.0	N
Ni	1.920	59.67	0.05	N	0.2	N	1.0	N
Cu	1.303	67.99	0.02	N	0.2	N	1.0	N
Zn	1.339	86.25	5.0	Y	2.0	Y	2.0	Y
Al	1.679	88.21	-	N/A	10	Y	15	Y
As	ND	-	0.05	Y	0.05	Y	0.1	Y

Appendix A17: Metal Concentrations of AMD Treated Using Dosage of 0.50 g/L PCC Synthesized By P123/CTAB Template.

Elements	P123 0.50							
	Original		NWQS		EQA Effluent Discharge Standard			
	Results (mg/L)	Removal (%)	Class IIA	Comply	Standard A	Comply	Standard B	Comply
Mn	16.600	43.65	0.1	N	0.2	N	1.0	N
Fe	10.300	86.53	1.0	N	1.0	N	5.0	N
Ni	0.359	92.46	0.05	N	0.2	N	1.0	Y
Cu	1.034	74.59	0.02	N	0.2	N	1.0	N
Zn	1.142	88.27	5.0	Y	2.0	Y	2.0	Y
Al	1.569	88.98	-	N/A	10	Y	15	Y
As	ND	-	0.05	Y	0.05	Y	0.1	Y